STRATIFIED INERTIAL FLOW IN THE GULF STREAM

Thesis by

Robert Roy Blandford

In Partial Fulfillment of the Requirements

For the Degree of

Doctor of Philosophy

California Institute of Technology

Pasadena, California

1964

(Submitted May 11, 1964)

ACKNOWLEDGEMENTS

I would like to thank Professors Kamb and Stommel for their help and encouragement, Professors Robinson and Fofonoff for several fruitful discussions, and Professor Malkus for introducing me to this topic. The work was performed with the assistance of funds from the National Science Foundation.

ABSTRACT

Earlier theoretical models of the Gulf Stream have treated the motion of a single fluid layer of constant density and vertically uniform flow velocity. As a step toward models with continuous stratification, the present work analyses inviscid, steady-state, purely inertial flow using two moving layers of different density and velocity.

The first type of Gulf Stream model analysed consists of two layers of different densities flowing over a denser layer at rest (baroclinic model). The second has two layers of different densities flowing over a rigid, horizontal bottom (mixed barotropic-baroclinic model).

In both models there exist, at any latitude, either 0, 2, or 4 theoretical solutions to the flow problem. Only one such solution, however, is realistic and satisfies the boundary condition of vanishing northward velocity at the southern latitude boundary of the flow region considered. This is called the correct solution, while the others are called incorrect solutions. As the parameters of the two-layer models converge to limiting values corresponding to one-layer models (for example, vanishing density difference between the upper and lower layers), the solutions may or may not converge to the one-layer solutions. If a correct solution converges uniformly, the limit is called a correct limit. If convergence is non-uniform at some value of the latitude coordinate, the limit is called an incorrect limit. If no solutions exist as the limit is approached, it is an impossible limit.

The most important limits discussed are as follows:

1. As the density contrast between the upper and lower moving layers becomes large in a baroclinic model for which the upper layer increases in thickness with latitude in the interior of the ocean to the east of the stream, the upper layer goes, via a correct limit, to the one-layer baroclinic model.

2. As the density contrast between the upper and lower layers becomes small in a baroclinic model, the solution for the sum of the two layers converges, via an incorrect limit, to the one-layer baroclinic model.

3. As the thickness of the upper layer becomes small while the density difference across it remains proportional to the thickness (a constant density "gradient" in the upper layer), the range of latitude over which there exists a correct solution tends to zero. The incorrect solution goes to the one-layer model via an incorrect limit. This result suggests that continuously stratified, purely inertial models of the Gulf Stream are impossible for finite density gradients.

4. In the limit as the interface between the lower moving layer and the resting layer becomes horizontal, the lower layer velocity goes to zero. No solution exists as the limit is approached. It is an impossible limit.

5. As the density contrast between the upper and lower layer becomes small in the barotropic-baroclinic model, the solution goes via a correct limit to the homogeneous barotropic model.

In an attempt to model the actual Gulf Stream, parameters are selected for a model of two moving layers, the upper about 600 meters

thick and the lower about 400 meters. This model is close to the impossible limit of 4. above, and no solution exists. The physical reason for this is that because of the small transport in the lower layer, the velocity in the lower layer must be small, which is incompatible with the large velocity gradient needed for conservation of potential vorticity as required in an inertial model. It therefore seems questionable that the deeper waters of the Gulf Stream can be modelled by a purely inertial theory.

No off-shore countercurrents can be found, despite fairly accurate modelling of boundary conditions which might be expected to give them.

The general implication of this work is that steady, purely inertial models are inadequate to describe even the lower latitude growth region of Gulf Stream if density stratification is taken into account, and that viscosity or unsteadiness must therefore be introduced.

TABLE OF CONTENTS

CHAPTER I

INTRODUCTION

1.1 The observational data

The modern view of the Gulf Stream is that it is a swiftly moving boundary current driven by fluxes of water from the rest of the North Atlantic. Both the wind stresses and temperature differences are thought to act as driving forces for these fluxes. Figure 1 from (1) shows schematically the chief features of the North Atlantic. The part of the ocean distinct from the Gulf Stream is commonly called the "interior," and the stream itself is called the "boundary layer." The mean velocities in the interior are 1 cm sec^{-1}, and in the Gulf Stream a typical velocity along the axis of the stream is 100 cm sec^{-1}. Stommel (1) has given an account of the early explorations and theories of the Gulf Stream.

The topography of the interior region is dominated by the eastern boundaries and by the Mid-Atlantic ridge. The effect of the Mid-Atlantic ridge on the ocean circulation is not too well understood. In the upper regions of the ocean, the observed distributions of temperature and salinity do not show any perturbations obviously associated with the ridge. However, they do show that the ridge effectively blocks the deep water, causing the water on either side of the ridge between about 4000 and 6000 meters to have significantly different temperatures and salinities. The basic mechanism of the circulation in the interior is presently thought to consist of a flow of cold

water upward to balance the downward diffusion of heat. This water then returns near the surface to colder regions of the ocean where it sinks to form the bottom water, thus completing the cycle.

A schematic diagram, figure 2, incorporating these ideas has been given by Stommel (1). Diagram 2a shows the upper layer, and diagram 2b shows the lower layer, roughly below 2000 meters. South of Greenland, surface water is thought to sink into the lower layer and move south-westward along the continental shelf. Two-thirds of this water flows to the South Atlantic, and one-third to the North Atlantic. In these general areas the cool water rises through the thermocline to act as the source for the upper layer circulations.

In the upper circulations, there is a certain amount of water constantly circulating, driven by the wind, which is represented by the three streamlines in figure 2a which do not end in sources. These other streamlines consist of water which has passed through the deep circulation. In more recent work this diagram has been modified to include, in the lower layer, a recirculation in the North Atlantic, and a zonal jet at 50°S. The observational and experimental evidence supporting this overall scheme has been discussed by Stommel and Arons (2,3), and by Stommel, Arons, and Faller (4); but as is the case with most oceanographic theories, the data are so sparse and so confused that it is not yet known to what degree this description is more than a working hypothesis.

Several authors (5,6,7,8) have discussed the mechanism of the thermocline in which the downward diffusion of heat warms the upward

flux of cold water. This mechanism is important because it determines the upward flux of cold water at the bottom of the thermocline which, when integrated over the globe, determines the total amplitude of the abyssal circulation. One of the most critical objections to these theories is the recent discovery by Swallow (9) of large scale velocity fluctuations in the thermocline and deep water. These fluctuations have amplitudes of 40 cm sec^{-1}, wavelengths of 300 km, and periods of a week. They seem to invalidate the equations which are used in all these theories of the interior which assume the steady state, and give amplitudes of 1 cm sec^{-1}. Perhaps the theories as given are correct for the mean motion, but that remains to be shown.

Figure 3 gives a density section in the Western Atlantic drawn from the data used by Fuglister (10) in his figure 51. It extends from Nova Scotia to Bermuda through the Mona Passage to Venezuala, roughly along latitude 66°W. The discontinuity at Bermuda is caused by the data being gathered on different cruises. The large slopes of the isotherms around 42°N mark the path of the Gulf Stream after it has turned east.

Figure 4 from Stommel (1) shows the depth of the 10°C isothermal surface in the western North Atlantic.

It is generally thought that the explanation for high velocity jets in certain regions of the ocean is that the equations appropriate to slow, steady motions do not have high enough order derivatives to satisfy boundary conditions on all of the coasts. As a result other terms in the equations of motion must be called into play, and these terms can become of importance only in a fast, narrow stream.

The Gulf Stream is just such a fast stream which satisfies the boundary conditions on the west coast of the North Atlantic. The additional terms in the stream are now thought to include inertia, turbulence, and time variations, all the terms available. Although the present work is primarily concerned with those streams which satisfy the boundary conditions using only the inertial terms, the second chapter will give some account of theories using other terms.

Figures 1 and 4 give some idea of the observed flow of the Gulf Stream. Figure 5 from Stommel's (1) book shows the topography of the Florida straits through which the stream passes. The depths are given in fathoms. (One fathom equals six feet.) It is apparent that the topography must exert a profound effect on the water in order to guide it through this channel. After passing through the straits the stream continues over a shelf of about 800 m to about 33°N., where it leaves the shelf. This shelf (the Blake Plateau) may be seen in figure 6.

Figure 7 shows a temperature and velocity section across the Gulf Stream from Chesapeake bay to Bermuda taken from Worthington (11). The "warm core" around station 4860 is a common feature of the Gulf Stream and usually has associated with it a countercurrent to the east, which is an object of considerable interest theoretically, since no theory so far has given a satisfactory account of it. Many workers have suggested that the countercurrent is a dynamical necessity because the hot water of the core, bounded by cold water to the east, should create a pressure gradient opposite to that of the main stream. However, this idea has not yet been fitted into a coherent model.

Figure 7 also clearly shows the leveling off of the isotherms as they approach the coast. It is not known whether this is due primarily to a frictional layer or to a hydraulic jump. These possibilities will be discussed in more detail in later chapters, especially chapter IV. The deep countercurrent that was discussed in the previous section is, of course, distinct from the one associated with the warm core, and since the former is thought to flow along the base of the continental shelf, it is below 2000 meters and not in this figure. It should be mentioned that inshore countercurrents have been observed in the Gulf Stream, but to my knowledge there are no accurate measurements of them. Probably they are basically a frictional phenomenon, even though inshore countercurrents of questionable significance are found in the present, purely inertial, theory.

When the stream leaves the coast at Cape Hatteras it rides out over deep water, and north of this point elaborate meanders are observed with wave lengths of 300 km, and a velocity of propagation of about 5 cm $sec.^{-1}$ For some time these waves were thought to be instabilities in the Gulf Stream, however, one of the most surprising results in recent oceanography is the seemingly conclusive demonstration by Bruce Warren (12) that the detailed path of the stream is determined by the angle at which it leaves the coast (which, perhaps, is due to some unstable fluctuation) and by the detailed topography over which it passes. This illustrates the powerful effect which topography exercises on the stream.

1.2 Aims of the present work

The purpose of this paper is to abstract from the maze of influences on the Gulf Stream the effects of inertial flow in a stratified system. The hope is, of course, that this will give the dominant behavior of the stream and that the other influences can be treated as perturbations. The interior will be completely parameterized by giving, *a priori*, its structure and the flux which it delivers at the eastern edge of the boundary layer.

The best previous theoretical models (chapter II) treat the Gulf Stream in terms of a single flowing water layer of constant density overlying a rigid bottom or a layer of stationary water of greater density. The dynamics are dominated by inertial forces, including, predominantly, the Coriolis "force."

The present work treats for the first time the case of two moving layers of different density. When the problem was undertaken, I expected to be able to fit observation in more detail than is possible with one-layer models, on the grounds that one could hope that two layers would allow a closer approach to the actual continuous density distribution. One could hope, for example, to account for the countercurrent associated with the warm core, and to show some of the characteristics which continuous inertial models would have to possess. The results could hardly be more different. Adding more detail to the models seems only to increase the detail of disagreement with observation. No warm core countercurrent can be found, and the principle result of the work is that steady, purely inertial models of any type

probably cannot account for the observations in any detail. The emphasis in the work has therefore been altered toward a study of the analytical properties of the inertial solutions, and in particular the various limits that the two-layer models approach as the defining parameters (e.g., density contrasts) are allowed to tend to certain limiting cases, like the one-layer model.

These results are contained in chapter III, where two-moving-layer models are calculated both analytically and numerically. Chapter II prepares the ground by reviewing earlier viscous and inertial one-moving-layer models, and chapter IV applies the calculations of chapter III to observed data in an attempt to account for the observations as closely as possible. Chapter V summarizes all the results and gives suggestions for further research.

1.3 Summary of Results

Analytic and numerical solutions are obtained for purely inertial, steady-state Gulf Stream models of two types. The first is a "completely baroclinic" stream consisting of two moving layers of different densities, flowing above water at rest, and therefore out of contact with the ocean bottom. The second is a "mixed barotropic and baroclinic model" comprising two layers of different density flowing over a rigid, horizontal bottom. In both models the flow along the axis of the stream is in geostrophic balance in accordance with a "boundary layer" concept, as in the one-layer models (chapter II).

The detailed results may be divided into two classes, those of interest for a comparison with observation, and those of primarily theoretical interest.

I. The results of observational interest for the "baroclinic" models are:

a. Large density gradients near the surface are necessary for flows to exist over large ranges of latitude.

b. The countercurrent associated with the warm core of the Gulf Stream almost certainly cannot be accounted for, within the boundary layer regime considered, by a model in which warm water is carried to higher latitudes in the upper layer.

c. Existing one-moving-layer models have generally been thought to apply to the water in the Gulf Stream between, say, 100 and 800 meters depth. The most obvious extensions for a two-layer model would be for the second layer to go from 0 to 100 meters, or from 800 to, say, 1600 meters. However, when possible models of these types are constructed, the disagreement with observation is extreme, leading one to suspect that adding further detail to the one-layer theory only increases the detailed disagreement with observation.

II. Of observational interest for the "mixed baroclinic-barotropic" models is an indication that the water flowing along the bottom with the stream through the Florida Straits and over the Blake Plateau cannot preserve the integrals of the inertial motion, because the analytical results based on these integral conditions disagree greatly with observation.

III. The results of theoretical interest for the "baroclinic" model are:

a. For most modelling parameters, as a solution is extended north from a chosen latitude of origin a latitude is reached at which more than one Gulf Stream cross section which satisfies all the integral conditions on the motion can be found. Only one of these cross sections belongs to a sequence of cross sections possessing the proper boundary conditions in the area of origin to the south, and only this one can be considered as the "correct" solution. However, the existence of these multiple solutions could be a stumbling block to further theoretical studies. It will be necessary to ensure that solutions from the same sequence are being discussed at all latitudes.

The "incorrect" sequences of cross-sections are also important theoretically because in some cases it is they, rather than the "correct" solutions that converge to the one-moving-layer solution in the limit where some parameter such as density difference tends to the corresponding one-layer limiting value. Because each of the solutions in this sequence tending toward the limiting solution is "incorrect," in that it does not connect properly to the area of origin to the south, the limit is called an incorrect limit. An incorrect limit represents non-uniform convergence to the one-moving-layer solution.

b. The correct limit for passing from a two-moving-layer to a one-moving-layer model is an increasing density contrast between the upper and lower layers. As noted above, vanishing density contrast between the two moving layers is an incorrect limit.

If the interface between the lower layer and the "level of no motion" below it were horizontal, the lower layer would be stationary and the upper layer would be a one-layer "baroclinic" model. However, there does not exist a sequence of realistic solutions converging to this limit as the lower interface becomes horizontal. In this work such a limit is called an impossible limit.

IV. The results of theoretical interest for the "mixed barotropic-baroclinic" models are:

a. Multiple solutions occur just as for the "baroclinic" case.

b. The correct limit by which to pass from the stratified to the homogeneous case is simply to let the density contrast vanish. For finite density contrast, if the interface between the two layers becomes horizontal there is non-uniform convergence to the homogeneous solution at some latitude dependent on the "stratification," hence this is an incorrect limit. The limit in which the lower layer becomes a level of no motion, and the upper layer passes into a one-layer baroclinic solution is an impossible limit.

CHAPTER II

EARLIER THEORIES OF THE GULF STREAM

2.1 Introduction

Analytical theories about the Gulf Stream can be separated into two groups, linear and non-linear. The linear theories have the disadvantage that eddy viscosity terms of doubtful validity are used to balance the driving forces, but they have the advantage that a steady state solution for an entire ocean basin may be found. This is true because the constant input of vorticity by the wind, and the changes of relative vorticity along a stream line because of changes in latitude, may be dissipated by the viscous terms.

The non-linear theories have the advantage that they do not use these questionable terms in the equations of motion, but because they have no dissipation, they are not able to model a complete ocean basin if the circulation is driven by a wind stress. An attempt has been made by Carrier and Robinson (13) to include just enough dissipation in the non-linear models to give a steady state solution without destroying the "essential" non-linearities. However, enough problems have been discovered in their work to make it seem that this is still a topic to be explored.

Bryan (14) has performed numerical solutions of equations with both viscous and inertial terms, and has obtained solutions over the entire basin which cannot be brought to a steady state when the inertial terms are large. This result suggests that time variation may be a necessary feature of a proper model.

The steady-state theories give different kinds of agreement with observation. The viscous theories give a general sort of agreement with the observed flow in the interior, but their picture of the Gulf Stream itself is inaccurate. The inertial theories cannot even discuss most of the interior, but in the rapidly moving regions of the Gulf Stream between the Florida Straits and Cape Hatteras, indications are that they can be at least a first approximation to observation. It is to this region that the present work is confined.

The remainder of this chapter will be devoted to discussing the above points in more detail, and in so doing, laying the groundwork for the new results to be discussed in the next chapter.

2.2 Linear theories

Stommel (1) has given a complete discussion of the important linear theories. Here only the principle results will be mentioned.

Sverdrup (15) in 1947 produced one of the first important results in modern oceanography when he wrote the equations of motion for the interior of the ocean as a balance between pressure gradients, Coriolis forces, and vertical steady-state stresses. By vertically integrating these equations, assuming that the stress vanished at great depths, and then cross-differentiating to eliminate the pressure, he was able to obtain

$$\beta \bar{v} = \mathrm{curl}_z \vec{\tau} \qquad (2.2.1)$$

where $\bar{v}$ is the vertically integrated north-south mass-transport, $\mathrm{curl}_z \vec{\tau}$ is the vertical component of the curl of the wind stress at the surface

of the ocean, β is the derivative of the Coriolis parameter, $2\Omega \sin \theta$, with respect to θ, where θ is the latitude. This relation between the horizontal transport and the vertical component of the curl of the wind stress enabled Sverdrup to discuss the currents of the interior by assuming that $\bar{u}$, the east west mass transport was zero at some longitude and by using the observed wind field and the continuity equation

$$\bar{u}_{,x} + \bar{v}_{,y} = 0 \ .$$

(Commas indicate differentiation with respect to the variables immediately following.)

Stommel's (16) important contribution was to show that the westward intensification of flow in the oceans is due to the variation of the Coriolis parameter with latitude. His basic equations were the same as those of Sverdrup's with the single addition of a dissipative force proportional to the horizontal transport. The resulting equations were cross-differentiated to eliminate the pressure, and streamlines for an exact solution were found for the cases of a nonrotating ocean, a rotating ocean, and a nonuniformly rotating ocean. The latter would correspond to the variation of the Coriolis parameter with latitude, and only for this case was there a westward intensification.

Munk (17) replaced Stommel's expression for the dissipation by horizontal eddy viscosity terms, and carefully examined the observed wind data to get a good representation of the driving force. The principle new theoretical result from his theory was an offshore countercurrent which can be traced to the biharmonic operator gener-

ated by the eddy viscosity expressions. The ratio of the transport of the countercurrent to that of the main stream is rather close to the observed ratio, and this is a feature which has not been duplicated to this day by any steady inertial theory including the present one. Of course the significance of the result is open to question because of the hypothetical nature of the eddy viscosity. Bryan's (14) work indicates that the inertial-viscous features corresponding to Munk's countercurrent are currents returning from the north, forming a complicated pattern in which even a small eddy viscosity can dissipate the advected vorticity. This sort of countercurrent probably corresponds in its effect on the stream to the eddies north of Cape Hatteras, and not to the countercurrent closely associated with the warm core which is of interest in the present work.

Stommel (18) pointed out that a value of the eddy viscosity small enough to give the proper width to the stream, and to be in agreement with order of magnitude observations of the Reynolds stresses, would also cause the inertial terms to be large, and this observation ushered in the inertial models of the Gulf Stream.

2.3 A history of inertial theories

Immediately after the paper by Munk was published, it was thought that inertial forces might be small compared to the viscous forces, so that Munk, Groves, and Carrier (19) discussed the perturbation problem. In an earlier paper Munk and Carrier (20) brought out the boundary-layer character of the Gulf Stream, which has been an essential point in all work on the subject since that time.

Following a suggestion by Stommel, Morgan (21) and Charney (22) developed inertial theories. These are also presented in Stommel's (1) book. Morgan considered both homogeneous and stratified models of the Gulf Stream, and drew the appropriate qualitative conclusions. He also gave a careful discussion of the basic equations and showed that coastal friction could not be inferred as necessary simply to balance the wind torques on the ocean.

Charney's work was aimed, on the other hand, at achieving a close agreement between theory and observation in the growth region of the Gulf Stream where the present theory also concentrates. By using a one-moving-layer stratified model and observed boundary conditions he did achieve good agreement with observation and this result has served as a source of confidence for all subsequent investigators.

Instead of discussing these papers in more detail, the solutions for stratified and homogeneous streams will be derived in the notation of this work, and Morgan's and Charney's papers will be discussed in terms of them. This will also provide the foundation for the new results of the next chapter.

2.4 A homogeneous ("barotropic") model

In the present work the equations used will be those of ordinary shallow water theory, which are derived from the basic equations in, for example, Stoker (23). The conditions for shallow water theory are that the flow be inviscid, adiabatic, incompressible, laminar, and that the characteristic length of the flow be much larger than the depth. In addition, in the present work the flow will be

assumed steady, and the variation of the free surface will be assumed small compared to the ocean depth.

The surface of the earth, over which the fluid flow takes place, is represented by a tangent cartesian plane, called the beta plane. In this plane the Coriolis parameter is allowed to vary in order to model the dynamical effects of the earth's curvature. The approximation was first introduced by Rossby (24), and is fairly good in a mathematical sense in the region between 15° and 35°N where it is used in this work. Experience with other theories indicates that it almost certainly will not lead to incorrect qualitative features in this range of latitude. To my knowledge the only complete discussion in the literature of this point is contained in the paper by Morgan (21). He carried through an unexceptionable derivation of the appropriate equations from the full spherical equations. His final results, including the integrals of motion for a one-moving-layer model, are indistinguishable from those of the beta plane except that his coordinates measure distances along latitude and longitude circles instead of along a tangent beta plane. The only serious approximation which he used was to expand the Coriolis parameter in a Taylor series and retain only the first term, which is also done in the beta-plane approximation. Thus it is fairly clear that the most serious approximation in the beta-plane treatment of the Gulf Stream is the expansion of the Coriolis parameter. The third term in the expansion becomes of the same size as the second term, for ranges of latitude of the order of the radius of the earth, when the plane is tangent at 45°N.

This latitude is therefore past the formal limit of validity of the approximation. However, qualitatively correct solutions may even be obtained north of 45° because the Coriolis parameter does increase monotonically, and because the approximation of the beta plane to the spherical geometry is always equally good (or bad) at any latitude.

The general expectation, mostly as a result of Charney's work, is that properly interpreted results from these equations will bear semi-quantitative comparison with observation.

In chapter III, models with two moving layers of different densities will be discussed. As additional layers are added, it is to be expected that a continuum model would be approached. This is correct, and in Appendix I it is shown that this limit corresponds to a continuum model in a "quasi-Lagrangian" coordinate system.

Historically, the equations used have been derived by vertically integrating the complete equations. However, as shown in Appendix I this is an untrustworthy approach. In this work, shallow water theory is used.

The following fundamental equations (23) are those of shallow water theory for steady flow of a homogeneous fluid layer on a cartesian plane tangent to a sphere, where the elevation of the free surface is negligible compared to the ocean's depth.

$$u'u'_{,x'} + v'u'_{,y'} - f'v' + \frac{1}{\rho} p'_{,x'} = 0 \qquad (2.4.1)$$

$$u'v'_{,x'} + v'v'_{,y'} + f'u' + \frac{1}{\rho} p'_{,y'} = 0 \qquad (2.4.2)$$

$$p' = - \rho g(z' - \eta') \qquad (2.4.3)$$

$$(D'u')_{,x'} + (D'v')_{,y'} = 0 \qquad (2.4.4)$$

Primes indicate variables having the usual physical dimensions as appropriate. In these equations $\underline{u}'$ is the east-west component of the flow velocity (assumed constant with depth) in the layer, $\underline{x}'$ is the east-west coordinate, $\underline{v}'$ is the north-south velocity component, $\underline{y}'$ is the north-south coordinate, D' is the thickness of the flowing layer, $\underline{z}'$ is the vertical coordinate, and η' is the elevation of the free surface, p' the pressure, and ρ the fluid density. (2.4.1) and (2.4.2) are the dynamical equation for horizontal motion, and express a balance between Coriolis forces (in terms of the parameter f'), pressure forces, and mass inertia. (2.4.3) describes vertical "hydrostatic" equilibrium, which is assumed to hold, and (2.4.4) is the flux continuity condition. The linear approximation to the Coriolis parameter, $\underline{f}'$, is obtained as follows:

$$f' = 2\Omega \sin\theta = 2\Omega \sin\theta_o \{1 + \cot\theta_o(\theta-\theta_o) - \tfrac{1}{2}(\theta-\theta_o)^2 + \cdots\}$$

$$\approx 2\Omega \sin\theta_o \{1 + \cot\theta_o(\theta-\theta_o)\} \approx 2\Omega \sin\theta_o \{1 + \cot\theta_o \frac{y'}{R}\}, \qquad (2.4.5)$$

where Ω is the angular velocity of the earth, θ_o is the latitude where $\underline{y}' = 0$, and $\underline{R}$ is the radius of the earth. Throughout this work, f' will be identified with the linear expression in y' given in (2.4.5).

To non-dimensionalize, a convenient set of characteristic sizes of the variables, consistent with the boundary-layer character of the stream as discussed by Morgan and Charney (21,22) is

$$y' \sim R, \qquad v' \sim \sqrt{g\eta_o},$$

$$\eta' \sim \eta_o, \qquad u' \sim \sqrt{g\eta_o}\,\frac{\lambda}{R}, \tag{2.4.6}$$

$$x' \sim \frac{\sqrt{g\eta_o}}{2\Omega \sin\theta_o} = \lambda \qquad f' \sim 2\Omega \sin\theta_o,$$

where η_o is a characteristic size for η'. A resulting non-dimensional parameter is,

$$\epsilon = \frac{\lambda}{R}\,. \tag{2.4.7}$$

The above quantities will be taken as coefficients of corresponding dimensionless variables, for example $x' = \lambda x$, dimensionless variables being identified by the unprimed symbols. If these dimensionless variables are substituted in 2.4.1-2.4.4, the result is, after eliminating $\underline{p}'$ by using the hydrostatic equation 2.4.3,

$$\epsilon^2 \{uu_{,x} + vu_{,y}\} - fv + \eta_{,x} = 0, \tag{2.4.8}$$

$$uv_{,x} + vv_{,y} + fu + \eta_{,y} = 0, \tag{2.4.9}$$

$$(Du)_{,x} + (Dv)_{,y} = 0. \tag{2.4.10}$$

Sizes of the scaling constants characteristic of the Gulf Stream are,

$$\eta_o \sim 1.0 \text{ m}, \qquad \Omega \sim .7 \times 10^{-4} \text{ sec}^{-1},$$

$$g \sim 10^3 \text{ cm sec}^{-2}, \qquad \theta_o \sim 20^{\circ}\text{N}\,. \tag{2.4.11}$$

$$R \sim 6.3 \times 10^3 \text{ km},$$

The value for η_o is derived from observations of the density structure by assuming that the pressure gradient vanishes at some great depth, e.g. 2000 meters, and observing that the difference of the vertical integral of ρdz at two different points in the Gulf Stream differs by as much as one meter of water. (See Stommel (1).)

These constants give

$$v' \sim 3.6 \text{ m sec}^{-1}, \qquad x' \sim 84.0 \text{ km}, \qquad \epsilon \sim 10^{-2}. \tag{2.4.12}$$

Since the sizes of $\underline{y}'$ and $\underline{x}'$ are similar to those observed, all the non-dimensionalized variables may be regarded as of order unity for a description of the Gulf Stream, and the terms multiplied by ϵ^2 in 2.4.8 may be neglected.

Two first integrals of the motion, the Bernoulli integral and the integral of potential vorticity, are of great importance in the present work. For two-layer models they may be derived in ways exactly parallel to the derivations given below for the one-layer case.

To derive the Bernoulli integral, multiply 2.4.8 by $\underline{u}$ and 2.4.9 by $\underline{v}$ and add. The result may be written as

$$\frac{d}{dt}\left[\tfrac{1}{2}\left(\epsilon^2 u^2 + v^2\right) + \eta\right] = 0. \tag{2.4.14}$$

where $\frac{d}{dt}(g)$ is the symbol for the substantial derivative $u\frac{\partial g}{\partial x} + v\frac{\partial g}{\partial y}$. The quantity in the brackets is a constant following the motion. For steady motion, the particles move along the stream-lines. Therefore the constant is a function only of the stream-function, ψ, that is

$$\tfrac{1}{2}\left(\epsilon^2 u^2 + v^2\right) + \eta = G(\psi), \tag{2.4.15}$$

where G is an arbitrary function of ψ. The expressions for the velocities in terms of a stream function are defined as

$$u = -\psi_{,y} \quad , \quad v = \psi_{,x} \ .$$

The layer depth, D, is not needed in the definition of ψ because the depth is constant for the barotropic model.

The potential vorticity integral is derived by first cross-differentiating and adding equations 2.4.8 and 2.4.9 to eliminate the pressure gradients. The quantity $u_{,x} + v_{,y}$ is then eliminated between the result and the continuity equation, to give, upon re-writing,

$$\frac{d}{dt}\left[\frac{v_{,x} - \epsilon^2 u_{,y} + \zeta}{D}\right] = 0 \ , \qquad (2.4.16)$$

or

$$\frac{v_{,x} - \epsilon^2 u_{,y} + \zeta}{D} = F(\psi) \ , \qquad (2.4.17)$$

where F is an arbitrary function of ψ, and where the symbol ζ has been written in place of f. This is done because this quantity ζ turns out in the subsequent development to have a special role as the natural "latitude" coordinate to use in place of y, to which it is related by the linear transformation

$$\zeta = (1 + \cot \theta_o \, y) \ .$$

The basic equation to be solved for this homogeneous model is found by substituting 2.4.8 into 2.4.7 to obtain, neglecting terms multiplied by ϵ^2,

$$\frac{1}{\zeta}\,\eta_{,xx} + \zeta = DF(\psi) \ . \qquad (2.4.18)$$

For the homogeneous model, the ocean depth is taken as a constant; the depth is normalized to D = 1.0.

This equation will now be applied to flow in the region illustrated by figure 8. The water flows toward the coast from the interior. The streamline at $\zeta = 1.0$, which is the (straight) southern boundary of the flow region, turns north at the coast $x = 0$ and becomes the $\psi = 0$ streamline.

The structure of the interior will be specified to ensure computational simplicity, since all that is desired here is a framework in which to discuss previous work and to introduce the ideas of the new calculations in the next chapter. The interior will be specified by giving the form of η as a function of latitude, ζ, just outside the boundary layer. In a more complete theory, the transport as a function of latitude would be determined by the wind stress, and this would fix the variation of the free surface.

In the interior then, η is assumed to be

$$\eta(\infty,\zeta) = \tfrac{1}{2}\,\zeta^2 \ . \qquad (2.4.19)$$

In the interior the non-linear terms in 2.4.9 are small and so

$$u(\infty,\zeta) = -\cot\theta_o \ . \qquad (2.4.20)$$

Integration with 2.4.14 gives

$$\psi(\infty,\zeta) = (\zeta-1) \ . \qquad (2.4.21)$$

But, because the velocity in the interior is small, $F(\psi)$ in 2.4.18 is

$$F(\psi) = \zeta\ (\infty, \psi),$$

so from 2.4.21

$$F(\psi) = \psi + 1\ . \tag{2.4.22}$$

But by using 2.4.8, integrating across the stream, and setting $\psi = 0$ at the coast,

$$\psi(x,\zeta) = \frac{1}{\zeta}\ \{\eta(x,\zeta) - \eta_c(\zeta)\}\ , \tag{2.4.23}$$

where η_c is the value of η at the coast.

Combining 2.4.22, 2.4.23, and 2.4.18 gives

$$\eta_{,xx} - \eta = -\ [\zeta(\zeta-1) + \eta_c]\ , \tag{2.4.24}$$

and the decaying solution gives,

$$\eta = A(\zeta)e^{-x} + \zeta(\zeta-1) + \eta_c\ . \tag{2.4.25}$$

Since $\eta = \eta_c$ at $x = 0$,

$$A(\zeta) = -\ \zeta(\zeta-1)\ , \tag{2.4.26}$$

so

$$\eta = \zeta(\zeta-1)(1-e^{-x}) + \eta_c\ . \tag{2.4.27}$$

There are two ways to complete the solution by determining η_c. The first is to use the Bernoulli condition, 2.4.15 (neglecting terms of order ϵ^2), along the ψ=0 streamline. Then by 2.4.19, $G(0) = \frac{1}{2}$.

The geostrophic relation applied to 2.4.27 gives the velocity at the coast, and so the Bernoulli condition may be solved for η_c. The result is,

$$\eta_c = \tfrac{1}{2}\,\zeta(2-\zeta)\ . \qquad (2.4.28)$$

The same result could be obtained by equating the expression 2.4.21 for the stream function to the expression 2.4.23 with $\tfrac{1}{2}\,\zeta^2$, the expression for η in the interior, substituted for $\eta(x,\zeta)$. In either case the final results are

$$\eta = \zeta(1-\zeta)e^{-x} + \tfrac{1}{2}\,\zeta^2\ , \qquad (2.4.30)$$

$$v = (\zeta-1)e^{-x}\ , \qquad (2.4.31)$$

$$\psi = (\zeta-1)(1-e^{-x})\ . \qquad (2.4.32)$$

Note that this homogeneous stream can extend to indefinitely large values of ζ . It will be found in chapter III that introducing density structure into the homogeneous model adds constraints on the motion so that the solutions cannot extend indefinitely far north.

As a check on this solution, it can be shown that continuity is explicitly satisfied by calculating $\underline{u}$ from (2.4.9), (2.4.30), and (2.4.31), and substituting in (2.4.10). From the inertial equation 2.4.9 the expression for $\underline{u}$ is

$$u = -\,\frac{vv_{,y} + \eta_{,y}}{v_{,x} + \zeta}\ .$$

By substituting 2.4.30 and 2.4.31 into this expression and setting $x = 0$, $\underline{u}$ is found equal to zero at the coast, in agreement with the flux condition applied in (2.4.23) by considering the $\underline{v}$ component of the velocity only. Still another check is to notice that the Bernoulli equation gives $\frac{1}{2} v^2 + \eta = G(\psi)$. Now $G(\psi) = \eta(\infty,\zeta) = \frac{1}{2} \zeta^2 = \frac{1}{2} (\psi+1)^2$, or $\frac{1}{2} v^2 + \eta = \frac{1}{2} (\psi+1)^2$ by equations 2.4.15, 2.4.19, and 2.4.21. Equations 2.4.30 through 2.4.32 satisfy the last relation, and thus the Bernoulli integral is satisfied for all values of ψ .

If instead of 2.4.19 there had been

$$\eta(\infty,\zeta) = - \frac{1}{2} \zeta^2 ,$$

then $\underline{u}$ would have been greater than zero, an eastward velocity, and η would have a plus sign in front of it in 2.4.24, implying only oscillatory solutions, that is, there would be no boundary layer. Generalized, this result says that there can be no steady inertial boundary layers on the west coast if the asymptotic velocity is eastward. Perhaps surprisingly the same result holds for inertial boundary layers on the east coast of the ocean. The only steady inertial boundary layers which can exist are those with asymptotic westward velocities. This result was obtained by Morgan and was extended by Robinson and Carrier, who showed that it was true for all plausible geometries and fluxes toward the coast.

A difficulty in constructing a purely inertial theory can be seen by 2.4.15 which shows that if water travels from a small value of ζ to a large value, it must have a large negative value of the relative

vorticity, $v_{,x}$, so that in the steady state in the north it must exist as a jet even in the interior. A possible pattern of flow then is an inertial flow accepting a westward flux up the west coast to a given latitude, then a jet across the ocean at that latitude, and then a boundary current down the opposite coast with an asymptotic westward flux going directly across the ocean into the boundary current on the west coast. The transition between the jet and the boundary current has been discussed in Fofonoff's (25) review article in which he shows that the jets and boundary current discussed above may be regarded as the most important pieces of a "free" solution (a flow which goes on steadily without dissipation) that he obtains and that includes the "corners." Carrier and Robinson (13) suggested that an arbitrary amount of this free solution might be added on to a wind-driven component, if friction were not taken into account; and they tried to use the necessity for dissipation of the wind's vorticity input to determine this amount.

However, Bryan's numerical calculations indicate that no ocean-wide circulation is needed except that directly forced by the wind-stress.

2.5 A baroclinic model: constant potential vorticity

The previous section discussed homogeneous models, which are also called barotropic models. The word implies that the constant density surfaces are parallel to the pressure surfaces, and since there is only one density in the problem this is trivially true.

A baroclinic model is instead one in which the constant density surfaces are inclined to the constant pressure surfaces. It is necessary to consider models of this type because the baroclinicity of the Gulf Stream is one of its most striking features. The model will be that of a layer of density ρ_1 and thickness D moving over a resting layer ("level of no motion") of density ρ_2, and of undetermined thickness. The equations of motion for the upper layer are,

$$u'u'_{,x'} + v'u'_{,y'} - f'v' + \frac{1}{\rho_1} p'_{,x'} = 0 \ , \qquad (2.5.1)$$

$$u'v'_{,x'} + v'v'_{,y'} + f'u' + \frac{1}{\rho_1} p'_{,y'} = 0 \ , \qquad (2.5.2)$$

$$p' = -\rho_1 g(z' - \eta') \ , \qquad (2.5.3)$$

$$(D'u')_{,x'} + (D'v')_{,y'} = 0 \ , \qquad (2.5.4)$$

where the variables are all the same as in 2.4.1-2.4.4.

The pressure in the lower layer is,

$$\begin{aligned} p'_2 &= \rho_1 g D' - \rho_2 g(z' + (D' - \eta')) \ , \\ &= g(\rho_1 - \rho_2)D' + \rho_2 g\eta' - \rho_2 g z' \ . \end{aligned} \qquad (2.5.5)$$

If the lower layer is to be a level of no motion, then the horizontal pressure gradient must vanish, so

$$\eta' = \frac{\rho_2 - \rho_1}{\rho_2} D' + \text{constant} \ . \qquad (2.5.6)$$

The constant is taken to be zero.

By introducing the characteristic sizes of the variables, as in 2.4.6,

$$D' \sim D_o \equiv D(\infty,1), \qquad x' \sim \frac{\sqrt{g\eta_o}}{2\Omega \sin\theta_o} \equiv \lambda ,$$

$$\eta' \sim \frac{\rho_2-\rho_1}{\rho_2} D_o \equiv \eta_o , \quad v' \sim \sqrt{g\eta_o} \tag{2.5.7}$$

$$y' \sim R , \qquad u' \sim \sqrt{g\eta_o}\,\frac{\lambda}{R}$$

going through the same procedure used to get 2.4.8-2.4.10, and omitting the terms multiplied by ϵ^2, there results,

$$-\zeta v + D_{,x} = 0 , \tag{2.5.8}$$

$$uv_{,x} + vv_{,y} + \zeta u + D_{,y} = 0 , \tag{2.5.9}$$

$$(Du)_{,x} + (Dv)_{,y} = 0 . \tag{2.5.10}$$

The Bernoulli integral for these equations is derived just like 2.4.15, and, omitting the ϵ^2 terms is

$$\tfrac{1}{2} v^2 + D = G(\psi) . \tag{2.5.11}$$

Similarly, the vorticity integral is,

$$\frac{v_{,x} + \zeta}{D} = F(\psi) . \tag{2.5.12}$$

The stream function is defined by

$$Du = -\psi_{,y} \quad , \qquad Dv = \psi_{,x} \tag{2.5.13}$$

The fundamental equation to be solved is obtained by substituting 2.5.8 into 2.5.12.

$$\frac{1}{\zeta} D_{,xx} - DF(\psi) = -\zeta \tag{2.5.14}$$

This equation is now solved in the flow region shown in figure 8. A simple solution may be obtained if in the interior the layer thickness is given by

$$D(\infty,\zeta) = \zeta \ . \qquad (2.5.15)$$

Since the non-linear terms are negligible in the interior, 2.5.9 and 2.5.13 give, with $\psi = 0$ at $\zeta = 1.0$,

$$\psi(\infty,\zeta) = (\zeta-1) \qquad (2.5.16)$$

and by 2.5.12,

$$F(\psi) = 1 \ . \qquad (2.5.17)$$

Since $F(\psi)$ is a constant in this case, 2.5.15 represents the special situation of constant potential vorticity, which plays an important role in inertial theories of the Gulf Stream (1).

If 2.5.17 is substituted into 2.5.14, and the resulting equation is solved, there results

$$D = (h_o-\zeta)e^{-\zeta^{\frac{1}{2}}x} + \zeta \qquad (2.5.18)$$

where h_o is the thickness of the layer at the coast. Just as in the homogeneous case there are two ways to evaluate h_o, the Bernoulli integral or the boundary condition of no flux through the coast. It is simple to use either one to obtain

$$h_o = \{\zeta(2-\zeta)\}^{\frac{1}{2}} \ . \qquad (2.5.15)$$

The complete results are then

$$D = [\{\zeta(2-\zeta)\}^{\frac{1}{2}} - \zeta]e^{-\zeta^{\frac{1}{2}}x} + \zeta \ , \qquad (2.5.20)$$

$$v = \zeta^{-\frac{1}{2}}[\zeta - \{\zeta(2-\zeta)\}^{\frac{1}{2}}]e^{-\zeta^{\frac{1}{2}}x} \ . \qquad (2.5.21)$$

The tests that continuity is satisfied, that u = 0 at x = 0, and that the Bernoulli equation is satisfied for all ψ, can be performed just as they were for equations 2.4.30-2.4.32.

For a realistic solution, the positive square root must be taken. The negative root also gives a set of cross sections which satisfy the Bernoulli equation and mass flux condition, but the layer thickness is negative, which is physically meaningless. Also, the solution for negative h_o does not match the boundary condition v = 0 at ζ = 1.0. (See figure 8.) In the present work the adjective realistic will have the strict meaning that all layer thicknesses are positive.

If the two solutions of 2.5.19 are plotted as a function of ζ, they form a parabola with the nose at ζ = 2, h = 0. In chapter III, solutions will be found for which the nose of the curve analogous to this parabola occurs for h > 0, thus implying more than one "realistic" solution for a given ζ. However, such lower "branches" do not extend back to v = 0 at ζ = 1.0, and thus are not correct solutions to the problem. In the present work a correct solution is defined as a sequence of cross sections which has the proper boundary conditions at ζ = 1.0.

There are also solutions for the one-layer model for $\zeta < 1.0$. If the positive sign is taken in 2.5.19 then $v < 0$ for $\zeta < 1$ and this

gives the solution in which the $\psi = 0$ streamline turns south instead of north. The solution extends to $\zeta = 0$ where $D = 0$, and the velocity goes to the constant value, $-2^{\frac{1}{2}}$, independent of $\underline{x}$ because the exponential in 2.5.21 does not decay at $\zeta = 0$. If the negative sign in 2.5.19 is taken for $\zeta < 1.0$, an unrealistic solution is found which joins the realistic one at $\zeta = 0$, and connects to the solution with a negative layer thickness for $\zeta > 1.0$ at $\zeta = 1.0$. All of these "branches" have corresponding solutions in the two-moving-layer cases, as will be seen in the discussion of the first two-moving-layer solutions in chapter III.

The correct solution for $\zeta > 1.0$ contains the qualitative features of the baroclinic models of Morgan and Charney (21,22). Notice that the stream cannot extend beyond $\zeta = 2$. This was interpreted by Charney as a separation of the Gulf Stream from the coast. Notice the difference here from the barotropic model, which could extend to indefinitely large value of ζ, since negative values of η are physically meaningful.

To understand the failure of the solution at $\zeta = 2.0$ somewhat better, the following relation, valid for both constant and non-constant potential vorticity, is useful:

$$\frac{dh_o}{d\zeta} = -\frac{1}{h_o}\int_1^{\zeta} \frac{1}{\xi} D(\xi)D'(\xi)d\xi$$

It may be derived by equating the northward transport to the transport toward the coast, and differentiating with respect to ζ. The layer thickness at the coast is h_o, in the interior it is $\underline{D}$, and ξ is a dummy

variable. When $h_o = 0$, only special functions, $\underline{D}$, will give a finite $h,_\zeta$. If $h,_\zeta$ is not finite when $\underline{h} = 0$, then neither is $D,_\zeta$, so for $x > 0$, $u \to \infty$, the non-linear terms become important in equation 2.5.8, "cross-stream geostrophy" fails, and with it all the theory. Therefore it is better to say that the regime of flow gradually breaks down as $\zeta = 2$ is approached, rather than to say that it fails suddenly at $\zeta = 2$, or that it leaves the coast at this latitude. Perhaps the regime of flow in which cross stream geostrophy is invalid could extend the flow farther than $\zeta = 2$.

It is clear then that $D,_\zeta \to \infty$ if $h_o \to 0$. To show that h_o must vanish for some interiors, consider a fixed latitude ζ_f with a layer thickness in the interior, D_f. Then the maximum transport, given by $\int \frac{1}{\zeta_f} DD,_x dx$ occurs for $h_o = 0$ and is $\frac{1}{2\zeta_f} D_f^2$, independent of D for $\zeta < \zeta_f$. But by increasing D for $\zeta < \zeta_f$ an arbitrarily large flux can be forced toward the coast, and therefore, north. Eventually therefore at $\zeta = \zeta_f$, h_o must vanish.

CHAPTER III

TWO-MOVING-LAYER GULF STREAM MODELS

3.1 Introduction

In this chapter the equations for a Gulf Stream with two moving layers are derived and solved for a range of parameters which is large enough to give a good qualitative picture of the behavior of the fluid-dynamical system. The main purpose of the chapter is to provide this qualitative picture. Comparisons with observed data, such as can be made, are given in chapter IV.

The chapter begins with the derivation of the equations of motion for a two-moving-layer model with a level of no motion. Here, this model is called the baroclinic model. When a reference is made to the baroclinic model of chapter II, it is specifically called the one-layer baroclinic model.

The equations are first solved for the case of constant potential vorticity in both layers. A particular solution is discussed in detail, and it is shown that in a range of latitudes three cross-sections of the stream in which the $\psi = 0$ streamline runs along the coast may be found for each latitude. Each cross-section satisfies the conditions of conservation of mass, potential vorticity, and energy and has positive layer thicknesses. However, it is shown that only one of these cross-sections may be considered a correct solution, because the others belong to families of cross-sections which do not have the proper boundary conditions at $\zeta = 1.0$. (See figure 8.) It is shown that hy-

draulic jumps cannot occur between the cross-sections that are possible at the same latitude, because the conservation of mass and energy flux precludes momentum flux conservation, which must be satisfied in a hydraulic jump.

A different type of cross-section possible in the range of latitude that contains multiple solutions consists of one in which the $\psi = 0$ streamline for the upper layer has left the coast and lies at some distance off shore. This constitutes the first proof (by example) that such a solution, representing a stream that has "separated" from the coast, is possible.

If the ratio of the thicknesses of two constant-potential-vorticity layers in the interior is either large or small, it is possible to get completely analytical solutions in series form at those latitudes at which the upper layer goes to zero thickness at the coast. From these solutions it is possible to see that the proper limit by which the two-layer baroclinic model passes into the one-layer baroclinic model is the limit in which the quantity $\gamma = \frac{\rho_3 - \rho_1}{\rho_3 - \rho_2}$ becomes large, where ρ_1, ρ_2, and ρ_3 are the densities of the upper, middle, and lower layers respectively. γ measures the density contrast or "stratification" of the two-layer model.

It is also shown that the limit $\gamma = 1.0$ is incorrect (Section 1.3), because at $\zeta = 1.0$ there is non-uniform convergence of the incorrect solution to the limiting solution.

In none of these solutions is an off-shore countercurrent found.

A numerical method for solving the exact equations for non-constant potential vorticity is then introduced and with it are discussed the solutions resulting from various types of interiors. The principle new qualitative result here is that for the limit in which γ is fixed and finite, but the boundary between ρ_2 and ρ_3 in the interior becomes horizontal, thus making the middle layer a layer of no motion, there does not exist a converging sequence of solutions. This shows that the one-layer baroclinic model may not be thought of as this type of limit of a two-moving-layer model, and the limit is defined as an impossible limit.

Another qualitative result is that even for a large flow of warm water from southern to northern latitudes, which would be expected to form a warm core (see figure 7), no warm core or countercurrent is found.

Numerical methods are then applied to a model in which there is a rigid bottom beneath two moving layers of differing densities. Here this model is called the barotropic model. If a reference is made to the barotropic model of chapter II, it is called the one-layer barotropic model. (Of course this two-layer model is, strictly speaking, baroclinic, but it is barotropic in the limit of vanishing stratification, and it is named barotropic for convenience. (In the introduction, Section 1.3, it was referred to as the "mixed barotropic-baroclinic model.")

In chapter II the solution for a rigid bottom with no stratification extended to the north indefinitely. One of the principle results

of this chapter is that as stratification is introduced, the result is to restrict the solution to lower latitudes. The fact that as the stratification density contrast is reduced the barotropic model extends farther north shows that stratification decreasing gradually to zero constitutes the limit leading to the one-layer barotropic solution.

It is shown that the solution corresponding to finite stratification but infinitesimal slope of the interface in the interior has a discontinuity in the velocities and layer thicknesses at some value of ζ dependent on the stratification. There is a non-uniform convergence to the homogeneous model, and this is thus a case of an incorrect limit. The non-uniformity does not occur at $\zeta = 1.0$ as it does for $\gamma = 1.0$ for the baroclinic model.

For the barotropic model, as for the baroclinic, there is no warm core or countercurrent.

3.2 Equations for the baroclinic model

The characteristic thickness of the constant-density layers will be taken as the sum of the thicknesses of the upper and lower layer at $\zeta = 1.0$, $x = \infty$. Thus in nondimensional form this sum is normalized to unity.

Assuming a level of no motion below the second layer, the equations for the pressure gradients are,

$$p_{1,x} = \gamma D_{1,x} + D_{2,x} , \qquad (3.2.1)$$

$$p_{2,x} = D_{1,x} + D_{2,x} ,$$

where $\gamma = \frac{\rho_3-\rho_1}{\rho_3-\rho_2}$ and ρ_1, ρ_2, and ρ_3 are the densities of the upper, lower, and stationary layers respectively. As written, they have been non-dimensionalized, analogously to 2.5.7, by the expressions,

$$D_1' = [D_1'(\infty,1) + D_2'(\infty,1)]D_1 , \qquad x' = \frac{\sqrt{g\eta_o}}{2\Omega \sin\theta_o} x = \lambda x,$$

$$\eta' = \frac{\rho_3-\rho_2}{\rho_3} [D_1'(\infty,1) + D_2'(\infty,1)]\eta = \eta_o\eta , \quad v' = \sqrt{g\eta_o} ,$$

$$y' = Ry , \qquad u' = \sqrt{g\eta_o}\,\frac{\lambda}{R}\,u .$$

The first of equations 3.2.1 will now be derived. The derivation of the second equation is similar. The expression for the pressure in layer 1 is

$$p_1'(z) = g\,(\eta'-z')\rho' ,$$

where η is measured from $z = 0$. The level of no motion below layer 2 requires that the pressure gradient there vanish, or

$$\frac{\partial}{\partial x'} [g\rho_1 D_1' + g\rho_2 D_2' - g\rho_3(z' + D_1' + D_2' - \eta')] = 0 ,$$

or

$$\eta_{1,x} = \frac{\rho_3-\rho_1}{\rho_3} D_{1,x}' + \frac{\rho_3-\rho_2}{\rho_3} D_{2,x}' ,$$

so

$$p_{1,x}' = \frac{g(\rho_3-\rho_2)}{\rho_3} [\gamma D_{1,x}' + D_{2,x}'] ,$$

which when non-dimensionalized gives the first of 3.2.1.

It would be possible to ensure a constant flux into the coast between, say, $\zeta = 1.0$ and $\zeta = 2.0$ by relaxing the constraint that $D_1(\infty,1) + D_2(\infty,1) = 1.0$. However, because solutions do not even exist near $\zeta = 2.0$ for some values of the parameters, it seems more reasonable to normalize the thickness of the layers and let the transport be determined. [In any event, the transport may be adjusted to any value by changing the overall stratification, or $D_1' + D_2'$.]

The differential equations for the layers are

$$- \zeta v_1 + \gamma D_{1,x} + D_{2,x} = 0 , \tag{3.2.2}$$

$$u_1 v_{1,x} + v_1 v_{1,y} + \zeta u_1 + \gamma D_{1,y} + D_{2,y} = 0 , \tag{3.2.3}$$

$$(D_1 u_1)_{,x} + (D_1 v_1)_{,y} = 0 , \tag{3.2.4}$$

$$- \zeta v_2 + D_{1,x} + D_{2,x} = 0 , \tag{3.2.5}$$

$$u_2 v_{2,x} + v_2 v_{2,y} + \zeta u_2 + D_{1,y} + D_{2,y} = 0 , \tag{3.2.6}$$

$$(D_2 u_2)_{,x} + (D_2 v_2)_{,y} = 0 . \tag{3.2.7}$$

These equations are just those of 2.5.8-2.5.10 for each individual layer, with the exception that the pressure gradients are given by 3.2.1, instead of $D_{,x}$ and $D_{,y}$ alone. The potential vorticity and Bernoulli integrals are

$$\frac{v_{1,x} + \zeta}{D_1} = F_1(\psi_1) , \qquad \tfrac{1}{2}v_1^2 + \gamma D_1 + D_2 = G_1(\psi_1) ,$$

$$\frac{v_{2,x} + \zeta}{D_2} = F_2(\psi_2) , \qquad \tfrac{1}{2}v_2^2 + D_1 + D_2 = G_2(\psi_2) . \tag{3.2.8}$$

These integrals are derived just as were 2.5.11 and 2.5.12. Only the equations for each individual layer are needed to derive the integrals for that layer. In the present work the thicknesses of the upper and lower layers in the interior will be limited to being linear functions of latitude, thus

$$D_1(\infty,\zeta) = a + b\zeta \ ,$$
$$D_2(\infty,\zeta) = c + (1-a-b-c)\ \zeta \ , \qquad (3.2.9)$$

where the coefficient of ζ in D_2 guarantees the normalization at $\zeta = 1.0$. It may be that restricting the interiors to this class makes it impossible to consider some important qualitative change associated with a change in the derivative of a layer thickness with latitude. For example, as one result, the manner in which the stream leaves the coast may not be discussed because the sign of the east-west velocity in the interior cannot change as a function of latitude. However, it is shown in chapter IV that this problem lies beyond the scope of the present work. Another question is whether the countercurrent might be excluded by 3.2.9. I do not believe that it is, because I have been able to model, to almost complete satisfaction, every type of two-layer interior which I thought a-priori might create a countercurrent.

3.3 Methods of solution for constant potential vorticity

The only interiors for which analytical results are obtainable are those with constant potential vorticity. In this case 3.2.9 becomes,

$$D_1(\infty,\zeta) = b\zeta \ , \ D_2(\infty,\zeta) = (1-b)\zeta \ . \qquad (3.3.1)$$

This gives $F_1(\psi_1) = \frac{1}{b}$, $F_2(\psi_2) = \frac{1}{1-b}$; the potential vorticity is thus constant. The ratio δ is defined by

$$\delta = \frac{b}{1-b} , \qquad (3.3.2)$$

and measures the ratio of thicknesses in the interior of the upper and lower layers.

If 3.2.2 and 3.2.5 are inserted into the corresponding potential vorticity integrals, 3.2.8, and both sides of the resulting equations are multiplied by the corresponding D, there result the following equations for the baroclinic model,

$$\gamma D_{1,xx} + D_{2,xx} - \zeta D_1 F_1(\psi_1) = - \zeta^2 , \qquad (3.3.)$$

$$D_{1,xx} + D_{2,xx} - \zeta D_2 F_2(\psi_2) = - \zeta^2 . \qquad (3.3.4)$$

For the special case of constant potential vorticity the functions of ψ are constant and,

$$F_1(\psi_1) = \frac{\delta}{1+\delta} , \quad F_2(\psi_2) = \frac{1}{1+\delta} . \qquad (3.3.5)$$

Then 3.3.3 and 3.3.4 become

$$\gamma D_{1,xx} + D_{2,xx} - \frac{1+\delta}{\delta} \zeta D_1 = - \zeta^2 , \qquad (3.3.6)$$

$$D_{1,xx} + D_{2,xx} - (1+\delta)\zeta D_2 = -\zeta^2 . \qquad (3.3.7)$$

Particular solutions to these equations are

$$D_1^p = \frac{\delta}{1+\delta} \zeta , \qquad D_2^p = \frac{1}{1+\delta} \zeta . \qquad (3.3.8)$$

The characteristic equation for the system of differential equations is

$$\begin{vmatrix} \gamma a^2 - \frac{(1+\delta)}{\delta} & \alpha^2 \\ \alpha^2 & \alpha^2 - (1+\delta) \end{vmatrix} = 0 \ . \qquad (3.3.9)$$

This gives

$$\alpha^2 = (1+\delta)\left\{\frac{\gamma + \delta^{-1} \pm ((\gamma-\delta^{-1})^2 + 4\delta^{-1})^{\frac{1}{2}}}{2(\gamma\ 1)}\right\}. \qquad (3.3.10)$$

It is easy to verify by rewriting the term under the square root sign that α^2 is always greater than zero, because γ is always greater than 1.0 for $\rho_1 < \rho_2 < \rho_3$, stable stratification. Since α has four possible roots, expressions for the layers are,

$$\begin{aligned} D_1 &= a_1 e^{\alpha_1 \zeta^{\frac{1}{2}} x} + a_2 e^{-\alpha_1 \zeta^{\frac{1}{2}} x} + a_3 e^{-\alpha_2 \zeta^{\frac{1}{2}} x} + a_4 e^{+\alpha_2 \zeta^{\frac{1}{2}} x} + \frac{\delta\,\zeta}{1+\zeta}\ , \\ D_2 &= b_1 e^{\alpha_1 \zeta^{\frac{1}{2}} x} + b_2 e^{-\alpha_2 \zeta^{\frac{1}{2}} x} + b_3 e^{-\alpha_2 \zeta^{\frac{1}{2}} x} + b_4 e^{\alpha_2 \zeta^{\frac{1}{2}} x} + \frac{\zeta}{1+\delta}\ , \end{aligned} \qquad (3.3.11)$$

where the convention is adopted that α_1 is the absolute value of the square root of the right hand side of 3.3.10 using the plus sign, and α_2 is the same expression using the minus sign. There are eight unknown constants in 3.3.11. This number is reduced to four by substituting in 3.3.6 or 3.3.7, and insisting that the coefficient of each exponential be zero. Using 3.3.7 this gives,

$$a_2 = n_1 b_2 \qquad a_4 = n_2 b_4 \qquad (3.3.12)$$

where $$n_1 = \left\{\frac{(1+\delta)-\alpha_1^2}{\alpha_1^2}\right\},\ n_2 = \left\{\frac{(1+\delta)-\alpha_2^2}{\alpha_2^2}\right\}.$$

The other constants are coefficients of growing exponentials and are set equal to zero so that velocities go to zero in the interior. This gives finally

$$D_1 = b_2\, n_1\, e^{-\alpha_1 \zeta^{\frac{1}{2}} x} + b_4\, n_2\, e^{-\alpha_2 \zeta^{\frac{1}{2}} x} + \frac{\delta\zeta}{1+\delta}\,, \qquad (3.3.13)$$

$$D_2 = b_2 e^{-\alpha_1 \zeta^{\frac{1}{2}} x} + b_4\, e^{-\alpha_2 \zeta^{\frac{1}{2}} x} + \frac{\zeta}{1+\delta}\,.$$

From 3.2.8, 3.2.9, 3.3.1, and 3.3.2 the Bernoulli constants for the zero streamline are

$$G_1(0) = \frac{1+\gamma\delta}{1+\delta}\,, \quad G_2(0) = 1\,. \qquad (3.3.14)$$

so along $\psi=0$,

$$\gamma h_1 + h_2 + \tfrac{1}{2}v_1^2 = \frac{1+\gamma\delta}{1+\delta}\,, \qquad (3.3.15)$$

$$h_1 + h_2 + \tfrac{1}{2}v_2^2 = 1\,,$$

where h_1 and h_2 are the layer thicknesses at $x = 0$. From 3.2.2, 3.2.5, and 3.3.13, at $x = 0$,

$$\begin{aligned} v_1 &= -\zeta^{\frac{1}{2}}[\alpha_1 (\gamma n_1+1)\, b_2 + \alpha_2\, (\gamma n_2+1)\, b_4]\,, \\ v_2 &= -\zeta^{-\frac{1}{2}}[\alpha_1 (n_1+1)\, b_2 + \alpha_2\, (n_2+1)\, b_4]\,. \end{aligned} \qquad (3.3.16)$$

An explicit formula for h_1 in terms of h_2 will now be found. In the interior, applying 3.2.3 and 3.2.6, noting that the inertial terms are small, to 3.3.1

$$u_1 = \frac{1}{\zeta}\left(\frac{\gamma\delta+1}{\delta+1}\right) \tan\theta_o\,, \quad u_2 = \frac{1}{\zeta}\tan\theta_o\,. \qquad (3.3.17)$$

If these expressions are multiplied by the layer thicknesses and integrated with respect to $\underline{y}$, there results

$$\psi_1(\infty,\zeta) + \psi_2(\infty,\zeta) = \left[\frac{\gamma\delta^2+2\delta+1}{(1+\delta)^2}\right](\zeta-1) \ . \qquad (3.3.18)$$

But by integrating across the stream, using 3.2.2 and 3.2.5

$$\psi_1(\infty,\zeta) = \frac{1}{\zeta}\int_0^\infty D_1(\gamma D_{1,x}+D_{2,x})\,dx \ ,$$

$$\psi_2(\infty,\zeta) = \frac{1}{\zeta}\int_0^\infty D_2(D_{1,x}+D_{2,x})\,dx \ , \qquad (3.3.19)$$

so

$$\psi_1(\infty,\zeta) + \psi_2(\infty,\zeta) = \left\{\frac{1}{2\zeta}(\gamma D_1^2+2D_1D_2+D_2^2)\right\}\Bigg|_0^\infty \ . \qquad (3.3.20)$$

Combining 3.3.20 and 3.3.18 and using 3.3.1 and 3.3.2

$$\gamma h_1^2 + 2h_1h_2 + h_2^2 = \frac{\zeta(2-\zeta)}{(1+\delta)^2}\left\{\gamma\delta^2 + 2\delta + 1\right\} \ . \qquad (3.3.21)$$

This equation shows that there can be no realistic solution north of $\zeta = 2.0$, for constant potential vorticity, because, assuming $(\gamma,h_1,h_2) \geq 0$, the right hand side is negative, whereas the left hand side must be positive. Furthermore, if there is a realistic solution at $\zeta = 2.0$, then $h_1 = h_2 = 0$.

Solving 3.3.2 for h_2 gives

$$h_2 = h_1\left[-1 \pm \left\{1 - \left(\gamma - \frac{\zeta(2-\zeta)}{h_1^2(1+\delta)^2}(\gamma\delta^2+2\delta+1)\right)\right\}^{\frac{1}{2}}\right]. \qquad (3.3.22)$$

Only the positive value of the radical may be used for realistic solutions, otherwise either h_1 or h_2 would be negative.

The next step is to take 3.3.13 at x = 0, and solve them for b_2 and b_4. The result is

$$b_2 = \left\{h_1 - n_2 h_2 - \frac{\zeta}{1+\delta}(\delta - n_1)\right\} \frac{1}{n_1 - n_2}, \qquad (3.3.23)$$

$$b_4 = \left\{h_1 - n_1 h_2 - \frac{\zeta}{1+\delta}(\delta - n_1)\right\} \frac{1}{n_2 - n_1}.$$

If equations 3.3.23 are substituted in equations 3.3.16, and the results substituted in equation 3.3.12, two quadratic equations in h_1 and h_2 are obtained. The solution to the problem can then be found as the roots of a quartic equation. The two quadratics might be any conic sections in principle. They can be pictured as in figure 9 for the case of two ellipses. Thus either 0, 2, or 4 real solutions for (h_1, h_2) are to be expected for any value of ζ.

Any pair of values (h_1, h_2) which are solutions to equations 3.3.15 must satisfy 3.3.21 (a centered ellipse), and since 3.3.21 is a simpler equation, the solutions have actually been computed using 3.3.21 and one of equations 3.3.15. Instead of solving directly for the roots of a quartic, a numerical technique was used to find the solution. For any latitude ζ the method of solution was as follows. First a guess for h_1 was made and substituted in 3.3.22 to obtain h_2. Then b_2 and b_4 were obtained from 3.3.23 and were substituted in 3.3.16 to obtain the velocities. The results were tested to see if

they satisfy one of equations 3.3.15, and if not, a new value of h_1 was chosen and the process repeated. When this iteration has produced a solution, the result satisfies the other equation 3.3.15. Then equations 3.3.23 give the values for b_2 and b_4, and equations 3.3.13 give the functional form for the layer thicknesses.

The discussion of solutions will begin with the specific case $\gamma = 2.0$, $\delta = 1.0$. Figure 10 shows the behavior of this solution. In figure 10, h_1 is plotted as a function of ζ. The symbols such as (++-+) give the signs of (h_1,h_2,v_1,v_2) at the closest computed point. The correct solution extends from $h_1 = .5$, $\zeta = 1.0$, to a "maximum" at $h_1 = 0.112 \pm .001$, $\zeta = 1.464 \pm .005$. From $h_1 = 0$, $\zeta = 1.4565 \pm .0002$, another branch of realistic solutions moves north toward the "maximum." Another segment of realistic solutions lies between the brackets at $\zeta = 1.43$ and 1.9. Outside of these brackets $h_2 < 0$ in the first quadrant.

For a small range of latitude around $\zeta = 1.45$ there are three realistic solutions. Only one of these, however, connects to the proper boundary conditions at $\zeta = 1.0$. It is called the <u>correct solution</u>.

In the graphs discussed in sections 3.8 and 3.9, only realistic solutions in which the velocities v_1 and v_2 at the coast are positive are plotted. However, in figure 10 all solutions corresponding to real roots of the pair of quadratics have been plotted.

The branch of solutions beginning at $h_1 = 0.5$, $\zeta = 1.0$ and extending to $\zeta = 0$ is realistic and has $(v_1,v_2) < 0$. It corresponds

to the case in which the streamlines turn south instead of north. The solution which begins at $h_1 \approx 0.4$, $\zeta = 1.0$ and goes to $\zeta = 0$ and $\zeta = 1.94$, is unrealistic $(h_1,h_2) < 0$. Between the bracket at $\zeta = 1.9$ and the point $h_1 = 0$, $\zeta = 1.94$, the solution has $h_1 > 0$, $h_2 < 0$, and $(v_1,v_2) > 0$. For the unrealistic solution extending from $\zeta = 1.45$ to $\zeta = 0$, and around to near $\zeta = 1.2$, v_1 has the opposite sign from v_2, and h_1 has the opposite sign from h_2.

All of (h_1,h_2,v_1,v_2) change sign as they pass through $\zeta = 0$. The solution passing through $h_1 = .5$, $\zeta = 1.0$ corresponds in the limit $\gamma \to \infty$ to taking the positive sign in 2.5.19, and the solution through $h_1 \approx -0.4$, $\zeta = 1.0$ corresponds to the negative sign. The two solutions together form a closed curve, and one might say that the other closed curve gives the effect of the second layer. The new realistic cross-sections added by this layer are, therefore, those between the brackets in the first quadrant.

The maximum at $\zeta = 1.463$ corresponds to the infinite slope at $\zeta = 2.0$ in the curve $h = \pm\sqrt{\zeta(2-\zeta)}$ for the one-layer, constant-potential-vorticity model. It will be seen in the next section that as the stratification, γ, increases in the two-layer model, the upper layer will become more like a one-layer model and the maximum will move toward $\zeta = 2.0$, $h_1 = 0$. The "lower branch" thus corresponds, as has been mentioned, to taking the negative sign in equation 2.5.19. Just as in the one-layer solution, if $h_1,\zeta = \infty$ at the maximum, the east-west velocity is infinite, and cross-stream geostrophy fails, thus invalidating the basic assumptions of the model.

Figure 11 gives an expanded view of the region of figure 10 near $\zeta = 1.463$. Figure 12 shows cross-sections of this solution at selected latitudes. Two of them are at the same latitude to emphasize the possibility of multiple cross-sections at the same latitude. The velocities are positive everywhere, and the velocities at the coast are noted on the figures.

In the upper left-hand corner of figure 28 the correct solution is plotted in more detail. The long dashed lines show the two layers in the interior, and the lines with computed data points show h_1 and h_2. At the left is an indication of the density structure. Because the absolute density differences have been scaled out of the problem, only the ratio of density differences, i.e., γ, is significant. Thus the function $\hat{\rho}(z)$ in figure 28 conveys in graphical form all the essential information about the density structure. It is defined by

$$\hat{\rho} = 1 \quad \text{for } z \text{ below } D_2 \ ,$$

$$\hat{\rho} = \frac{\gamma-1}{\gamma} \quad \text{for } z \text{ in } D_2 \ ,$$

$$\hat{\rho} = 0 \quad \text{for } z \text{ in } D_1 \ .$$

Therefore in the graph of this function in figure 28, the ratio of the sum of the two horizontal line segments $(\rho_3-\rho_1)$, to the lower line segment $(\rho_3-\rho_2)$, is γ. One may therefore think of the vertical lines at 0, $\frac{\gamma-1}{\gamma}$, and 1 as indicating the densities ρ_1, ρ_2 and ρ_3.

In figure 28 the sum of the thickness of the two layers at the coast remains very close to 1.0, its value at $\zeta = 1.0$. It is noteworthy that for correct cross-sections north of $\zeta = 1.45$ the maximum velocity in the lower layer occurs for $x > 0$. To see this note that the conservation of potential vorticity gives $v_{2,x} = 2h_2 - \zeta$. Since at $\zeta = 1.46$, $h_2 = 0.790$; $v_{2,x}(x=0) > 0$ and the maximum velocity is for $x > 0$.

It is natural to ask if there can be a transition between the multiple solutions at a given latitude. If so, it could be imagined that one solution would hold up to a particular latitude and that, north of that latitude, another which did not extend down to $\zeta = 1.0$ would take over. However, the transitions cannot occur between the cross-sections at the same latitude in figure 10, because it is well known that in hydraulic jumps energy is dissipated whereas the momentum flux integral and the mass flux are constant. For all of these cross-sections, on the other hand, the energy and mass flux are the same at a given latitude, which implies that the momentum flux integral cannot be.

3.4 Off-shore solutions

It is possible to find solutions in two layer models in which the upper layer has moved away from the coast. In this section they will be discussed only for constant potential vorticity solutions.

If the upper layer has moved away from the coast, then in the interval between it and the coast there are only the single layer equations, and the solution for D_2 in this interval is the same as for

the one layer model in chapter II, except that the thickness of the layer in the interior is multiplied by $\frac{1}{1+\delta}$. Taking this into consideration, the expression for D_2 in this interval is

$$D_2^L = a_1 e^{-\zeta^{\frac{1}{2}}(1+\delta)^{\frac{1}{2}}x} + a_2 e^{\zeta^{\frac{1}{2}}(1+\delta)^{\frac{1}{2}}x} + \frac{\zeta}{1+\delta} , \qquad (3.4.1)$$

where D_2^L stands for D_2 to the left of the two layer system.

If the argument leading to 3.3.21 is repeated, but including the one layer system to the west of the two layer system, it is found that the same result, 3.3.21, is obtained, so that if the upper layer departs from the coast, resulting in $h_1 = 0$, then h_2 is completely determined and is given by,

$$h_2 = \frac{\zeta(2-\zeta)}{(1+\delta)^2} (\gamma\delta^2 + 2\delta + 1) . \qquad (3.4.2)$$

From the Bernoulli integral, 3.3.15, the velocity v_2^o at $x = 0$

$$v_2^o = \pm \{2(1-h_2)\}^{\frac{1}{2}} \qquad (3.4.3)$$

The sign must be determined by the behavior of the entire solution as a function of ζ.

Equations 3.4.1, 3.4.2, and 3.4.3 give two conditions on a_1 and a_2 in 3.4.1, thus completely determining D_2^L. The conditions are

$$h_2 = a_1 + a_2 + \frac{\zeta}{1+\delta} , \qquad (3.4.4)$$

$$v_2^o = \zeta^{-\frac{1}{2}}(1+\delta)^{\frac{1}{2}}(-a_1 + a_2) ,$$

and the solutions are,

$$a_1 = \tfrac{1}{2}\left[h_2 - v_2^o \zeta^{\frac{1}{2}}(1+\delta)^{-\frac{1}{2}} - \zeta(1+\delta)^{-1}\right],$$

$$a_2 = \tfrac{1}{2}\left[h_2 + v_2^o \zeta^{\frac{1}{2}}(1+\delta)^{-\frac{1}{2}} - \zeta(1+\delta)^{-1}\right]. \qquad (3.4.5)$$

Thus D_2^L is a known function of x. The problem can now be solved in a manner similar to that of section 3.3. First consider equations 3.3.13. To use them for off-shore solutions, take a new coordinate system to change them to the form

$$D_1 = b_2\, n_1\, e^{-\alpha_1 \zeta^{\frac{1}{2}}(x-x_t)} + b_4\, n_2\, e^{-\alpha_2 \zeta^{\frac{1}{2}}(x-x_t)} + \frac{\delta\zeta}{1+\delta}$$

$$D_2 = b_2\, e^{-\alpha_1 \zeta^{\frac{1}{2}}(x-x_t)} + b_4\, e^{-\alpha_2 \zeta^{\frac{1}{2}}(x-x_t)} + \frac{\delta}{1+\delta}, \qquad (3.4.6)$$

where x_t is the value of $\underline{x}$ at which layer 1 begins. To determine b_2 and b_4, equations 3.3.23 are now used with $h_1 = 0$, and $D_2(x_t)$, a known function of x_t, replacing h_2.

$$D_2(x_t) = a_1\, e^{-(1+\delta)^{\frac{1}{2}}\zeta^{\frac{1}{2}}x_t} + a_2\, e^{(1+\zeta)^{\frac{1}{2}}\zeta^{\frac{1}{2}}x_t} + \frac{\zeta}{1+\delta} \qquad (3.4.7)$$

Then equations 3.3.16 are used to find v_1 and v_2. Thus the layer thicknesses and the velocities are completely determined as functions of x_t. The functions may be substituted in

$$\tfrac{1}{2} v_1^2 + D_2 = \frac{\gamma\delta+1}{\delta+1}, \qquad (3.4.8)$$

the $\psi_1 = 0$ Bernoulli integral. The result is a transcendental equation for x_t, which can be solved by a trial-and-error process.

Figure 13 shows the location of x_t as a function of x, for the parameters $\delta = 1.0$, $\gamma = 2.0$, the same parameters as were discussed in section 3.3. An off-shore cross section exists between $\zeta = 1.4475 \pm .0005$, and $1.4705 \pm .001$, with a pair of cross-sections between the lower limit and $\zeta = 1.4565$, the latitude at which h_1 vanishes in figure 10.

In this case then, the off-shore cross-sections are not physically realistic because they do not connect to a correct solution. Another reason why these cross sections are not realistic is that when x_t is plotted against ζ as in figure 13, the resulting line gives the plan view of the trace on the surface of the boundary between the upper and middle layer; and the trace moves south instead of north, moving into latitudes where there is already some other cross-section.

For no solutions having $\delta = 1.0$ are there any off-shore solutions which connect in a physically reasonable way to $\zeta = 1.0$, because there is no physically reasonable sequence of cross-sections as a function of ζ by which h_1 can go from $h_1 = h_1(1) = 0.5$ to $h_1 = 0$. This is because, for all values of γ, noting the discussion at the end of section 3.3, there are figures similar to figures 10 and 11 for the depth of the upper layer at the coast as a function of ζ.

3.5 Analytical results for small δ

In this section analytical results are obtained for cross sections in which δ is small. The terms obtained in the expansions converge only if the quantity $\gamma\delta^2$ is small, thus providing an expansion for γ also. It turns out that the $h_1 = 0$ cross sections, the only ones for

which explicitly analytical expression can be obtained for the layer thicknesses and velocities, correspond to the solution on the lower "branch" in figure 10, so that they do not represent correct solutions. However, the results will tell us that constant potential vorticity solutions with γ of order unity and small δ cannot extend very far north.

For analysis it is convenient to introduce the parameter θ representing the ratio of the density "gradients" of the upper and lower layers.

$$\theta = \frac{\frac{\rho_2-\rho_1}{\delta/1+\delta}}{\frac{\rho_3-\rho_2}{1/1+\delta}} = \frac{1}{\delta}\,\frac{\rho_2-\rho_1}{\rho_3-\rho_2} \tag{3.5.1}$$

This implies

$$\gamma = 1 + \theta\delta \,. \tag{3.5.2}$$

An expansion of 3.3.10 gives, for small δ

$$\begin{aligned} \alpha_1 &\approx \theta^{-\frac{1}{2}}\delta^{-1}(1+\delta)^{\frac{1}{2}}\left\{1 + \delta/2 - \delta^2/8 + \left(\frac{\theta}{2} + \frac{1}{16}\right)\delta^3 + \cdots\right\} \\ \alpha_2 &\approx (1+\delta)^{\frac{1}{2}}\left\{1 - \delta/2 + 3/8\ \delta^2 - \frac{1}{16}\,(8\theta + 5)\,\delta^3 + \cdots\right\} . \end{aligned} \tag{3.5.3}$$

If 3.3.23 is combined with 3.3.16 with $h_1 = 0$, there results

$$\begin{aligned} v_1 = -\zeta^{-\frac{1}{2}}\Bigg[&\alpha_1(\gamma n_1+1)\left\{-n_2\,h_2 - \frac{\zeta}{1+\delta}\,(\delta-n_2)\right\}\frac{1}{n_1-n_2} \\ &+ \alpha_2\,(\gamma n_2+1)\left\{-n_1\,h_2 - \frac{\zeta}{1+\delta}\,(\delta-n_1)\right\}\frac{1}{n_2-n_1}\Bigg], \end{aligned} \tag{3.5.4}$$

$$v_2 = -\zeta^{\frac{1}{2}} \left[\alpha_1 (n_1+1) \left\{ -n_2 h_2 - \frac{\zeta}{1+\delta} (\delta - n_2) \right\} \frac{1}{n_1 - n_2} \right.$$

$$\left. + \alpha_2 (n_2+1) \left\{ -n_1 h_2 - \frac{\zeta}{1+\delta} (\delta - n_1) \right\} \frac{1}{n_2 - n_1} \right] . \qquad (3.5.5)$$

If expansions for the n's and α's are entered in the above expressions, and the results are inserted in 3.3.15 with $h_1 = 0$, then, after lengthy calculations, the final result is a pair of algebraic equations with terms in $h_2\zeta$, h_2^2, ζ, and ζ^2; and with power series in θ and δ. If the term in ζ is eliminated between these two equations then the quadratic formula produces the result

$$\frac{h_2}{\zeta} = (1+\delta)^{-1} \left\{ 1 + (1 - \tfrac{1}{2}\theta^{\frac{1}{2}}) \delta - (\tfrac{1}{2}\theta^{\frac{1}{2}} + \tfrac{1}{4}\theta) \delta^2 + \cdots \right\} . \qquad (3.5.6)$$

When this expression is substituted into one of the quadratic equations to eliminate h_2, the resulting equation in ζ yields,

$$\zeta = 1 + \frac{1}{2} \theta^{\frac{1}{2}} \delta + \frac{3}{8} \theta \delta^2 + \cdots , \qquad (3.5.7)$$

and thus,

$$h_2 = 1 - \frac{1}{8} \theta \delta^2 + \cdots . \qquad (3.5.8)$$

Expressions for the velocities using only the largest terms are

$$v_1 \approx \delta \theta^{\frac{1}{2}} \left[e^{-\theta^{-\frac{1}{2}} \delta^{-1} x} + \tfrac{1}{2} e^{-x} \right] ,$$

$$v_2 \approx \tfrac{1}{2} \delta \theta^{\frac{1}{2}} e^{-x} . \qquad (3.5.9)$$

The upper diagram in figure 14 is a plot of h_1 as a function of ζ for the parameters $\Theta = 1.0$, $\delta = 0.1$. It was obtained by calculations using the methods of 3.3. This diagram shows that the cross section, which has been obtained analytically by putting $h_1 = 0$, lies on the lower branch and is thus not part of a correct solution.

The accuracy of the expansion is quite good. Equation 3.5.7 gives $\zeta = 1.05375$ for the latitude at which $h_1 = 0$, whereas the exact solution gives $1.0527 \pm .0002$. The expansions for the other variables give comparable accuracy. From figure 14 it can be seen that the "nose" extends north to a value of $(\zeta-1)$ of the same order as that at which $h_1 = 0$. Therefore in the present theory, thin upper layers with finite Θ are restricted to low latitudes. This result is quite general and will be seen to apply to non-constant potential vorticity cases also.

Even though expressions like 3.5.3 do not appear to converge for small Θ, presumably the higher terms do give convergence because 3.5.7 and 3.5.8 give good agreement with numerical calculations for small Θ, in addition to small δ. Thus 3.5.7 and 3.5.8 are valid expansions for small δ and Θ.

The solutions fail at the points analogous to the "nose" in figure 14 because cross-stream geostrophy breaks down. Perhaps a thin upper layer can be carried smoothly north by purely inertial, a-geostrophic dynamics. However, if not, the suggestion is strong that no purely inertial, continuously stratified model of the Gulf Stream can be constructed.

Off-shore solutions exist for small δ, but they are qualitatively the same as figure 13.

The lower diagram in figure 14 shows the sequence of cross-sections for $\delta = 0.1$, which corresponds to the incorrect solution between $\zeta = 1.4$ and 1.9 in figure 10, in 3.4. As $\delta \to 0$ it goes to the one-layer baroclinic model of chapter II. To see this, imagine that the one-moving-layer baroclinic model were separated into two layers of equal density, of constant potential vorticity, and of thickness ratio δ. Then at the coast the ratio $\frac{h_1}{h_2}$ would always be δ, and therefore $h_1 = \frac{\delta}{1+\delta} \sqrt{\zeta(2-\zeta)}$. This is close to the behavior of the incorrect solution in figure 14b. The results of the calculations for h_2 are close to $\frac{1}{1+\delta} \sqrt{\zeta(2-\zeta)}$. The only difficulty is that the incorrect solution is not close to the proper value at $\zeta = 1.0$. As $\delta \to 0$, $h_1(1)$ does not go to $\frac{\delta}{1+\delta}$ even though for $\zeta = 1 + \epsilon$, for any small ϵ, there is convergence. The convergence is non-uniform at $\zeta = 1.0$. A limit which behaves in this way is called an <u>incorrect limit</u>. If the convergence is non-uniform at some latitude other than $\zeta = 1.0$, the limit is also called an <u>incorrect limit</u>.

The incorrect solution in figure 14 turns toward larger ζ near $\zeta = 1.1$, but eventually turns again and crosses $\zeta = 1.0$ at $h_1 = 2.875$, where $h_2 = -3.292$. So as $\delta \to 0$, h_1 at $\zeta = 1.0$ appears to go to a large value. In fact, for $\theta = 1.0$, $\delta = 0.01$, $\gamma = 1.01$ there is $h_1 = 3.85$, $h_2 = -4.77$, at $\zeta = 1.0$; the value of h_1 at $\zeta = 1.0$ appears to diverge. It seems clear that there is non-uniform convergence near $\zeta = 1.0$. The sharp turn near $\zeta = 1.1$ corresponds to the slight inflection for the incorrect solution in figure 10.

The behavior of the solution for constant θ and small δ obtained here is one of the most important results of the present work. Because θ represents the ratio of the density gradients, the fact that the correct solution for small δ cannot extend far north indicates that no solutions can exist for continuously stratified models with finite density gradients. It might be that a thin upper layer cannot correspond to a thin surface portion of a continuously stratified model; or that a continuously stratified model will "join" the correct and incorrect solutions. However, such conjectures can only be resolved by an explicit treatment of continuously stratified models. Until this is done, the existence of continuously stratified solutions is thrown into question.

The limit $\theta \to 0$ is also incorrect, as can be seen from figure 20 which is discussed in section 3.8. It will be seen that it has the same type of behavior at $\zeta = 1.0$ as the limit $\delta \to 0$. This is reasonable because in both cases $\gamma \to 1.0$.

3.6 Analytical results for large δ

For large δ an expansion of 3.3.10 gives,

$$\alpha_1 \approx (1+\delta)^{\frac{1}{2}} \left\{1 + \tfrac{1}{2}\theta^{-1}\delta^{-1} - \frac{1}{8}\theta^{-2}\delta^{-2} + (\tfrac{1}{2}\theta^{-2} + \frac{1}{16}\theta^{-3})\,\delta^{-3} + (-\frac{3}{4}\theta^{-3} - \frac{5}{128}\theta^{-4})\,\delta^{-4} + (\tfrac{1}{2}\theta^{-3} + \frac{11}{16}\theta^{-4} + \frac{7}{256}\theta^{-5})\,\delta^{-5} + \cdots\right\},$$

$$\alpha_2 \approx \theta^{\frac{1}{2}}\delta^{-1}(1+\delta)^{\frac{1}{2}} \left\{1 - \tfrac{1}{2}\theta^{-1}\delta^{-1} + \frac{3}{8}\theta^{-2}\delta^{-2} - (\tfrac{1}{2}\theta^{-2} + \frac{5}{16}\theta^{-3})\delta^{-3} + \cdots\right\}. \qquad (3.6.1)$$

By obtaining two quadratics in h_1^2, $h_1\,\zeta$, ζ^2 and ζ and eliminating ζ as in section 3.5, there results

$$\zeta = 2\left\{1 - \theta^{-1}\delta^{-2} - 2\theta^{-3/2}\delta^{-5/2} + (2\theta^{-3/2}+\theta^{-2})\delta^{-3} + (6\theta^{-2}+\theta^{-5/2})\delta^{-7/2}+\cdots\right\}, \tag{3.6.2}$$

and

$$h_2 = \frac{2\delta^{\frac{1}{2}}}{1+\delta}\left\{1 + \theta^{-\frac{1}{2}}\delta^{-\frac{1}{2}} + (\theta^{-\frac{1}{2}} + \tfrac{1}{2}\,\theta^{-1})\,\delta^{-1} - 2\,\theta^{-1}\,\delta^{-3/2} + \cdots\right\}. \tag{3.6.3}$$

Taking only the largest terms, the expansions for the velocities are,

$$v_1 = (2\theta)^{\frac{1}{2}}\left[e^{-2^{\frac{1}{2}}\theta^{-\frac{1}{2}}\delta^{-\frac{1}{2}}x} + \theta^{-3/2}\delta^{-5/2}e^{-2^{\frac{1}{2}}\delta^{+\frac{1}{2}}x}\right], \tag{3.6.4}$$

$$v_2 = 2^{\frac{1}{2}}\delta^{-\frac{1}{2}}\left[\theta^{-\frac{1}{2}}e^{-2^{\frac{1}{2}}\theta^{-\frac{1}{2}}\delta^{-\frac{1}{2}}x} - (\theta^{-\frac{1}{2}} + \delta^{\frac{1}{2}}-1)e^{-2^{\frac{1}{2}}\delta^{+\frac{1}{2}}x}\right] \tag{3.6.5}$$

There are two cases of interest here,

a. $\theta \sim 1$, $\delta \gg 1$,

b. $\theta \gg 1$, $\delta < 1$.

In both cases all the expansions converge. However in case a, 3.6.5 shows an inshore countercurrent for this limit. As has been mentioned before in connection with the off-shore solutions, there is no possible source for such countercurrent water since its ψ value is less than zero.

In case b there is no countercurrent in the lower layer. The fact that $\delta < 1.0$ and $\theta \gg 1$ for this good behavior is suggestive of a rule that a physical stream, to flow smoothly, must have a large

difference in density gradients and that the large density gradients must be concentrated near the surface, as is observed in the Gulf Stream.

Figure 15 shows the exact solution for the case $\Theta = 1.0$, $\delta = 10.0$, case a. The solution consists entirely of the upper "branch." However, the unrealistic aspect of the solution consists of an inshore countercurrent in the lower layer which sets in between $\zeta = 1.3$ and 1.4. Once again the expansions give good agreement with the exact solution for the latitude at which $h_1 = 0$. The exact solution gives $1.9734 \pm .0001$, and the expansion, 1.978. An off-shore solution extends tc the north from where $h_1 = 0$ to $\delta = 1.982$ where $x_{t,\zeta}$ appears to be infinite at $x_t = 1.0 \pm .1$. The offshore solution also has the countercurrent along the coast in the lower layer.

Figure 16 shows the exact solution for the parameters $\delta = 1.0$, $\Theta = 16.0$. This is not strictly case b because $\delta \not< 1$, however; it has the same behavior as case b because of smaller terms not written down in 3.6.15. This solution has no countercurrent. The latitude where h_1 becomes zero is $\zeta = 1.8970 \pm .0001$, while the expansion gives 1.8954. Since the cross-section for $h_1 = 0$ is on the lower branch, there can be no physically reasonable offshore solutions.

3.7 Numerical techniques for baroclinic models

Despite considerable unpublished work by several investigators, no analytical solution of the case of more than one layer of non-constant potential vorticity has been carried out. Even perturbations on the case of constant potential vorticity seem intractable. Thus, if the qualitative features associated with different interiors are to

be discussed, and if theoretical results are to be compared in any detail with observation, then numerical solutions are necessary.

For numerical integration, the equations 3.3.3 and 3.3.4 are reduced to four first-order differential equations by first defining

$$\begin{aligned} D_1 &= Y_1 , & D_2 &= Y_3 , \\ D_{1,x} &= Y_2 , & D_{2,x} &= Y_4 . \end{aligned} \tag{3.7.1}$$

The stream-functions constitute two other variables in the set of numerical equations,

$$\psi_1 = Y_5 , \qquad \psi_2 = Y_6 . \tag{3.7.2}$$

The geostrophic equations 3.2.2 and 3.2.5 may be expressed in terms of the Y's.

$$\begin{aligned} v_1 &= \frac{1}{\zeta} [\gamma Y_2 + Y_4] \\ v_2 &= \frac{1}{\zeta} [Y_2 + Y_4] \end{aligned} \tag{3.7.3}$$

Equations 3.3.3 and 3.3.4 may be separated as

$$\begin{aligned} D_{1,xx} &= \frac{\zeta}{\gamma-1} [F_1(\psi_1)D_1 - F_2(\psi_2)D_2] \\ D_{2,xx} &= \frac{\zeta}{\gamma-1} [\gamma F_2(\psi_2)D_2 - F_1(\psi_1)D_1] - \zeta^2 \end{aligned} \tag{3.7.4}$$

So an appropriate set of six first-order differential equations is,

$$Y_{1,x} = Y_2 , \tag{3.7.5}$$

$$Y_{2,x} = \frac{\zeta}{\gamma-1} [F_1(Y_5) \cdot Y_1 - F_2(Y_6) \cdot Y_3] , \tag{3.7.6}$$

$$Y_{3,x} = Y_4 \ , \tag{3.7.7}$$

$$Y_{4,x} = \frac{\zeta}{\gamma-1} \left[\gamma F_2(Y_6) \cdot Y_3 - F_1(Y_5) \cdot Y_1\right] - \zeta^2 \ , \tag{3.7.8}$$

$$Y_{5,x} = \frac{1}{\zeta} Y_1 \left[\gamma Y_2 + Y_4\right] = D_1 v_1 \ , \tag{3.7.9}$$

$$Y_{6,x} = \frac{1}{\zeta} Y_3 \left[Y_2 + Y_4\right] = D_2 v_2 \ . \tag{3.7.10}$$

For the initial conditions on these equations, a trial guess is made for h_1. Then an equation analogous to 3.3.22 gives h_2. The two Bernoulli conditions will then give v_1 and v_2, and 3.7.3 can be used to derive Y_2 and Y_4. The stream functions Y_5 and Y_6 are, of course, zero at the coast. Equations 3.2.9 give the structure of the layers in the interior, and the equation for obtaining h_2 in terms of the guess for h_1 is derived in the same way as 3.3.22, and is,

$$h_2 = -h_1 + \{h_1^2 - K_1\}^{\frac{1}{2}} \ , \tag{3.7.11}$$

where

$$\begin{aligned} K_1 = {} & 2\zeta \ (\psi_1(\infty,\zeta) + \psi_2(\infty,\zeta)) \\ & - \{ -\gamma h_1^2 + \gamma(a+b\zeta)^2 + 2(a+b\zeta)(c + (1.0-a-b-c)\ \zeta) \\ & + (c + (1.0-a-b-c)\ \zeta)^2 \} , \end{aligned} \tag{3.7.12}$$

and

$$\psi_1(\infty,\zeta) = (\gamma b + (1-a-b-c)) \{a \log \zeta + b(\zeta-1) \} \tag{3.7.13}$$

$$\psi_2(\infty,\zeta) = (1-a-c) \{c \log \zeta + (1-a-b-c)(\zeta-1) \} \tag{3.7.14}$$

Once the initial conditions are specified, the equations 3.7.5-3.7.10 may be integrated, provided only that the expressions F_1 and F_2 are given. For any value of $\underline{x}$, F_1 may be evaluated by equating $\psi_1(\infty,\zeta)$ and Y_5. The value of ζ that satisfies this equation is the latitude of origin of the water at the value of $\underline{x}$ under consideration, and the potential vorticity of this water may thus be calculated. Writing this process out explicitly, first the value of ζ that satisfies

$$Y_5 - \{\gamma b + (1-a-b-c)\}\{a \log \zeta + b(\zeta-1)\} = 0 \qquad (3.7.15)$$

must be found. This is done by the method of false position. (See Todd (26).) In the numerical solution this method is used until an accuracy is attained an order of magnitude greater than that maintained in the integration of the differential equations. Then, if the value for ζ is found to be, say, ζ_c then F_1 is given by

$$F_1 = \frac{\zeta_c}{a+b\zeta_c} \quad .$$

A similar procedure applies for finding F_2.

The actual integrations are performed by a combination of Runge-Kutta-Gill and Adams-Moulton-predictor-corrector formulas (see Todd (26)) which are used in a program to provide the option of variable spacing while maintaining a constant level of accuracy. When the solution changes so rapidly with $\underline{x}$ that the interval spacing must be reduced to less than 10^{-3} times a value of Δx set by the programmer, in order to maintain a stated accuracy, the program gives an error return and stops. This generally means that one has tried to integrate

through a singularity, although in this work it frequently means that growing exponential terms have become large. The integration scheme is described in detail in Appendix II.

As was shown above, all of the initial conditions are functions of the single variable h_1. Thus, to find the solution, integrations may be performed for a series of values of h_1 until that value is found for which the asymptotic values of D_1, D_2, ψ_1, and ψ_2 approach the values given by 3.2.9, 3.7.13, and 3.7.14; and the velocities go to zero.

For the offshore solutions, $h_1 = 0$; and as has been shown for the constant-potential-vorticity case, this completely determines h_2. There are only the one-layer equations between the coast and the two-layer system, and the solution to these equations is completely determined by h_2. To find the offshore solution, the one-layer equations are integrated out to some selected value of $\underline{x}$, say x_c, and then the two-layer system is introduced. All the boundary conditions at this point are easy to determine, and the two-layer system is integrated outward in $\underline{x}$. Successive values of x_c are chosen until that value is found which gives the proper asymptotic behavior for the two-layer system.

The greatest difficulty with this technique, both for solutions offshore and at the coast, is that incorrect values of h_1 or x_c imply non-zero coefficients of growing exponentials, which were discarded from equations 3.3.11 in the analytical solutions for constant potential vorticity. As an example, for $\delta = 1.0$, $\gamma = 2.0$, the largest

exponent for D_1, D_2, v_1, and v_2 is $(1+\delta)^{\frac{1}{2}}\zeta^{\frac{1}{2}}\alpha_1 x = 2.80\ \zeta^{\frac{1}{2}}\underline{x}$, and since the stream-functions are products of these variables, the largest exponential in their expressions is $5.60\ \zeta^{\frac{1}{2}}\underline{x}$. As a result h_1 must be accurate to about 10^{-3} for a solution accurate to 10% at $x = 1.0$, and to about 10^{-6} for $x = 2.0$.

However, it is fairly simple to iterate toward the proper value of h_1, because as h_1 passes through its proper value, the coefficients of all the growing exponentials change sign, so that by examining the behavior of the solutions at large values of $\underline{x}$ it is possible to bracket the solution. The program is constructed to iterate to as many decimals as are desired for h_1 once the solution is bracketed.

If the routine is required to keep an accuracy of 10^{-5} in each interval of $\Delta x = .1$, then there is no change in the fifth decimal place when the accuracy is changed to 10^{-7}. This shows that the numerical error control is conservative. It appears that when the routine is required to keep an accuracy of 10^{-5} it manages to maintain close to 10^{-6}. These results show that the integration does not introduce significant random coefficients of the growing exponentials which would render the solutions erratic. A typical integration to $x = 2.0$ requires one second on the 7090, and four-figure accuracy for h_1 requires about six iterations.

Figure 17 shows the convergence of the machine solutions for $\delta = 1.0$, $\gamma = 2.0$, $\zeta = 1.4565$, $h_1 = .2100$ which is, of course, a cross section which was discussed in previous sections of this chapter by analytical methods.

3.8 Behavior of baroclinic models

The numerical technique of the previous section will give solutions for various values of a, b, c, and γ. In this section the chief purpose will be to reveal the behavior as a function of these parameters; comparison with observation is deferred to the next chapter.

The discussion centers on figures 18-23. They show h_1 as a function of ζ for those realistic solutions which have $(v_1, v_2) > 0$ for $x = 0$. The plots are only for $\zeta > 1.0$. This restricts the figures to the first quadrant of figure 10.

In the upper left-hand corner of each figure are diagrams of two north-south sections through the interior. The arrow between them indicates a particular sequence of boundary conditions which is treated in the main part of the figure. For example in figure 18 the stratification, γ, is held constant while the layers change their rate of thickness increase with latitude. The diagrams are at opposite limits of the sequence, and the data beneath them give the parameters of the limits. The data in the upper right part of the figure give the parameters for the boundary conditions which are actually computed and plotted in the figure, and identify the plotted curves. Data are listed only for those parameters which vary as the sequence is traversed. The asterisks by some of the listings indicate that the correct portion of the solution for those parameters is plotted in more detail in figure 28.

The computations are indicated either by circled points or by thin horizontal or vertical lines. A dot means that the value of h_1 is

known with a limit of accuracy that would plot as a dot of the size shown. A line indicates the limits between which the solution must lie. If the line is vertical, there is uncertainty in h_1, if horizontal, in ζ. A heavy bar, as in figure 24, means that there are no realistic solutions for values of ζ beyond that bar, although there may be unrealistic ones (i.e., solutions outside the range $(h_1, h_2, \zeta > 0)$.

If h_2 becomes negative, then the end of the realistic solution is indicated by a bracket, as was done in figure 10. If the solution is unknown beyond some point, the line simply stops. If there is some evidence about the line, for example, a knowledge of where it is not, the conjectured position is indicated by short dashes.

The figures will now be discussed individually.

Figure 18.--This figure shows that the correct solution will extend farther north as the layers become more nearly horizontal. It is plausible that this should happen because it can be shown by the equation analogous to 3.3.21 that a single layer which increases more slowly with latitude than a constant-potential-vorticity layer can have an inertial boundary layer farther north than $\delta = 2.0$.

Figure 19.--Here, the sequence explores what happens as the interface between the lower and bottom layers becomes horizontal. Since $v_2 = \frac{1}{\zeta} \frac{\partial}{\partial x} (D_1+D_2)$ by the geostrophic equation (3.2.5), this means that the lower layer becomes a level of no motion. Since the upper layer in this sequence is held at constant potential vorticity, then the solution in the limit should be the solution of chapter II of

a one-moving-layer baroclinic model of constant potential vorticity. This limit is shown by the crosses in figure 19.

This one-moving-layer model is certainly the limit if $u_2 = v_2 \equiv 0$. But as the limit is approached, as $(u_2, v_2) \to 0$, the situation is quite different from $u_2 - v_2 \equiv 0$, because water continues to move, however slowly, from the interior through the boundary layer, and in the theoretical formulation used it must preserve the integrals of the motion. One might well suspect that this is impossible as the limit is approached because of the following argument. Along a streamline both $\frac{1}{2}v_2^2 + D_1 + D_2$ and $\frac{v_{2,x}+\zeta}{D_2}$ must remain constant. If the velocities are small then both $D_1 + D_2$ and $\frac{\zeta}{D_2}$ must simultaneously remain constant along each lower layer streamline. One might well imagine that this would prove impossible.

In figure 19, the question marks on solutions 2 and 3 indicate that it was not possible to determine certainly that there was, or was not, a solution for values near the points plotted. (The numerical computations do however show that there is no solution anywhere else for c near the limiting value of 1.0.)

It is impossible to determine if there is a solution because the numerical criteria for a solution become equivocal near these points. For values of h_1 on either side of the line for $c = .9$ at large x, only five of the six variables (D_1, D_2, v_1, v_2, ψ_1, ψ_2) changed sign. Furthermore, although increasingly accurate values for h_1 give solutions that extend to larger values of x before diverging, the convergence is very slow. The value of x attained was proportional to

the logarithm of the precision of h_1. Because of the slow convergence, the maximum seven-figure accuracy gave, for the parameters $\zeta = 1.5$, $c = 0.9$, a solution only to $x = 1.5$, where either $v_{2,x}$ became large or D_1 became negative, ending the computation. (For a typical set of other parameters the corresponding value of x attained would be 5.0 or 6.0.) The same behavior, with slower convergence, and with only three variables changing sign, is found for $c = .99$. Because the convergence is so slow, and because some of the variables do not change sign, I do not believe that there is any solution for 2 or 3 in figure 19, for any value of ζ.

However, since the numerical results show clearly that the plotted curves define the only trajectories that could conceivably be realistic solutions, it is important to show that, in the limit as $c \to 1.0$, there is no solution here either. This proof below, draws on the qualitative ideas discussed three paragraphs ago.

First note that the numerical results for $c = .9, .99$, establish that there is no solution anywhere except possibly for $h_1 \to \frac{1}{2}\{\zeta(2-\zeta)\}^{\frac{1}{2}}$ and $h_1 + h_2 \to 1$, the trajectory marked by the crosses. From the Bernoulli integral for the lower layer in (3.2.8) this means that v_2 $(x=0)$ may be as small as desired. The potential vorticity integral, on the other hand, shows that $v_{2,x}(0)$, and, by differentiation and use of the geostrophic equations, all higher derivatives, are of order unity. For example,

$$v_{2,xx} = \frac{\partial}{\partial x}(D_2F_2-\zeta) = \frac{\zeta}{1-\gamma}(v_1-\gamma v_2)F_2 + D_2F_2^1D_2v_2 = O(1) .$$

As $c \to 1.0$, a reasonable solution would have v_2 a differentiable function of x, and it could, therefore, be expanded in a Taylor series around $x = 0$. So in some small, finite interval, ϵ_o, beyond $x = 0$, there must be $v_{2,x} = O(1)$, and the lower layer transport in this interval must be at least $O(\epsilon_o^2)$, since $D_2 = O(1)$. But by letting $c \to 1.0$, the transport toward the coast from the interior may be made arbitrarily small. Thus the finite transport close to the coast can only be a recirculation, which constitutes a physically unrealistic solution, even should it exist. Thus there do not exist realistic cross-sections at any latitude, in the limit as the lower interface becomes horizontal. (In the last two sentences "realistic" was used in its conventional sense.) This is the definition of an impossible limit, as used here.

The very slow convergence, which I regard as a sign of the non-existence of a solution, sets in for a value of $c > 0.4$ and probably $c < 0.6$. It should be emphasized that the non-existence of solutions in the limit rests critically on the numerical result that the only possible solution is for $h_1 \to \frac{1}{2}\{\zeta(2-\zeta)\}^{\frac{1}{2}}$, $h_1+h_2 \to 1$.

Figure 20.--This shows how, as γ is increased, the correct solution moves toward the solution for a one-moving-layer model. This same result was obtained by the analytic methods of section 3.3. As γ goes to 1.0 ($\theta \to 0$), the incorrect solution goes to the one-moving-layer solution, an incorrect limit.

Beyond the brackets, the solution crosses $\zeta = 1.0$ for $h_1 = 2.033$, $h_2 = -1.251$, an unrealistic solution. From figure 10, $\gamma = 2.0$, it crosses for $h_1 = 1.04$. Evidently the value of h_1 at $\zeta = 1.0$ diverges

as $\gamma \rightarrow 1.0$; there is non-uniform convergence at $\zeta = 1.0$.

Figure 21.--This covers the types of interiors from which an off-shore inertial countercurrent might have been expected. However, in none of the solutions, correct or incorrect, is any countercurrent found. Solutions of this type will be discussed in detail in the next chapter where comparisons with observation are made.

As γ is increased, the correct solution penetrates farther north, but γ cannot increase indefinitely for a fixed negative value of b because by 3.2.9 and 3.2.3, $\gamma b + (1-a-b-c)$ must be greater than 0 for a westward flux in the upper layer. As the limit is approached, the upper layer becomes a level of no motion. So, as in a previous case (figure 19), it would be remarkable if there were a solution. In fact, there is no realistic, incorrect solution for $\gamma = 2.6$, and for $\gamma = 4.5$ there is no solution anywhere. Therefore $\gamma = 5$ is an impossible limit.

As γ goes toward 1.0, the correct solution disappears increasingly close to $\zeta = 1.0$, and the incorrect solution converges non-uniformly to the solution for a single layer of thickness equal to the sum of the two layers, this is an incorrect limit. In figure 21, the cases plotted have been picked so that this limiting solution for the two layers together is of constant potential vorticity, and the limiting solution is shown by the crosses.

It is reasonable that the upper layer should increase in thickness along the coast, because the sequence of solutions is tending, as $\gamma \rightarrow 5$, to the limit of an upper level of no motion. Now if the upper

and bottom layers are levels of no motion, and the middle layer is of constant potential vorticity, the solution can be calculated analytically, just as was done in chapter II. In the result, h_1 does increase along the coast. Since the solutions in this sequence are tending to this limit, shown by x's in figure 21, it is not surprising that h_1 increases for them also.

North of $h_2 = 0$, as at $\zeta = 1.45$ in figure 21, one might expect that the lower layer would move away from the coast beneath the upper layer. However, these would be such physically unreasonable cross sections that they have not been computed.

Figures 22 and 23.--These show the changes as an upper layer thickness passes from an increase to a decrease with latitude in the interior. In all of these cases the sum of the two layers is held at constant potential vorticity.

As the thickness of the upper layer in the interior increases less rapidly with latitude, its profile along the coast changes from a decrease as a function of latitude, to an increase. For no value of b can the solution extend much beyond $\zeta = 1.5$.

Summary.--If in the interior, both layers increase slowly with latitude, the inertial boundary layer extends far north. Small values of γ keep the correct solutions far south, as do large negative or positive derivatives of the layers with latitude. To increase the northward extension, then, a rule of thumb is to have strong stratification and to minimize variations of the layer thicknesses with latitude in the interior.

3.9 Equations for barotropic models

In this section the elevation of the free surface will appear explicitly in the calculations. In the interior it will be taken as a linear function of ζ.

$$\eta' = \eta_i \zeta \tag{3.9.1}$$

The characteristic thickness of the layers will be taken as D_o, the depth of the ocean, neglecting the elevation of the free surface. And the characteristic size of the variation in elevation of the free surface is η_o as in 2.4.6. Then if

$$\gamma = \frac{\sqrt{g\eta_o}}{2\Omega \sin\theta_o} , \tag{3.9.2}$$

then the characteristic sizes of the velocities and horizontal dimensions are, as in 2.4.6,

$$\begin{aligned} x' &\sim \lambda , & u' &\sim \frac{\lambda}{R}\sqrt{g\eta_o} , \\ y' &\sim R , & v' &\sim \sqrt{g\eta_o} . \end{aligned} \tag{3.9.3}$$

The non-dimensionalized equations of motion take the form

$$-\zeta v_1 + \eta_{,x} = 0 , \tag{3.9.4}$$

$$u_1 v_{1,x} + v_1 v_{1,y} + \zeta u_1 + \eta_{,y} = 0 , \tag{3.9.5}$$

$$(D_1 u_1)_{,x} + (D_1 v_1)_{,y} = 0 , \tag{3.9.6}$$

$$-\zeta v_2 + \eta_{,x} - eD_{1,x} = 0 , \tag{3.9.7}$$

$$u_2 v_{2,x} + v_2 v_{2,y} + \zeta u_2 + \eta_{,y} - eD_{1,y} = 0 \ , \qquad (3.9.8)$$

$$(D_2 u_2)_{,x} + (D_2 v_2)_{,y} = 0 \ , \qquad (3.9.9)$$

$$D_1 + D_2 = 1 \ . \qquad (3.9.10)$$

Equation 3.9.10 gives the connection between D_1 and D_2, the sum of whose thicknesses has been normalized to unity. The parameter $\underline{e} = \frac{\rho_2 - \rho_1}{\rho_2} D_o/\eta_o$ measures the relative effect of the density stratification versus the free surface on the velocities. In these equations, the approximation $\frac{\rho_2 - \rho_1}{\rho_2} \ll 1$ and $\eta_o \ll D_o$ have been used. The density in the upper layer is ρ_1 and in the lower layer is ρ_2.

The integrals of motion are,

$$\frac{v_{1,x} + \zeta}{D_1} = F_1(\psi_1) \quad , \quad \tfrac{1}{2} v_1^2 + \eta = G_1(\psi_1) \qquad (3.9.11)$$

$$\frac{v_{2,x} + \zeta}{D_2} = F_2(\psi_2) \quad , \quad \tfrac{1}{2} v_2^2 + \eta - eD_1 = G_2(\psi_2) \ .$$

In the interior the expression for η is $\eta = \frac{\eta_i}{\eta_o} \zeta$. The coefficient η_i/η_o may be normalized to unity. This does not restrict the choice of physically different boundary conditions. This can be verified by noting that the expressions for η and D_1 in the interior are taken to be

$$\eta(\infty, \zeta) = \zeta \ , \quad D_1(\infty, \zeta) = a + b\zeta \ . \qquad (3.9.12)$$

With 3.9.5 and 3.9.8, both with the non-linear terms discarded, this implies that

$$\frac{u_1(\infty,\zeta)}{u_2(\infty,\zeta)} = \frac{1}{1-eb} \ . \qquad (3.9.13)$$

So the physical ratios of velocities and layer thicknesses may independently assume any values by means of the parameters e, a, and b. Other normalizations are possible, but this one seems most convenient.

Using the potential vorticity integrals 3.9.11, and the geostrophic relations, the equations analogous to 3.3.3 and 3.3.4 are,

$$\eta_{,xx} - \zeta D_1 F_1(\psi_1) = - \zeta^2 \ , \qquad (3.9.14)$$

$$\eta_{,xx} - eD_{1,xx} - \zeta(1-D_1)F_2(\psi_2) = - \zeta^2 \ . \qquad (3.9.15)$$

These may be changed, by addition and subtraction, to the following equations,

$$\eta_{,xx} - \zeta D_1 F_1(\psi_1) = - \zeta^2 \ , \qquad (3.9.16)$$

$$eD_{1,xx} + \zeta\{F_2(\psi_2) - D_1[F_1(\psi_1) + F_2(\psi_2)]\} = 0 \ . \qquad (3.9.17)$$

If

$$\begin{aligned} \eta &= Y_1 \ , \quad & D_1 &= Y_3 \ , \\ \eta_{,x} &= Y_2 \ , \quad & D_{1,x} &= Y_4 \ , \\ \psi_1 &= Y_5 \ , \quad & \psi_2 &= Y_6 \ . \end{aligned} \qquad (3.9.18)$$

Then

$$Y_{1,x} = Y_2 \ , \qquad (3.9.19)$$

$$Y_{2,x} = \zeta Y_1 F_1(Y_5) - \zeta^2 \ , \qquad (3.9.20)$$

$$Y_{3,x} = Y_4 \ , \qquad (3.9.21)$$

$$Y_{4,x} = -\frac{\zeta}{e}[F_2(Y_6) - D_1\{F_1(\psi_1) + F_2(\psi_2)\}] , \qquad (3.9.22)$$

$$Y_{5,x} = \frac{1}{\zeta} Y_3 Y_2 , \qquad (3.9.23)$$

$$Y_{6,x} = \frac{1}{\zeta} (1-Y_3)(Y_2-eY_4) . \qquad (3.9.24)$$

The use of the geostropic equations, together with 3.9.12 gives, analogously to 3.3.18,

$$\psi_1(\infty,\zeta) = \{a \log \zeta + b(\zeta-1)\} , \qquad (3.9.25)$$

$$\psi_2(\infty,\zeta) = (1-eb)\{(1-a) \log \zeta - b(\zeta-1)\} \qquad (3.9.26)$$

Then the equation for η at the coast, η_c, is obtained in the same way as 3.7.11.

$$\eta_c = \zeta \{\psi_1(\infty,\zeta) + \psi_2(\infty,\zeta)\}$$
$$- e\{\tfrac{1}{2} h_1^2 - h_1 - \tfrac{1}{2} (a+b\zeta)^2 + (a+b\zeta)\} \qquad (3.9.27)$$
$$+ \zeta$$

The initial conditions for equations 3.9.16-3.9.24 can be obtained by first guessing a value for h_1 and then using 3.9.27 for the corresponding value of η_c. Then the Bernoulli integrals give the values for the velocities, which may be entered into the geostrophic equations to give $\eta_{,x}$ and $D_{1,x}$. Y_5 and Y_6 are set to zero at x = 0. The offshore solutions are obtainable by a simple extension of these ideas, as was discussed in 3.7 for the offshore level of no motion solutions. The same numerical technique is used here as in Section 3.7: guess h_1,

integrate the system of first order equations and use the behavior for large x to iterate toward a solution.

3.10 Behavior of barotropic models

The numerical technique of the previous section will give solutions for various values of a, b, and e. In this section the properties of the solutions as a function of these parameters will be discussed. Detailed comparison with observation is deferred to the next chapter. The purpose and format of the diagrams are the same as for figures 18-23, and are described in section 3.8.

Figures 24 and 25.--For the case in which the upper layer thickness was a constant increase or decrease as a function of latitude, as e increases from zero, the density effects restrict the correct solution to lower latitudes. For $b < 0$, as $e \to \infty$, $v_2 \to \infty$ and therefore $v_2 \gg v_1$. If this limit is properly scaled, it corresponds to the upper layer becoming a level of no motion. To show this, imagine that in equations 3.9.2 and 3.9.3 that (x,u,v) are scaled using $\frac{\rho_2-\rho_1}{\rho_2} D_o$ instead of η_o. Then the parameter e^{-1} would only appear as the coefficient of η in equations 3.9.4-3.9.10. That is, the equations containing e would be

$$-\zeta v_1 + \frac{1}{e}\eta_{,x} = 0 \qquad (3.9.4a)$$

$$u_1 v_{1,x} + v_1 v_{1,y} + \zeta u_1 + \frac{1}{e}\eta_{,y} = 0 \qquad (3.9.5a)$$

$$-\zeta v_2 + \frac{1}{e}\eta_{,x} - D_{1,x} = 0 \qquad (3.9.7a)$$

$$u_2 v_{2,x} + v_2 v_{2,y} + \zeta u_2 + \frac{1}{e}\eta_{,y} - D_{1,y} = 0 \; . \qquad (3.9.8a)$$

Thus, with this different scaling it is explicitly seen that $e \to \infty$ corresponds to the upper layer becoming a level of no motion. Since $e \to \infty$ corresponds to either $\eta_o \to 0$ or $\frac{\rho_2-\rho_1}{\rho_2} D_o \to \infty$, i.e., the stratification becoming dominant over the effect of the free surface; it may be said that the upper layer level of no motion corresponds to negligible effect of the free surface.

If the upper layer becomes a level of no motion, an impossible limit may be expected. When the upper layer velocity vanishes identically, the solution for h_2, and therefore for $h_1 = (1-h_2)$, is completely determined. But when the velocities are small but not identically zero, the conservation of potential vorticity gives, for the sequence in figure 18 if $v_{1,x} \to 0$, $\frac{h_1}{\zeta} = 2^{-1}$. This is different from the limit for h_1 when the velocity in the upper layer is identically zero.

In contrast to the discussion in 3.8 for figure 19, no simple conclusion like $h_1 + h_2 = 1$ can be drawn from the Bernoulli integral for the rescaled equations, $\frac{1}{2} v_1^2 + \frac{1}{e} \eta = \frac{1}{e}$, because all the terms are small. But an impossible limit is still to be expected because of the above potential vorticity argument, and indeed, for $e = 4.0$ no solution can be found. Thus $e \to \infty$ is an impossible limit.

The difference between $e \to \infty$ for $b < 0$, an impossible limit, and $\gamma \to \infty$ for the baroclinic case, a correct limit when $b > 0$, occurs because in the baroclinic case the thickness of the lower layer can adjust to satisfy the conservation of potential vorticity.

As e goes to zero, the correct solution goes to that limit in which the upper layer has the same thickness at the coast as it did at $\zeta = 1.0$, and goes to its proper asymptotic value for large x. Of course, in the limit, this variation in thickness of the upper layer across the stream has no effect on the velocity because $e = 0$. The disappearance of the solution as e gets larger for the case of positive b is not surprising, because when $e = 1/b$, the lower layer becomes a level of no motion, an impossible limit is expected, and, in fact, no solution can be found for $e = 3.8$. This shows that the one-moving-layer baroclinic model may not be regarded as the limit of a two-layer barotropic model. It is an impossible limit.

Figures 26 and 27.--If in the interior the interface between the two densities is horizontal, then, even if $e \neq 0$, the difference in density has no effect on the input fluxes, and it is clear that a possible solution is the one in which the solution for the homogeneous layer holds, and in which the interface is at the same depth throughout the entire region. These figures show, however, that for $e \neq 0$, the horizontal interior may not be regarded as equivalent to the homogeneous solution, because for arbitrarily small slopes a discontinuity in the solution appears at some latitude. In these figures $e = 1.0$, and the discontinuity appears at $\zeta = 1.7$. Thus the horizontal interface between ρ_1 and ρ_2 is an incorrect limit. If the upper layer thickness increases slightly with latitude in the interior, then along the coast its thickness decreases with latitude, and if it decreases in

the interior, then it increases along the coast. In both cases, no value of $\underline{e}$ gives an off-shore countercurrent.

These four figures show that the correct way to pass from a two-layer model to the homogeneous model, which can extend to indefinitely large values of ζ, is for $\underline{e}$ to go to zero, that is, for the effect of the free surface to be dominant over the density structure. Or to put it another way, the one-layer baroclinic model may be extended beyond the latitude to which it would otherwise extend by adding large components of the barotropic model.

3.11 Summary

The constant-potential-vorticity solutions showed that a thin upper layer could not extend very far north unless the stratification, γ, were large. For a thick upper layer, a solution with an inshore countercurrent in the lower layer could be found up to near $\zeta = 2.0$, but the water in this countercurrent could not have come from the interior, so that the solution is physically meaningless. The inshore countercurrent can be eliminated by large stratification together with making the upper layer in the interior less than roughly $\frac{1}{2}$ the total thickness, which is the kind of density structure observed in the ocean. This result suggests that if some other density structure existed, perhaps because of climatic change, the Gulf Stream in the growth region would not be as smooth as is observed. Large stratification is also the proper limit for passing from the two-moving-layer

model to the one-layer model. If the internal stratification goes to zero in a two-layer baroclinic model, then an incorrect solution approaches the one-layer solution.

Numerical computations with non-constant potential vorticity (baroclinic models) verify that large stratification extends the solutions northward and is the proper limit for passing to the one-moving-layer baroclinic case. The computations also show that the level-of-no-motion solution resulting from a horizontal lower interface is an impossible limit.

Numerical computations with barotropic models show that the proper limit for passing from the two-layer case to a homogeneous layer is for the effect of the free surface variation to dominate over the internal density structure. It was also shown that a one-moving-layer baroclinic solution may not be regarded as the limit of a two-moving-layer barotropic model in which the velocity in the lower layer goes to zero, because no solution exists as this limit is approached. It is an impossible limit.

The results of this chapter are summarized in figures 29 and 30 for baroclinic and barotropic models respectively. For example the upper portion of figure 29 shows that for passing to the one-layer baroclinic model, $\gamma \to \infty$ is a correct limit, $\gamma \to 1$ is an incorrect limit, and the lower layer becoming horizontal is an impossible limit.

CHAPTER IV

COMPARISON WITH OBSERVATION

4.1 Restrictions on comparison with observation

The primary purpose of this investigation of inertial boundary currents has been to discover the qualitative effects resulting from the density structure of the ocean. However, it would be interesting to see if more detailed agreement with observation can be obtained than was previously possible. Before these comparisons are attempted, however, some mention should be made of the effects of mechanisms which have been excluded from the model.

Perhaps the most fundamental objection arises from the discovery by Bryan (14) that as the horizontal eddy viscosity goes to zero, no steady state can be obtained in numerical solutions of the homogeneous, barotropic model with an imposed wind stress. In his solutions, the region of the boundary current in which the water fluxes toward the coast (which is the region of interest in this work) is well behaved, the time average is close to the analytical steady-state models. However, where the flux is away from the coast, the solution takes the form of a series of countercurrents in which even a small horizontal eddy viscosity can dissipate the relative vorticity caused by changes in latitude. This result was anticipated by Fofonoff (25) in his review article. It is not surprising that the time variation is present, because the large shears in the northern region must lead to instability. If it is instability which leads to the time variation, then a steady-state analytical solution may yet be found.

If Bryan's results are interpreted as meaning that no inertially dominated flow can be in a steady state, then the significance of steady state theories becomes questionable. However, since steady state inertial models give a good representation of Bryan's results in the growth region, it is plausible that close analogs of the present stratified-ocean results will be valid in the time varying case.

In addition to the instabilities of horizontal shear found in Bryan's work, there are instabilities related to the density structure. Ippen and Harleman (27) have observed in experimental fluid flows that internal waves on the interface between two moving layers begin to break for Froude number of order unity. In many of the models in this paper the Froude number exceeds unity, and these transitions might occur. More recent work on stratified hydraulic jumps has been performed by Long (28) and Yih (29).

Stern (30) has shown that infinitesimal disturbances will not grow on a one-layer baroclinic model if the gradient of potential vorticity across the stream does not vanish. Since the potential vorticity is monotonic in the present models, this would imply that all results in this paper, except perhaps for the constant potential vorticity case, are stable. Unfortunately, Stern does not include the variation of the Coriolis parameter in his analysis, and the results are strictly valid only for small values of the velocity (small values of the Rossby number, $\frac{UL}{\Omega}$) so that the significance of his result is not so clear in the present context as it is for zonal flow. However, in general, the possibility of infinitesimal disturbances drawing on the available kinetic and potential energy should be kept in mind.

Bottom topography is not discussed in the theory, yet it has an important effect. Greenspan (31) has emphasized the importance of bottom topography for the existence of steady boundary layer solutions. It is quite clear that if the depth changes, so must the relative vorticity; a variation in depth is equivalent in many ways to variation of the Coriolis parameter.

Warren (12) has shown that the bottom topography controls the detailed path of the stream after it has left the continental shelf. The path of the Gulf Stream through the Caribbean shows clear topographic influence, and the Florida Straits are shallow enough to cut off much of the water fluxing toward the coast between 10° and 17°N in figure 3. This water would otherwise play a role in the stream.

Figure 3 shows considerable density structure in the upper layers which cannot be adequately modeled by anything short of a continuum theory. The failure in this work to deduce an offshore countercurrent from a two-moving-layer model makes it seem possible that the countercurrent might be associated with a north-south gradient of density at $z = 0$, because that is practically the only qualitative feature which cannot be modeled with the class of interiors available. A continuum model is necessary for this question because it will avoid the infinite values of potential vorticity which result from a layer of zero thickness in the interior. I have not been able to handle these infinite values with numerical techniques. A continuum model might also "join" the correct and incorrect solutions and therefore show the discontinuities to be artifacts of the finite number of layers.

It might be thought that it would be possible with this numerical computation scheme to discuss how the upper layer could return to the interior with an eastward flux over a large range of latitude, while the lower layer maintained the boundary current by continuing to accept a westward flux. However, this topic lies beyond the scope of this work because a given value of the stream function, as it returns to the interior, must carry with it the same potential vorticity with which it entered the inertial regime. This requirement imposes a severe restriction on the density structure where the streamline returns to the interior. For some cases I have shown that it is not possible to determine <u>any</u> density structure to accept the return inertial flow. However, it is not necessary to give these results here because even if such density structures did exist, and if inertial solutions could be computed to fit them, the meaning of the result would be unclear, because the result would imply that the interior density structure at a lower latitude forces a particular density structure at a higher latitude by means of the inertial boundary current. It is more plausible to me to think of the Gulf Stream as a boundary layer on an internal thermocline region which is determined by a balance between diffusion and advection of heat. Bryan's results do indicate that the interior can be thought of as determined independently from the boundary layer and also that any search for broad, steady, purely inertial, fluxes returning to the interior from a simple boundary layer is likely to be fruitless.

The effects of vertical and lateral eddy diffusivity are difficult to evaluate. However, if one accepts as a typical vertical eddy kinematic viscosity, 1 cm^2 sec^{-1}, and as a typical horizontal viscosity, 10^5 cm^2 sec^{-1}, then the Navier-Stokes expressions indicate that over the course of the accelerating portion of the stream, eddy viscosities might easily destroy secondary inertial phenomena. However, there is no reasonable way to apply such comment about viscosity in a systematic manner. In summary, comparison with observation must be restricted to the lower growth region of the Gulf Stream. Effects of unsteadiness, instability, bottom topography, continuous stratification, and viscosity are neglected. Since I cannot put error limits on these effects, neglecting them can only be justified by comparison with observation.

4.2 Comparison of baroclinic models with observation

Figure 3 gives the data for the interior from which plausible two-moving-layer model boundary conditions must be extracted. Some approximation is inevitable, and choosing a proper model is to some degree a matter of guess or intuition. To me one of the most plausible models consists of an upper layer bounded below by $\sigma_t = 27.0$, and a lower layer with a bottom boundary of $\sigma_t = 27.5$. The parameters a, b, and c are evaluated by requiring the upper layer to change from a thickness of 400 meters at 15°N, which is taken as $\zeta = 1.0$, to a thickness of 750 meters at 30°N, which is approximately $\zeta = 2.0$. Between the same limits, the bottom of the lower layer is taken to vary between 900 and 1000 meters depth. Characteristic σ_t values chosen for

the layers are 26.0, 27.25, and 27.75 for the upper, lower, and bottom layers respectively. These data give as parameters of the normalized level of no motion model, a = .111, b = .333, c = .778, and γ = 3.5. This model is close to one consisting of an upper layer of constant potential vorticity overlying a layer whose lower boundary is horizontal (which would make it a layer of no motion). The level of no motion chosen is plausible because Stommel (1) gives the level of no motion in this section between 1000 and 1300 meters on the basis of water mass considerations.

Because the above parameters are close to the impossible limit of figure 19, it is to be expected that no solution exists. Indeed, the same indications of the non-existence of a solution found in section 3.8 in the discussion of figure 19 are found here also. That is, for each ζ there is no indication of a solution anywhere except in a small region where the convergence is exceptionally slow, and where one of the asymptotic fields does not change sign.

These criteria strongly indicate that for these modelling parameters there is no solution. It was shown in section 3.8 that the physical reason for this is that slow motions in the lower layer make it impossible for $v_{,x}$ to be large enough so that potential vorticity can be conserved.

Presumably, in the actual stream, as the water flows north, because $\underline{v}$ cannot be large, the relative vorticity caused by changes in latitude must be dissipated by horizontal eddy viscosity. Also presumably, if in the real flow, or in an imagined "model" or "ideal"

flow, the "natural" turbulence were not sufficient to dissipate this excess vorticity, then the steady, boundary layer flow would break down and sufficient unsteady turbulence would be generated to dissipate the advected vorticity. Perhaps, in fact, this is the cause of some unsteady motions in the ocean.

Figure 31 shows the "solution" for these model parameters. It may or may not be instructive to compare this with observation and to note that the "solution" for the upper layer is close to what it would be if the lower layer were a level of no motion. This latter solution is shown by the crosses. This behavior is, of course, the same as in figure 19. The upper layer comes to the surface at $\zeta = 2.08$, which, for a β plane tangent at 25°N corresponds to a latitude of 33°N. This is about 2° south of Cape Hatteras. The agreement of this upper layer with observation is good, as it should be since, in effect, it is Charney's (21) model.

On the other hand, for the lower layer, the agreement is poor. To see this, first note that the ρ_2, ρ_3 interface may be identified fairly accurately with the 6°C isotherm. In the computed "solution" this interface rises across the stream by no more than the equivalent of 100 meters between $\zeta = 1.0$ and 2.0. But from figure 7, the 6°C isotherm rises by 700 meters across the stream. So in the lower layer, where the inertial theory is expected to be worse, the "fake" solution gives excessively poor agreement with observation.

In summary, including the lower, slowly-moving layer in a baroclinic inertial theory seems to be impossible because the slow

velocities are incompatible with the large relative vorticities caused by changes in latitude. Because Charney (21) did not consider these lower layers, he was able to achieve good agreement with observation.

If the advection of warmer water from more southerly latitudes causes the warm core and the associated countercurrent, it might be possible to reproduce such features with a two-moving-layer model. Constructing such a model will be the next attempt in a comparison with observation.

From figure 3, one possible model is a horizontal interface between ρ_1 and ρ_2 at a depth of 160 meters (corresponding to $\sigma_t = 26.1$), and a lower layer bounded below by $\sigma_t = 27.0$ and going from 400 meters at $\zeta = 1.0$, to 750 meters at $\zeta = 2.0$. (Another possibility is certainly one in which the upper layer decreases in thickness with latitude. Such models have been computed and give essentially the same results as this one.) Characteristic σ_t values are 25.0, 26.6, and 27.5 for the upper, lower, and bottom layers respectively. These data give the parameters $a = 0.4$, $b = 0.0$, $c = -.15$, $\gamma = 2.7$. The solution for these parameters is shown in figure 32 by one of the standard diagrams and by a cross-section at $\zeta = 1.6$. There is no countercurrent in this cross-section, and there was none for any of a comprehensive class of other solutions computed for varying shapes of the upper layer and values of γ. In figure 32 the failure of the solution to go to the dashed lines which give the proper asymptotic values is, of course, due to the divergence of the solution for large $\underline{x}$.

To my knowledge no profile like that of the upper layer in figure 32 has ever been observed. It seems intuitively plausible that such structures would be especially subject to instabilities, and that they might easily be destroyed by the viscous layer in which the velocity goes to zero at the coast.

However, this type of profile is found for all cases in which the thickness of the upper layer in the interior decreases with latitude, and thus appears to be fundamental. This may be an indication that an inertial theory will never be able to discuss an offshore countercurrent, which exists, perhaps, only if turbulence is introduced. On the other hand, the countercurrent may depend crucially on the surface gradient of density in the interior, which can be discussed in an inertial continuum model.

The fact that none of the correct solutions have a warm core can be understood in a way already mentioned. In the analytic solution computed for a layer of constant potential vorticity between two levels of no motion, h_1 increases with latitude. Since for the present "warm-core" models the upper layer approaches a level of no motion, h_1 increases with latitude for them also, making a warm core impossible.

Warm cores can, however, be found in the incorrect class of solutions. (See figures 21 and 23), but they do not give a countercurrent. Figure 33 is a plot for such a warm core solution for $a = 0.75$, $b = -.25$, $c = -.75$, $\gamma = 2.0$, and $\zeta = 1.9$. It is on the incorrect branch for case 2 in figure 21. The two solutions represent the closest computed "bracketing" solutions. The velocity in both layers for both

solutions is positive out to x = 1.8. The warm core is shown by the fact that D_1 around x = 1.0 is greater than the asymptotic thickness as indicated by the dashed line.

Because cross-sections in which the warm core thickness vanishes at some non-zero value of x, like figure 34e, were not discussed numerically, it is important to show, if possible, that they will not give a countercurrent. I have obtained some results if the lower layer has constant potential vorticity, which is a very representative model. Unfortunately, however, I have not been able completely to exclude a countercurrent even for constant potential vorticity.

To begin the discussion, suppose the north-south cross-section looks like figure 34a, so that the lower layer has constant potential vorticity. The plan views of the boundary layer could look like figures 34 b, c, or d. It will be shown that countercurrents in the surface water are impossible in figures 34b and c, but no result is obtained for figure 34d. In these figures the solid curve represents the intersection with the free surface of the surface between ρ_1 and ρ_2. In 34b there is evidently a countercurrent in the upper layer. The dashed curve in each figure represents a ψ_1 streamline which enters the stream south of the ρ_1, ρ_2 intersection.

If figure 34b represented the solution to the boundary conditions given by 34a, then one would expect a countercurrent, as indicated by the dashed line, at a cross-section which is everywhere south of the solid curve. However, cross sections at analogous points have been computed, and give no countercurrents (see, for example, figure

21, the incorrect solution), indicating that figure 34b does not obtain.

So it is reasonable to ask next if there can be an off-shore countercurrent north of ζ_m in figure 34c. To show that there cannot, first note that at such a cross-section v_1 at the solid curve must be positive. Figure 34e gives the principle features of such a cross-section. Since $v_1 = \frac{1}{\zeta}(\gamma D_{1,x} + D_{2,x})$ and $v_2 = \frac{1}{\zeta}(D_{1,x} + D_{2,x})$, if $v_1 > 0$, then so is v_2. Since $D_1 = 0$ for $x > x_c$, then the velocity to the right of x_c must be $v_2 = v_2(v_c)\, e^{-\alpha\zeta^{\frac{1}{2}}(x-x_c)}$ where $v_2(x_c)$ is the positive value of v_2 at x_c, and α is some positive number. So the velocity is of one sign, positive, and there is no off-shore countercurrent.

Only figure 34d has not been excluded, but I can think of no way to do so. So the question of off-shore countercurrents remains open. Fortunately, it seems that the observed boundary conditions can be fitted satisfactorily by two-moving-layer models without requiring that $D_1 = 0$ for some ζ in the interior, so that this gap in knowledge may not be so serious.

In summary, the attempt to model the upper 200 meters, or the range 700-1000 meters of the Gulf Stream by one layer of a two-layer theory must be accounted a failure, so far as comparison with observation is concerned. In the range 700-1000 meters it appears that the reason is that the transport is so small that there cannot exist the relative vorticity necessary for large changes in latitude, so that the

vorticity must be dissipated either by "natural" turbulence, or turbulence caused by breakdown of the steady inertial flow system.

For the upper 200 meters the explanation is not so clear. It may be that turbulence is especially active in surface layers and destroys the inertial flow. Or perhaps continuously stratified models are needed in this region. For thin surface layers, as discussed in section 3.3, it may be that non-linear terms must be considered in the x momentum equation.

It is, however, just possible that continuously stratified models could solve all these problems.

4.3 Comparison of barotropic models with observation

The barotropic model is actually inappropriate for a comparison with observation because, as Stommel (1) has shown, the water below about 1500 meters appears to move eastward in the interior. However, it might still be expected that the upper layer would be insensitive to the lower layer and that a fairly realistic model might be constructed from an upper layer of approximately constant potential vorticity and a value of e sufficient to give a small westward value to the velocity in the lower layer. It turns out, not too surprisingly if the results of chapter III are remembered, that any plausible model of this type has no solution. Such models are close to impossible limits. For example, if the upper layer is taken to change from 400 to 800 meters between $\zeta = 1.0$ and 2.0, if the total depth is taken as 4000 meters, and if e is selected so that the ratio of the upper layer velocity to that of the lower is 5.0; then no solution can be found

even at $\zeta = 1.03$. The same result is obtained when, to take account of the fact that the stream in the Florida straits and along the Blake Plateau is in water of less than 1000 meters, a plausible barotropic model is given for only this upper region.

The failure of this latter model strongly suggests that if the bottom water through the Florida straits and on the Blake plateau flows in the same direction as the main stream, then it does not conserve the inertial integrals. Here, as in the comparison of baroclinic models with observation, viscosity might dissipate the advected vorticity.

4.4 Summary

Both baroclinic and barotropic models fail to give good, or in some cases any, description of the surface and deep layers of the Gulf Stream. These results suggest that the one-moving-layer inertial models very likely give almost the best result that can be obtained for a purely inertial flow of global dimensions, and that adding more detail to a purely inertial model will probably only increase the detail of disagreement with observation. This does not necessarily mean that the success of the single-layer models is illusory, only that they select that part of the stream which is most dominated by inertial effects. However, this conclusion must be preliminary until solutions for continuum models are available.

CHAPTER V

SUMMARY AND RECOMMENDATIONS FOR FURTHER RESEARCH

Although the solution of the mathematical problems posed is fairly complete and clear-cut, its net contribution to the physical problem of the Gulf Stream seems only to add more uncertainty than existed previously. It seems a general result that if any realistic detail is added to the one-moving-layer baroclinic models of Morgan and Charney, then either no solution can be found, or if a solution is found, it is valid only for small intervals of latitude. For example, an infinitesimal surface layer with a finite density gradient makes it impossible to find a correct solution outside of an infinitesmal range of latitude, at the northern end of which, cross-stream geostrophy breaks down, as at the "nose" in figure 14.

To the north of such points there are incorrect solutions, as in figure 18, and in a continuously stratified model, perhaps correct and incorrect solutions "join" and perhaps there is no discontinuity. However, if the results of the present work are really an indication that a steady, inertial Gulf Stream is impossible, what new terms must be added to the equations of motion to get a useful model? Will including non-linear inertial terms in the x momentum equation join the correct and incorrect solutions? Or is turbulence necessary? Is turbulence generated because steady inertial flows cannot exist? Or does "intrinsic" turbulence itself destroy the steady flows? Or can all the problems be resolved by a continuum approach? Until these

problems are resolved, the significance of the results of Morgan and Charney is thrown into question.

The meaning of the failure to find an inertial, off-shore countercurrent is also not clear. Is it possible that a type of interior boundary condition different from those considered could give a two-layer inertial countercurrent? Or is it necessary to introduce continuous stratification, a-geostrophy, or turbulence?

The principle positive result of the thesis is, of course, the understanding of the nature of the various limits--those of infinite and vanishing stratification, and those giving levels of no motion. This understanding should help in future attempts to solve the problems suggested above.

Some investigations which may be of value to settle these questions are:

1. Analysis of two-layer models using horizontal eddy viscosities.
2. Analysis of two-layer models, one viscous and one inertial.
3. Existence theorems for two-layer models, especially with regard to countercurrents.
4. Existence theorems for continuum models.
5. A discussion of what happens in the one and two-layer baroclinic models after cross-stream geostrophy breaks down.

APPENDIX I

CONTINUOUS STRATIFICATION, AND VERTICALLY AVERAGED MODELS

1. Continuous stratification

In the present work one- and two-moving layer models have been considered. But it is possible to imagine models with an indefinitely large number of layers, and the question arises, what is the continuum limit? If there are many layers, then each individual layer will be arbitrarily thin, and the vertical velocity, $\underline{w}$, can be calculated from $w = uz_x + vz_y$, where $\underline{z}$ represents the value of the vertical coordinate for the particular layer under consideration. This shows that although in the many-layer models $\underline{w}$ does not explicitly appear, just as it does not in the one- and two-layer models, it can be calculated, which is necessary for a continuum limit.

The value of $\underline{z}$ for a given layer would be found by integrating $\frac{\partial z}{\partial \rho} d\rho$ from the surface to the layer under consideration. The analog of the layer thickness is $\frac{\partial z}{\partial \rho}$, and ρ may be regarded as the coordinate replacing $\underline{z}$. In the momentum equations in chapter III, the non-linear and Coriolis terms were not changed by going from a one to a two-moving layer model. But the pressure gradients did change. In the continuum limit the pressure at density ρ is the integral from the layer to the surface of $g\rho \frac{\partial z}{\partial \rho} d\rho$.

When the changes outlined above are effected in the transition from a few layers to a continuum model, the result is exactly the equations of motion in the well-known quasi-Lagrangian coordinate

system of Starr (32). The quasi-Lagrangian equations are simply a transformation of the basic equations, using only the assumption of "hydrostatic balance" in the vertical momentum equation; the same assumption is used in the present work. Thus, in the limit of many layers, the present theory does go over to a continuum theory.

In the continuum theory the analog to the conservation of potential vorticity derived in the present work is

$$\frac{d}{dt}\left(\frac{v_{,x}-u_{,y}+f}{\frac{\partial z}{\partial \rho}}\right) = 0 \ .$$

This result is derived by Starr, and is in agreement with our previous discussion of the analogy between D and $\frac{\partial z}{\partial \rho}$.

For an arbitrary coordinate system, and without using the hydrostatic approximation, Ertel (33) has derived the more general theorem, valid also for compressible flow

$$\frac{d}{dt}\left[\frac{1}{\rho}\{\nabla \times \bar{v} + 2\,\bar{\Omega}\} \cdot \bar{\nabla}\rho\right] = 0 \ .$$

Jacobs (34) has found the corrections to the equations in a cartesian coordinate system if the "hydrostatic" condition is not valid. He shows that the equations become much more complicated.

2. Vertically averaged models

In the present work, the shallow-water equations have been used for one or two layers of constant density as an approximation to continuously stratified flow. Another way to get equations is to

vertically integrate the equations of motion, and divide by the depth to get an "average" equation of motion. When non-linear terms are of importance in the equations, as in the boundary layer in the present theory, some rather drastic assumption must be made in order to evaluate the integrals of the non-linear terms. All the assumptions which can be made are so arbitrary and untrustworthy that Carrier and Robinson (13), who used vertically averaged equations, evaluated the non-linear terms "by assumption," they simply set, for example,

$$\int u\, u_x\, dz = \int u dz \cdot \frac{\partial}{\partial x} \int u dz \ .$$

The motivation for using vertically integrated boundary layer equations is that in the interior, if the motions are presumed slow, the vertically averaged equations are far more reliable; and it is desired to fit this good interior theory to a suitable boundary layer.

However, at the present time, even the Sverdrup relation, a result of vertically averaged equations, seems untrustworthy. In the vertical average of pressure gradients there are terms due to bottom topography, and near the Mid-Atlantic ridge, these are of the same order as the β term. Also, if the unsteady motions observed by Swallow (9) have auto-correlations of only 10% then the resulting turbulent stresses will also be of the same order as the β term.

In general, then, even the Sverdrup relation is questionable, so that there is little motivation to used vertically averaged equations.

The best plan for steady models is probably to consider the interior by detailed, diffusive thermocline theories using the full equations, and to treat the boundary layer by shallow water equations, using layers of different densities.

APPENDIX II

NUMERICAL TECHNIQUE

The subroutine used for the actual integration is one which has been used by many workers at Caltech. It was written by K. H. Redner of the Computer Sciences Corporation. The user must give a supplementary routine for evaluating the derivatives and the subroutine will perform the integration and control the errors.

It has been programmed to allow the option of either fixed interval size or variable interval size with automatic error control. The method of Runge-Kutta-Gill is used to start the integration process and is used to restart the integration whenever the interval size has been changed. Let the system of equations to be solved be given in the form:

$$\text{II 1} \qquad \begin{cases} Y_i' = f_i\,(t, Y_1, Y_2, \cdots, Y_n), \; i = 1, 2, \cdots, n \\ Y_i(t_o) = Y_{io} \end{cases}$$

Let Y_{in} be the value of Y_i at $t = t_n$, f_{in} the derivative at $t = t_n$, and Δt the interval size of the independent variable t.

The Runge-Kutta-Gill method uses the formulas:

$$\text{II 2} \qquad \begin{cases} k_{io} = \Delta t\; f_i\,(t, Y_{in}) \\ Y_{in}^{(1)} = Y_{in} + \frac{1}{2} k_{io} \\ q_{i1} = k_{io} \end{cases}$$

$$\text{II } 3 \qquad \begin{cases} k_{i1} = \Delta t f_i \left(t + \frac{\Delta t}{2}, Y_{in}^{(1)}\right) \\ Y_{in}^{(2)} = Y_{in}^{(1)} + \frac{b_1}{2}\left(k_{i1} - q_{i1}\right) \\ q_{i2} = b_1 k_{i1} + c_1 q_{i1} \end{cases}$$

$$\text{II } 4 \qquad \begin{cases} k_{i2} = \Delta t\, f_i\, t + \frac{\Delta t}{2}, Y_{in}^{(2)}) \\ Y_{in}^{(3)} - Y_{in}^{(2)} + \frac{b_2}{2}\left(k_{i2} - q_{i2}\right) \\ q_{i3} - b_2 k_{i2} + c_2 q_{i2} \end{cases}$$

$$\text{II } 5 \qquad \begin{cases} k_{i3} = \Delta t f_i \left(t + \Delta t, Y_{in}^{(3)}\right) \\ Y_{i,n+1} = Y_{in}^{(3)} + \frac{1}{6} k_{i3} - \frac{1}{3} q_{i3} \end{cases}$$

where

$$b_1 = 2 - \sqrt{2} \qquad c_1 = -2 + \frac{3\sqrt{2}}{2}$$

$$b_2 = 2 + \sqrt{2} \qquad c_2 = -2 - \frac{3\sqrt{2}}{2}$$

The Adams-Moulton predictor-corrector formulas are:

$$\text{II } 6 \qquad Y_{i,n+1}^{(p)} = Y_{i,n} + \frac{\Delta t}{24}\left(55f_{i,n} - 59f_{i,n-1} + 37f_{i,n-2} - 9f_{i,n-3}\right)$$

$$\text{II } 7 \qquad Y_{i,n+1}^{(c)} = Y_{i,n} + \frac{\Delta t}{24}\left(9f_{i,n+1}^{(p)} + 19f_{i,n} - 5f_{i,n-1} + f_{i,n-2}\right)$$

The corrector formula is applied only once so that only two derivative evaluations are needed for each Adams-Moulton integration step. The starting values are obtained using the Runge-Kutta-Gill method.

If the variable interval size mode is chosen, the interval size is determined as follows:

Let

$$\text{II 8} \quad \begin{cases} E_{n+1} = \text{Max} \dfrac{\left| Y^{(p)}_{i,n+1} - Y^{(c)}_{i,n+1} \right|}{14 D_i} \\ D_i = \text{Max} \left\{ \left| Y^{(c)}_{i,n+1} \right| , .001 \right\} \end{cases} .$$

An upper bound, $\overline{E}$, on the truncation error estimate, E_{n+1}, is input to the program. This is equivalent to specifying the number of significant figures which are to be preserved locally throughout the integration. A lower bound, $\underline{E}$, is computed by $\underline{E} = .02\ \overline{E}$.

If $\underline{E} \leqslant E_{n+1} < \overline{E}$, the interval size, Δt, is unchanged. If $E_{n+1} \geqslant \overline{E}$, the program compares $\frac{\Delta t}{4}$ to Δt_{min} where $\Delta t_{min} = 2^{-12}\ \Delta t_{max}$ where Δt_{max} is inserted by the user. If $\frac{\Delta t}{4} < \Delta t_{min}$, an error return is made. If $\frac{\Delta t}{4} \geqslant \Delta t_{min}$, Δt is replaced by $\frac{\Delta t}{4}$, the conditions at time t_{n-1} are restored (i.e., $Y_{i,n-1}$, $f_{i,n-1}$), and three Runge-Kutta-Gill integrations, and two Adams-Moulton integrations are performed. It may be seen that the last Adams-Moulton integration step was an integration from time t_n to time $t_n + \frac{\Delta t}{4}$. The truncation error estimate, E_{n+1}, is computed at this point and the program continues as above.

If $\frac{1}{\Delta t} [t_o + j\Delta t_{max} - t_{n+1}] \equiv 0 \bmod 2$, where j is a positive

integer and $t_o + (j-1)\Delta t_{max} < t_{n+1} \leq t_o + j\Delta t_{max}$, the program compares E_{n+1} to $\underline{E}$. If $E_{n+1} < \underline{E}$, the program performs integrations to times t_{n+2} and t_{n+3} by the method of Adams-Moulton. If $E_{n+2} < \underline{E}$ and $E_{n+3} < \underline{E}$ and $2\Delta t < \Delta t_{max}$, then Δt is replaced by $2\Delta t$.

While the truncation error test will guarantee that the local error does not exceed $\overline{E}$, the cumulative error will usually exceed $\overline{E}$. Hence, $\overline{E}$ is chosen small enough to allow for an accumulation of truncation error.

Starting values for the Adams-Moulton method are always obtained using the Runge-Kutta-Gill method whenever the interval size is changed, just as at the beginning of the integration. An initial value for the interval size is input to the program when using the variable mode.

Both the Runge-Kutta-Gill method and the Adams-Moulton method incorporate round-off control features. This is accomplished by keeping the Y_{in} in double precision and forming the sums $Y_{in} + \Delta Y_{in}$ in double precision. The derivative evaluations are all performed in single precision. The procedure has been shown to be very effective in controlling the growth of round-off error.

FIGURE CAPTIONS

Figure 1.

Chief features of the surface water circulation in the North Atlantic. From Stommel (1).

Figure 2.

Schematic diagram of the surface and abyssal circulations in the Atlantic Ocean. From Stommel (1).

Figure 3.

North-south density section in the Atlantic near 66°W. Stations plotted are: Atlantis 5176-5202, 5232-5235, 5237-5263, Crawford 312-328. The symbol, σ_t is 1000 (ρ-1), where ρ is the density. The corresponding temperature and salinity sections have been plotted by Fuglister (10).

Figure 4.

Depth of the 10°C isothermal surface in the North Atlantic. Depth is given in meters. Stommel (1).

Figure 5.

Topography of the Florida Straits, depth is in fathoms. Stommel (1).

Figure 6.

Topography of the western North Atlantic. Depth is in fathoms. Stommel (1).

Figure 7.

Temperature and velocity sections across the Gulf Stream. From Worthington (11). It is the density which is dynamically important

in the stream, however the lines of constant salinity, and therefore of density, parallel the lines of constant temperature. In the upper figure the "warm core" is clearly visible, and in the lower figure is the countercurrent associated with the warm core.

Figure 8.

The general pattern of flow for all models in the present work. From the interior, x = oo, water flows toward the coast. At $\zeta = 1.0$ (or y = 0, since $\zeta = 1+\cot \theta_o \, y$), the water turns north, forming the boundary current, which extends northward to values of ζ dependent on the dynamics.

Figure 9.

The solution for a constant-potential-vorticity model with $\gamma = 2.0$, $\delta = 1.0$. Solution plotted in the h_1, ζ plane, where h_1 is the thickness of the upper layer at the coast and ζ is the latitude coordinate. The symbols like (++-+) give the signs of (h_1, h_2, v_1^o, v_2^o) at the nearest calculated point. The velocities at the coast are v_1^o and v_2^o. The correct solution has $h_1 = 0.5$ at $\zeta = 1.0$, and extends north.

Figure 10.

Representation of the solution of constant-potential-vorticity Gulf Streams by finding the solution of two simultaneous quadratics in h_1 and h_2, the layer thicknesses at the coast.

Figure 11.

Expanded view of the correct solutions in figure 9.

Figure 12.

Cross-sections of the Gulf Stream at selected points of figure 11. The layer of density ρ_1 is shown by the symbol D_1, and similarly for D_2.

Figure 13.

Shows the existence of off-shore solutions in which the upper layer moves away from the coast for parameters $\gamma = 2.0$, $\delta = 1.0$. The solid line shows the intersection of the $\psi_1 = 0$ streamline with the surface. Along this line, $D_1 = 0$. Note that more than one off-shore solution can exist for one value of ζ.

Figure 14.

Thickness of the upper layer, h_1, at the coast as a function of the latitude variable, ζ , for the case $\theta = 1.0$, $\delta = 0.1$ ($\gamma = 1.1$). The lower diagram shows an incorrect solution, and the non-uniformity near $\zeta = 1.0$ is shown in the text to indicate that $\delta \to 0$ is an incorrect limit.

Figure 15.

Thickness of the upper layer at the coast as a function of the latitude variable ζ for the case $\theta = 1.0$, $\delta = 10.0$. ($\gamma = 11.0$.) The velocity at the coast, v_2^o becomes negative at the coast for $\zeta > 1.4$. Therefore the limit $\delta \to \infty$ is not physically reasonable.

Figure 16.

The correct solution for $\delta = 1.0$, $\theta = 16.0$. ($\gamma = 17.0$.) The dashed lines show the layer thicknesses in the interior, the solid lines show the layer thickness at the coast. The solution is plotted

only to the point where $h_{,\zeta} = \infty$. To the left is a representation of the density structure. The variable $\hat{\rho}$ is defined in section 3.3. The small insert shows h_1, the thickness of the upper layer, as a function of ζ, the latitude variable, near the point where $h_1 = 0$. Note that the maximum value of ζ occurs for $h_1 > 0$.

Figure 17.

The thickness of the upper layer, h_1, as a function of $\underline{x}$, the east-west coordinate, showing convergence of machine integrations for successive approximations to h_1 for the parameters $a = 0$, $b = 0.5$, $c = 0$, $\gamma = 2.0$, $\zeta = 1.457$. The dashed line shows the correct asymptotic solution.

Figure 18.

The upper layer thickness at the coast, h_1, is plotted as a function of the latitude variable, ζ, for a sequence of baroclinic models showing that as the layer thicknesses increase less rapidly with ζ in the interior, the correct solution for the boundary layer can extend to larger values of ζ. The detailed format of the figure is discussed in section 3.8.

Figure 19.

The upper layer thickness at the coast, h_1, is plotted as a function of the latitude variable ζ for a sequence of baroclinic models showing that as the interface between ρ_2 and ρ_3 become horizontal it becomes impossible to find a solution. The sequence tends to an impossible limit. The crosses represent this limit which is the solution for a single layer of constant potential vorticity. The question marks

at the data points for c = 0.9 and 0.99 show that convergence to a solution was questionable at these points, indicating an approach to the impossible limit. The detailed format of the figure is discussed in section 3.8.

Figure 20.

The upper layer thickness at the coast, h_1, is plotted as a function of the latitude variable ζ for a sequence of baroclinic models, showing that as the stratification, γ , is increased, the correct solution goes to the limit of a single layer of constant potential vorticity, represented by the crosses. Large γ is a correct limit. As $\gamma \to 1.0$ it is the incorrect solution which approaches the limit. So $\gamma \to 1.0$ is an incorrect limit. The detailed format of the figure is discussed in section 3.8.

Figure 21.

The upper layer thickness at the coast, h_1, is plotted as a function of the latitude variable ζ for a sequence of baroclinic models, showing that if the upper layer decreases in thickness as a function of ζ in the interior, then increasing γ causes the correct solution to extend farther north. But γ cannot be greater than 5.0, for then the upper layer is a level of no motion, an impossible limit. And for $\gamma = 4.5$, no solution can be found. As $\gamma \to 1.0$, the incorrect solution goes to the solution for a homogeneous baroclinic layer, showing again that $\gamma \to 1.0$ is an incorrect limit. The crosses show the limit for $\gamma \to 1.0$, while the x's show the limit for $\gamma \to 5.0$. The detailed format of the figure is discussed in section 3.8.

Figure 22.

The upper layer thickness at the coast, h_1, is plotted as a function of the latitude variable, ζ , for a sequence of baroclinic models, showing that for fixed stratification, γ , as the upper layer changes from an increase toward a decrease with latitude in the interior as a function of ζ, its behavior at the coast changes from a decrease to an increase as a function of latitude. For no value of the slope does it extend beyond $\zeta = 1.5$. The slope of the ρ_2, ρ_3 interface, together with γ, restrictsthe solutions to lower latitudes. The detailed format of the figure is discussed in section 3.8.

Figure 23.

The upper layer thickness at the coast, h_1, is plotted as a function of the latitude variable, ζ , for a sequence of baroclinic models, showing that as the upper layer decreases more rapidly with latitude, the solution is restricted to lower latitudes. The detailed format of the figure is discussed in section 3.8.

Figure 24.

The upper layer thickness at the coast, h_1, is plotted as a function of the latitude variable, ζ for a sequence of barotropic models, showing that if the upper layer decreases in thickness with latitude in the interior, that increasing the stratification, e, restricts the correct solution to lower latitudes. The limit $e \to 0$ is clearly correct for a transition to a homogeneous, barotropic model. The limit $e \to \infty$, when scaled, gives $u_1 = v_1 = 0$, a level of no motion and an impossible limit. In fact, for $e = 4.0$, no solution can be

found. The detailed format of the figure is discussed in section 3.8.

Figure 25.

The upper layer thickness at the cost, h_1, is plotted as a function of the latitude variable, ζ, for a sequence of barotropic models, showing that if the upper layer increases in thickness with latitude that increasing the stratification, e, restricts the correct solution to lower latitudes. The limit $e \to 0$ is correct for a transition to a homogeneous barotropic model. For $e = 4.0$, the lower layer becomes a level of no motion, and is an impossible limit. For $e = 3.8$ no solution can be found. The detailed format of the figure is discussed in section 3.8.

Figure 26.

The upper layer thickness at the coast, h_1, is plotted as a function of the latitude variable, ζ, for a sequence of barotropic models, showing that as the upper layer increases more rapidly in thickness with latitude in the interior, that the correct solution is restricted to lower latitudes. Also, as the ρ_1, ρ_2 interface becomes horizontal there is non-uniform convergence to the homogeneous model limit in which the two layers have equal thicknesses and velocities everywhere. It is an incorrect limit. The detailed format of the figure is discussed in section 3.8.

Figure 27.

The upper layer thickness at the coast, h_1, is plotted as a function of the latitude variable, ζ, for a sequence of barotropic models, showing that as the upper layer decreases more rapidly in

thickness with latitude in the interior, that the correct solution is restricted to lower latitudes. Also, as the ρ_2, ρ_3 interface becomes horizontal there is non-uniform convergence to the homogeneous model limit in which the two layers have equal thicknesses and velocities everywhere. It is an incorrect limit. The detailed format of the figure is discussed in section 3.8.

Figure 28.

The correct solutions for those figures marked by an asterisk in figures 18-23. The dashed lines show the layer thicknesses in the interior, the solid lines show the layer thicknesses at the coast. To the left is a representation of the density structure. The variable $\hat{\rho}$ is defined in section 3.3. The solutions are not plotted past the points where either $h_2 = 0$ or $h_{,\zeta} = \infty$.

Figure 29.

Illustration of the character of the limits of various sequences of solutions for baroclinic models. For example, for the transition to a one-layer baroclinic model, $\gamma \to 1$ is an incorrect limit, $\gamma \to \infty$ is a correct limit, and letting the ρ_2, ρ_3 interface be horizontal is an impossible limit.

Figure 30. Illustration of the character of the limits of various sequences of solutions for barotropic models. For example the lower left-hand corner shows that $e \to 0$ is a correct limit.

Figure 31.

Results of calculations for a two-layer Gulf Stream using boundary conditions obtained from observed data. The question marks indicate that convergence to a solution is doubtful because the param-

eters are close to an impossible limit. To the left is a representation of the density structure. The variable $\hat{\rho}$ is defined in section 3.3. The dashed lines give the layer thicknesses in the interior, and the solid lines give the layer thicknesses at the coast. The corner gives the solution for an upper layer $D = .111 + .333\ \zeta$, just like D_1, over a level of no motion. The questionable solution is close to this limit.

Figure 32.

Results of calculations for a two-layer Gulf Stream using boundary conditions from observed data which might have given an offshore countercurrent, $a = .4$, $b = 0$, $c = -.15$ and $\gamma = 2.7$. In the upper figure the dashed lines indicate the layer thickness in the interior, and the solid lines show the layer thickness at the coast. To the left is a representation of the density structure. The variable $\hat{\rho}$ is defined in section 3.3. The solution ends when $h_2 = 0$. The lower diagram gives a cross-section at $\zeta = 1.6$. The failure of the solution to go to the dashed lines which give the proper asymptotic values shows the divergence of the numerical integration for large x.

Figure 33.

A "warm core" solution from the incorrect class of solutions in figure 23. The two solutions for large x are the two closest computed "bracketing" solutions. The existence of the warm core is shown by the fact that the layer thickness of the upper layer near $x = 1.0$ is greater than the asymptotic thickness as shown by the dashed lines.

Figure 34.

Sketches useful for discussing the existence of off-shore countercurrents. Figure 34a shows a north-south section through the interior. $D_1 = 0$ at ζ_m. The upper layer has density ρ_1 and the lower, ρ_2. Figures 34b,c,d show possible patterns for the streamlines. The solid line is the $\psi_1 = 0$ streamline where $D_1 = 0$. The dashed lines represent other streamlines. The possible existence of these various patterns is discussed in section 4.2. Figure 34e shows an east-west cross-section with a warm core.

Figure 35.

A "warm core" solution from the incorrect class of solutions in figure 26. The two solutions for large $\underline{x}$ are the two closest computed "bracketing" solution. The existence of the warm core is shown by the fact that the layer thickness of the upper layer near $x = 1.0$ is greater than the asymptotic thickness as shown by the dashed lines.

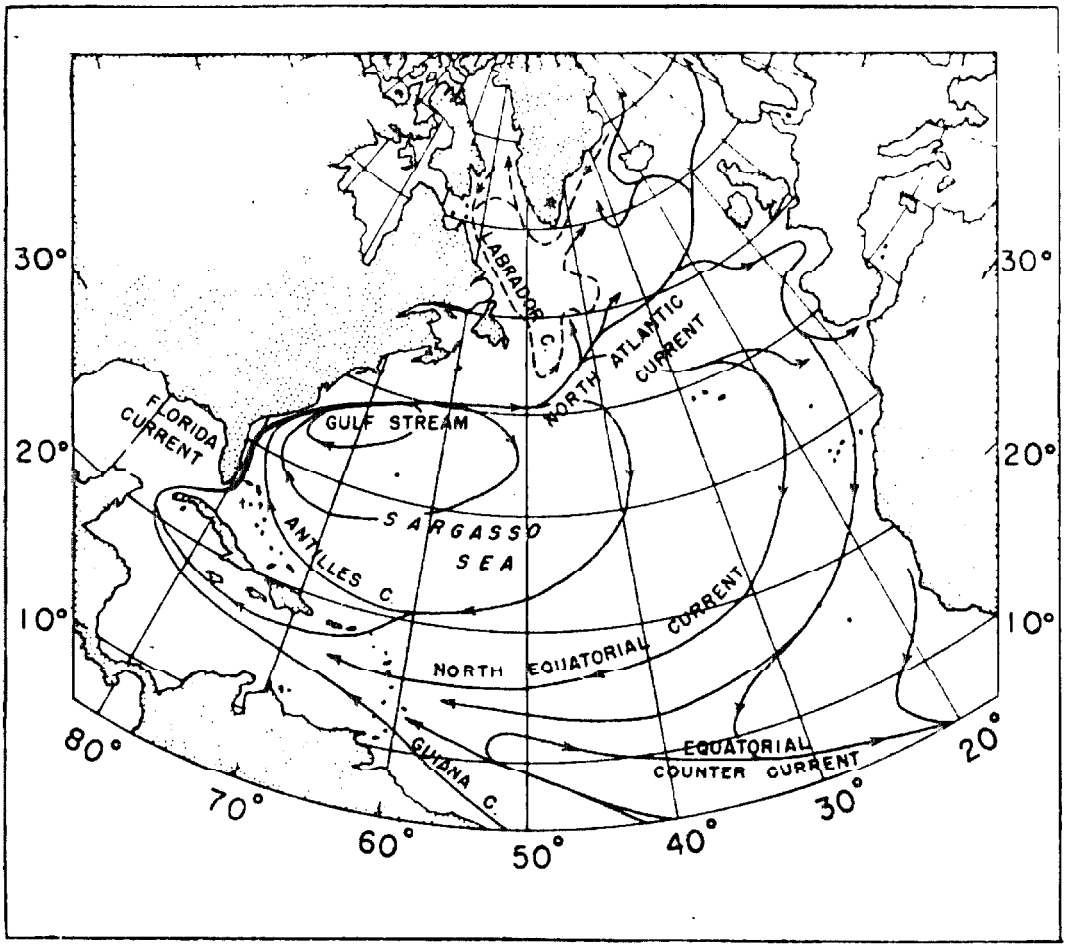

Figure 1. Chief features of the surface water circulation in the North Atlantic. From Stommel (1).

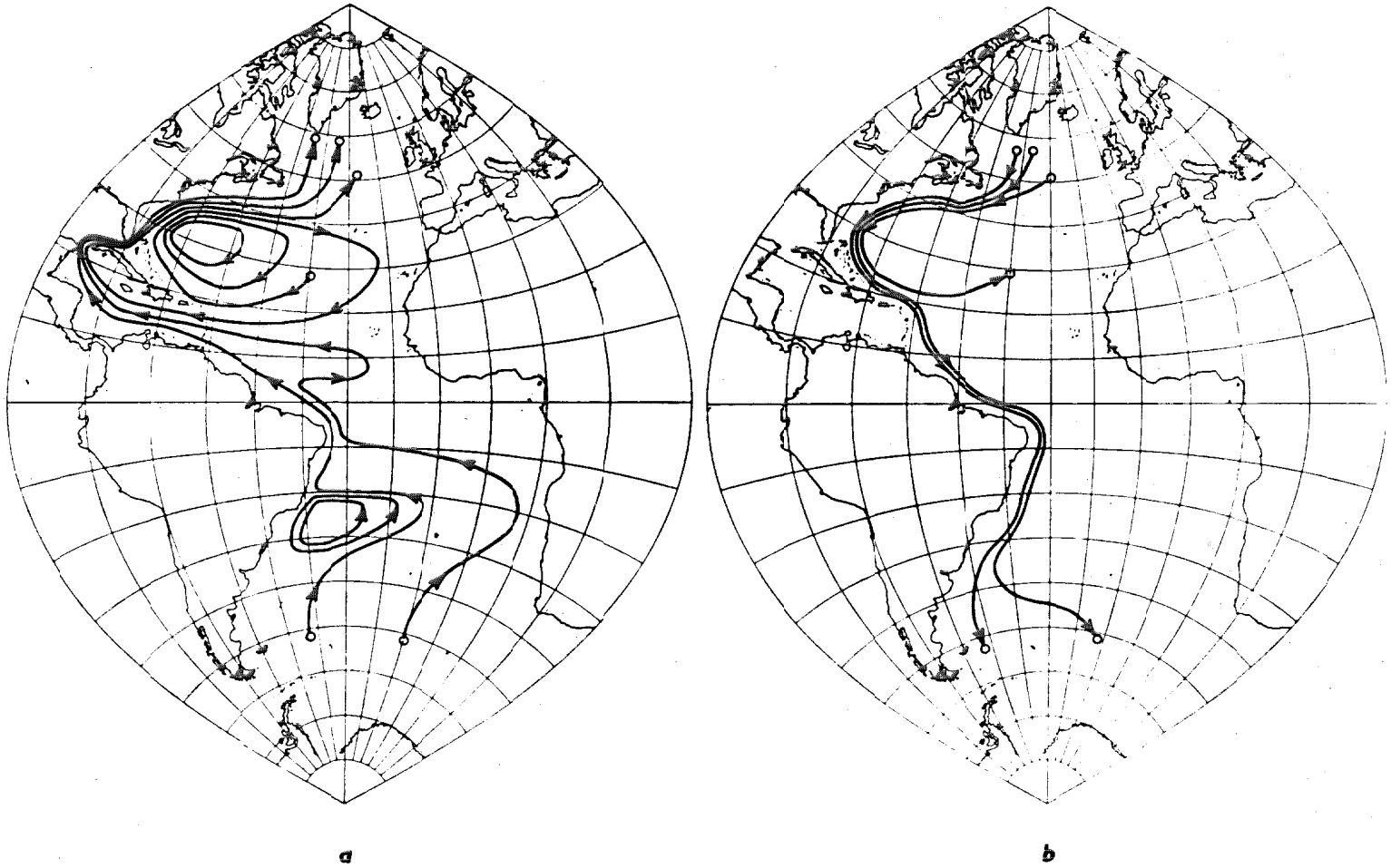

Figure 2. Schematic diagram of the surface and abyssal circulations in the Atlantic Ocean. From Stommel (1).

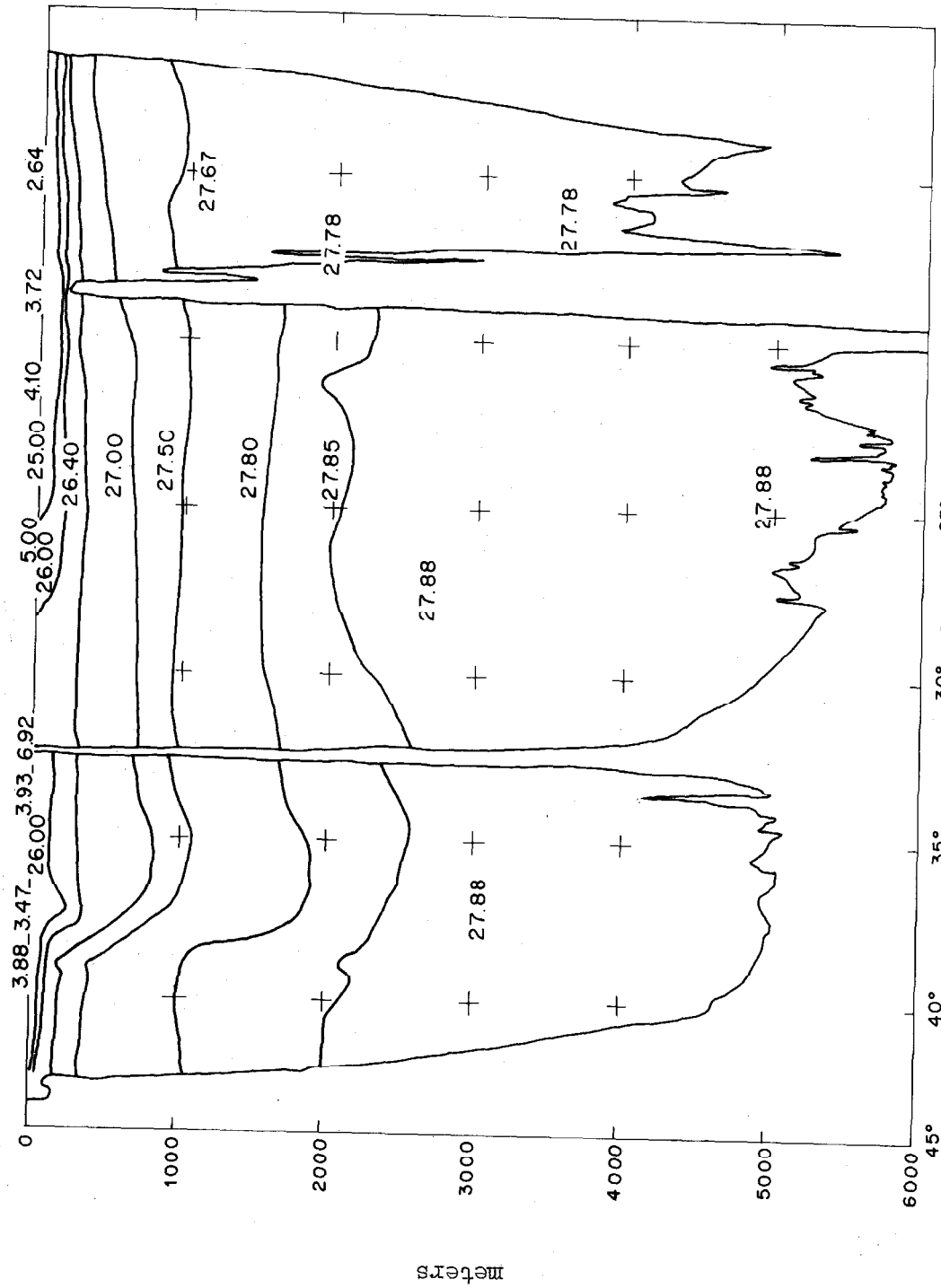

Figure 3. North-south density section in the Atlantic near 66°W. Stations plotted are: Atlantis 5176-5202; 5232-5235, 5237-5263, Crawford 312-328. The symbol, σ_t is 1000 (ρ-1), where ρ is the density. The corresponding temperature and salinity sections have been plotted by Fuglister (10).

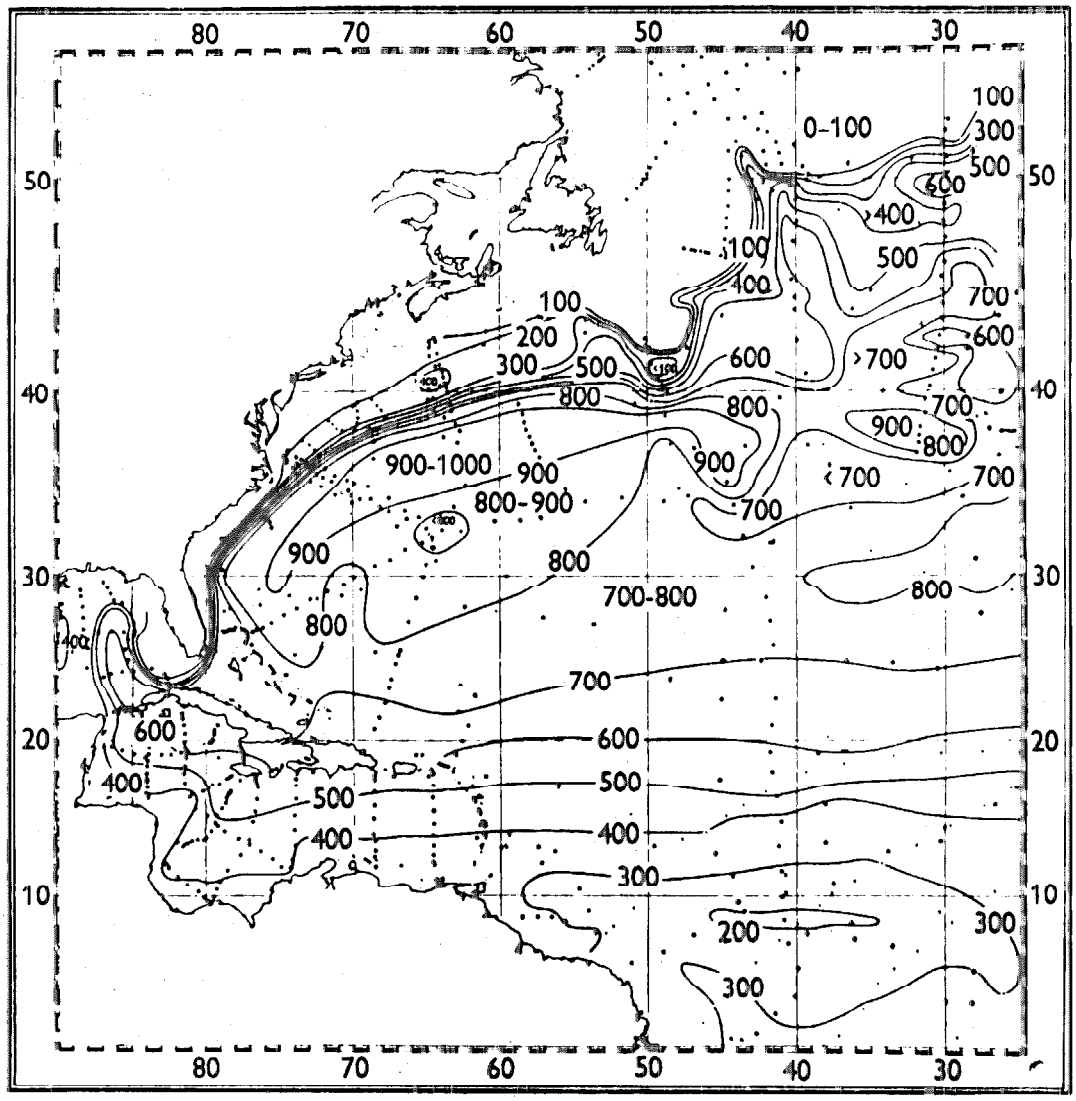

Figure 4. Depth of the 10°C isothermal surface in the North Atlantic. Depth is given in meters. Stommel (1).

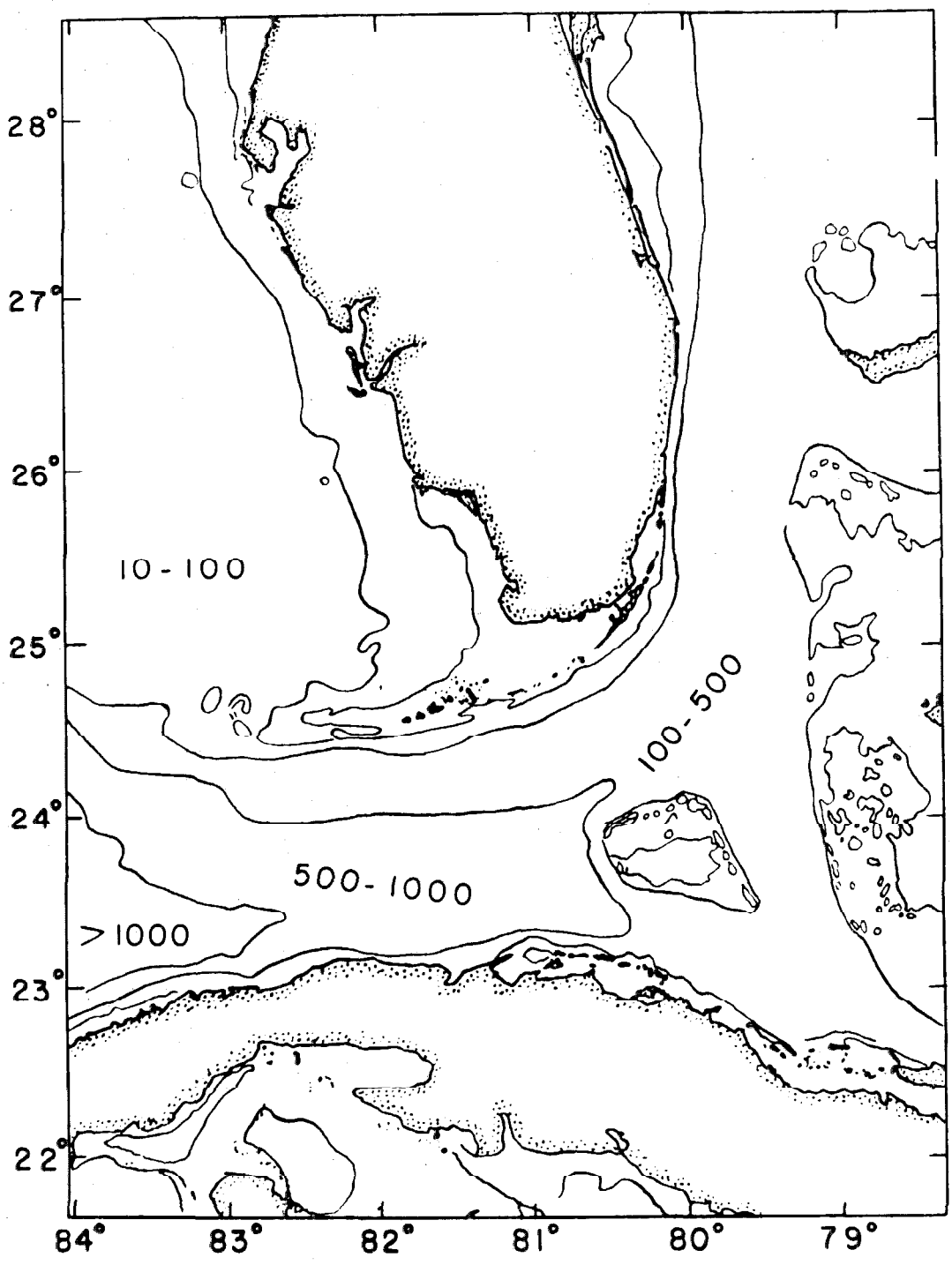

Figure 5. Topography of the Florida Straits, depth is in fathoms. Stommel (1).

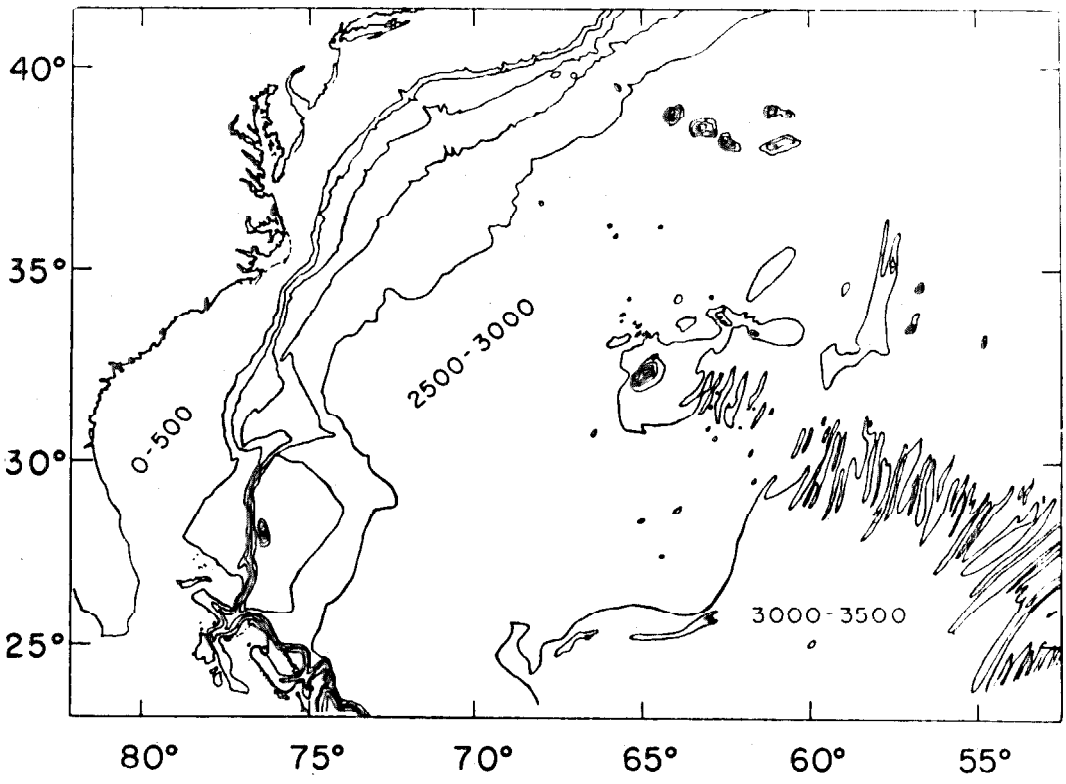

Figure 6. Topography of the western North Atlantic. Depth is in fathoms. Stommel (1).

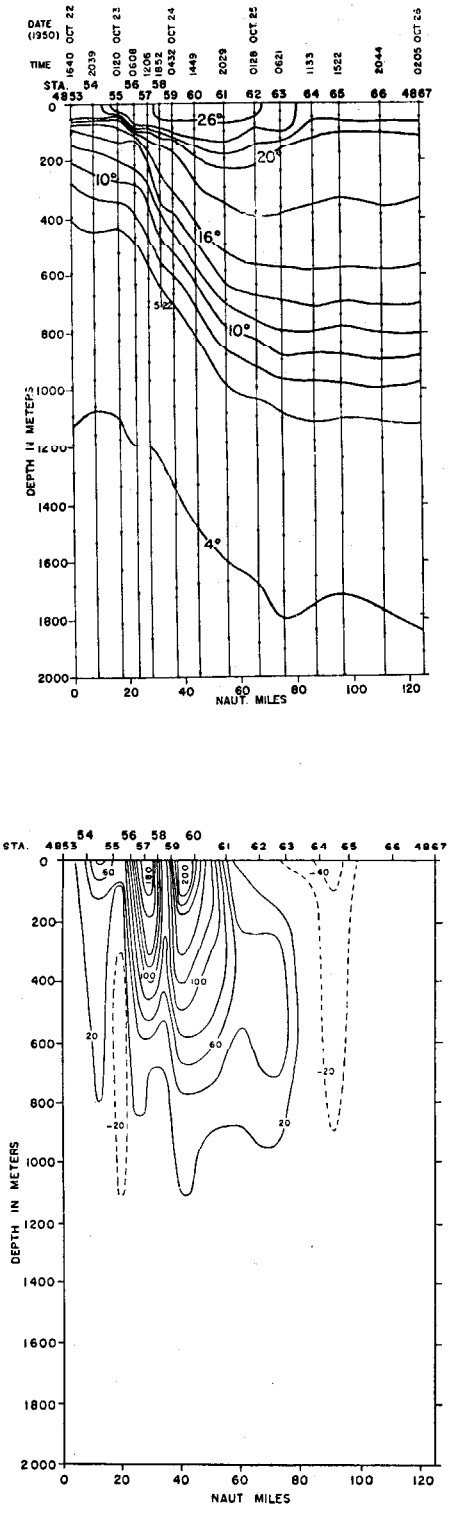

Figure 7. See caption beginning on page 105.

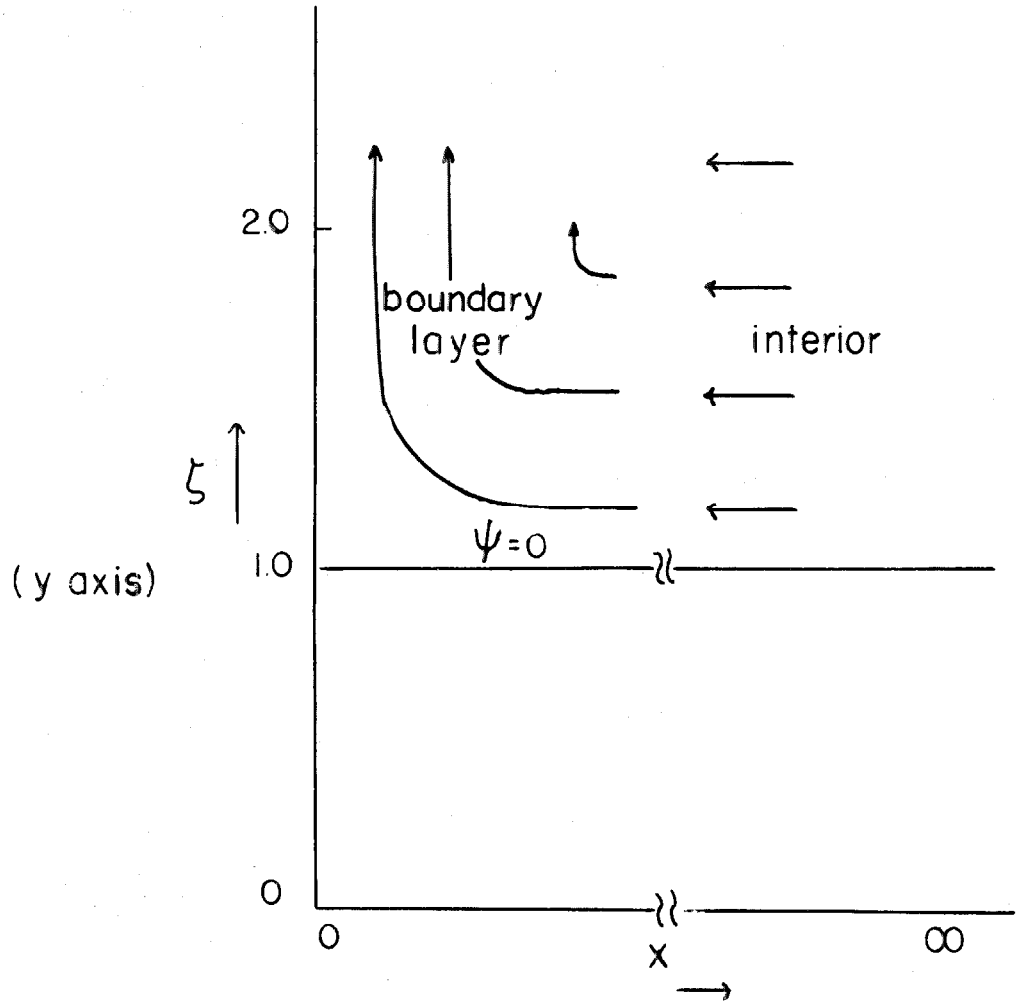

Figure 8. The general pattern of flow for all models in the present work. From the interior, $x = \infty$, water flows toward the coast. At $\zeta = 1.0$ (or $y = 0$, since $\zeta = 1 + \cot \theta_o \, y$), the water turns north, forming the boundary current, which extends northward to values of ζ dependent on the dynamics.

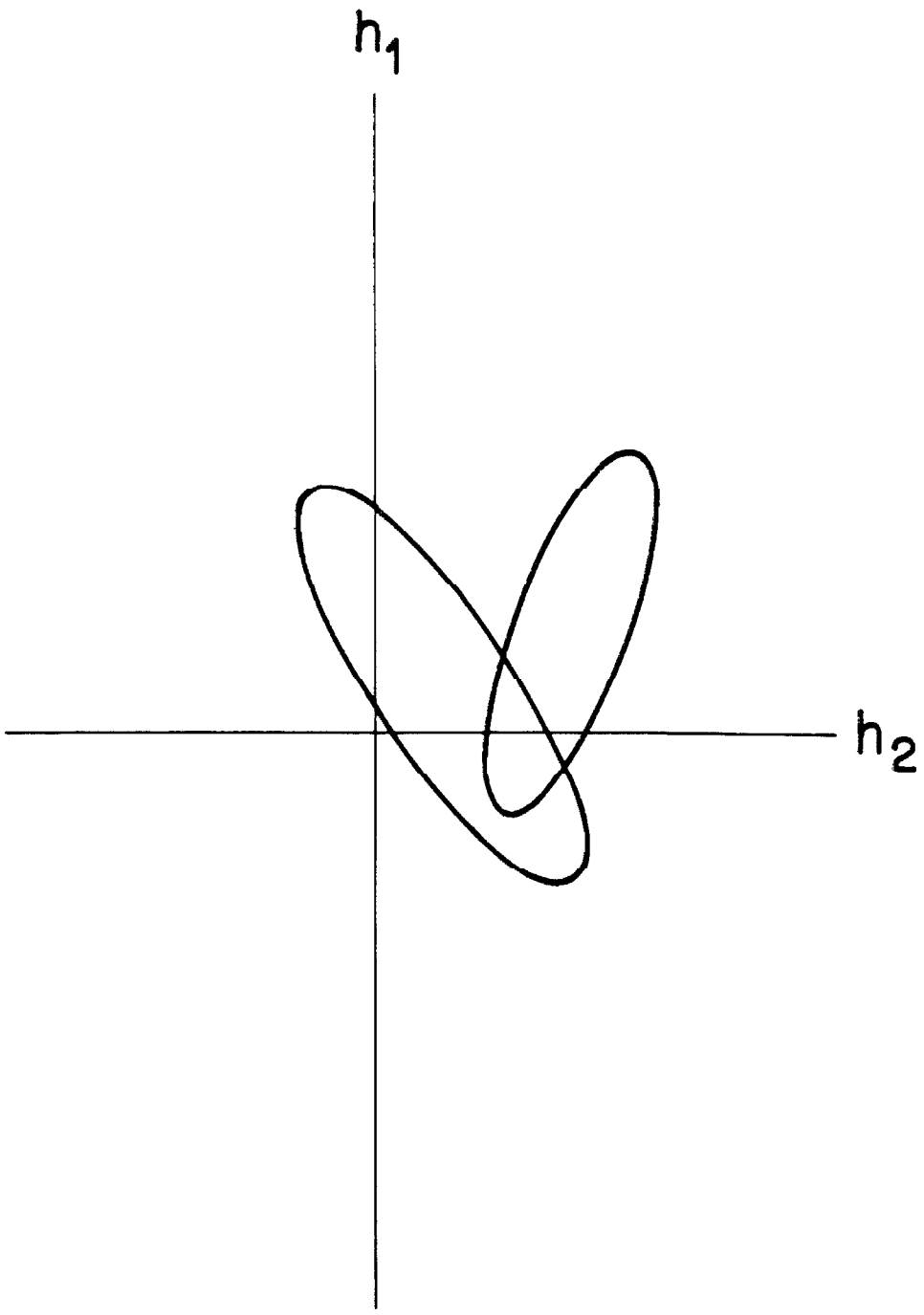

Figure 9. Representation of the solution of constant-potential-vorticity Gulf Streams by finding the solution of two simultaneous quadratics in h_1 and h_2, the layer thicknesses at the coast.

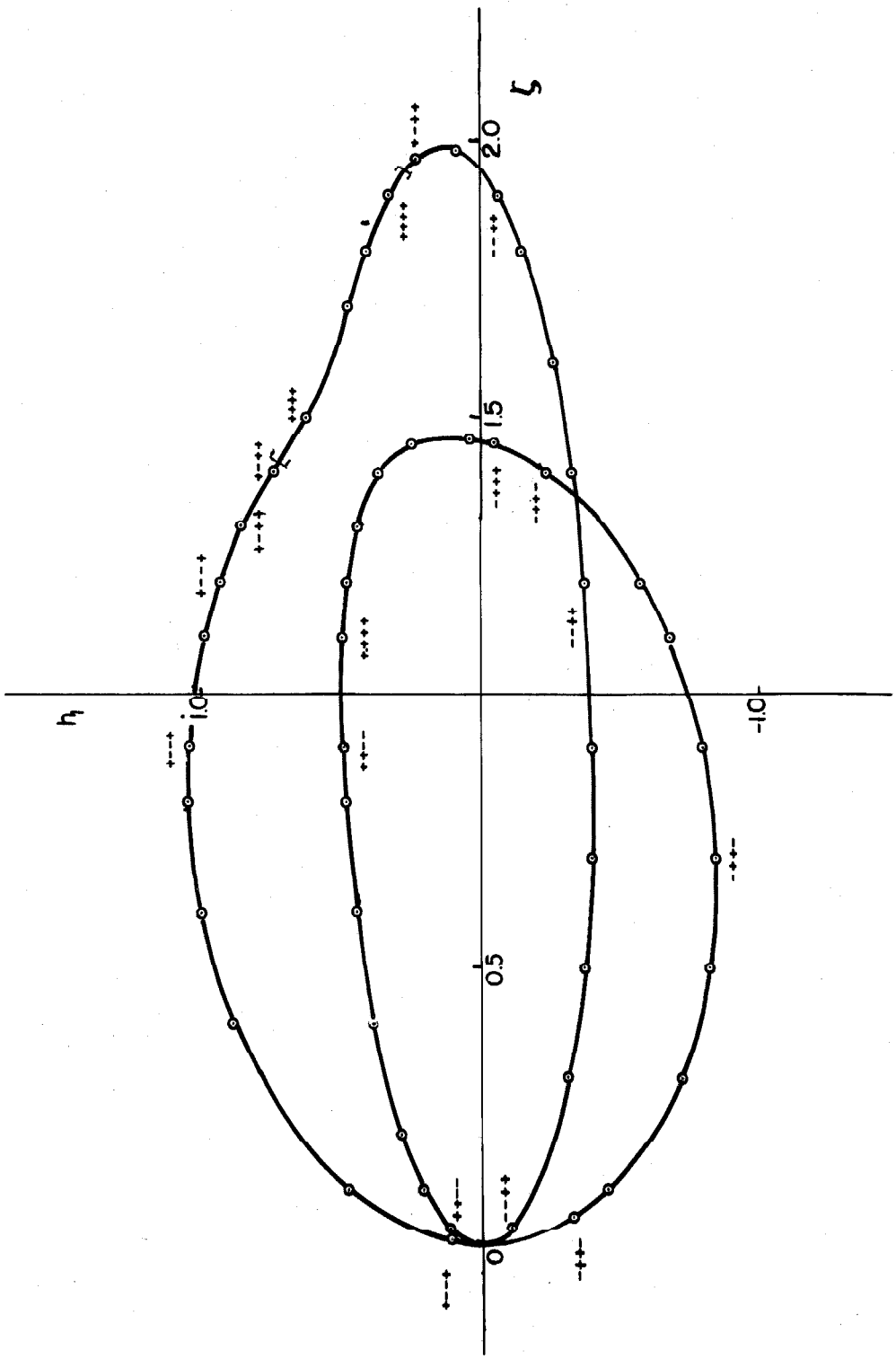

Figure 10. See caption on page 104.

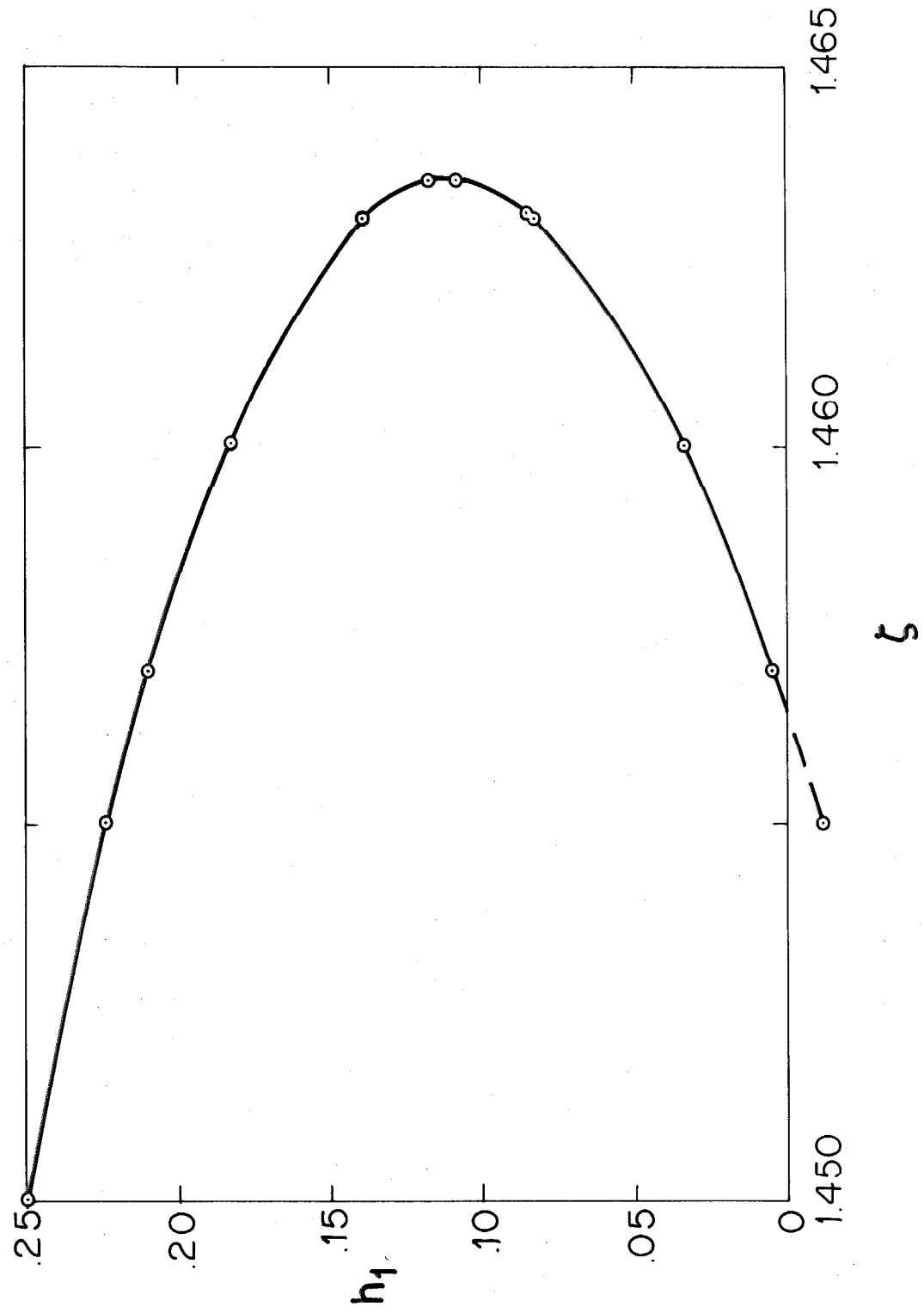

Figure 11. Expanded view of the correct solutions in figure 10.

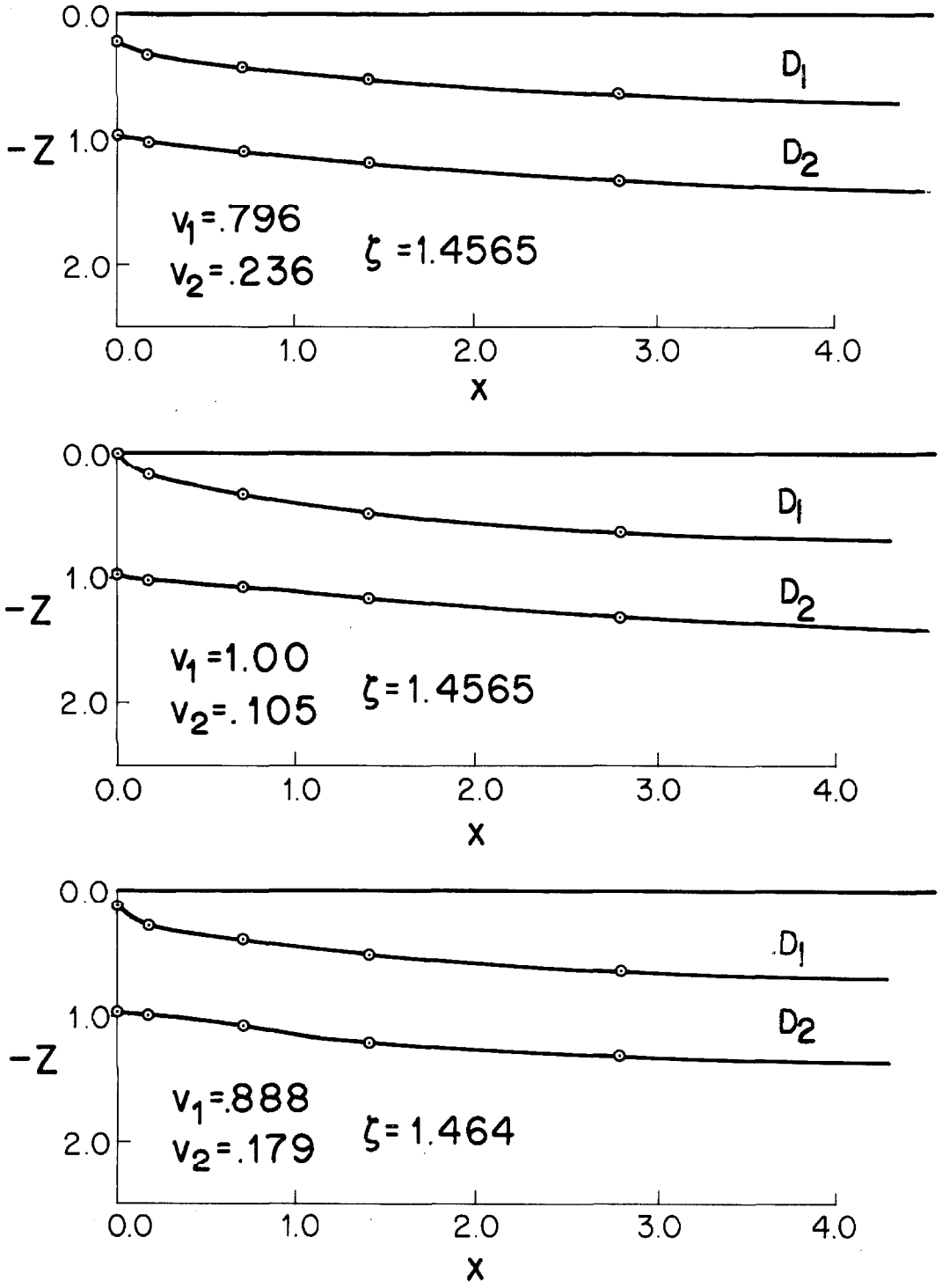

Figure 12. Cross-sections of the Gulf Stream at selected points of figure 11. The layer of density ρ_1 is shown by the symbol D_1, and similarly for D_2.

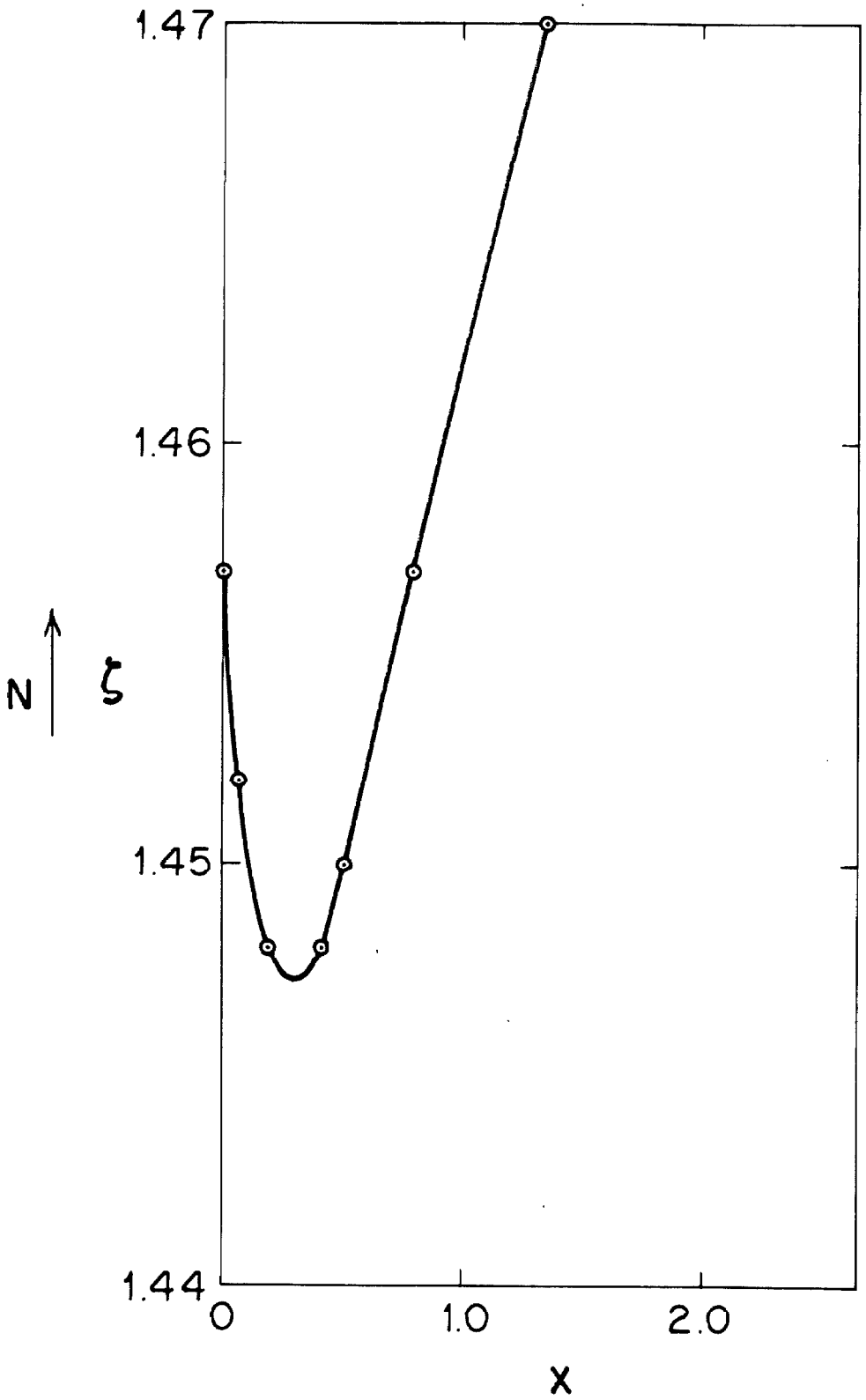

Figure 13. See caption on page 105.

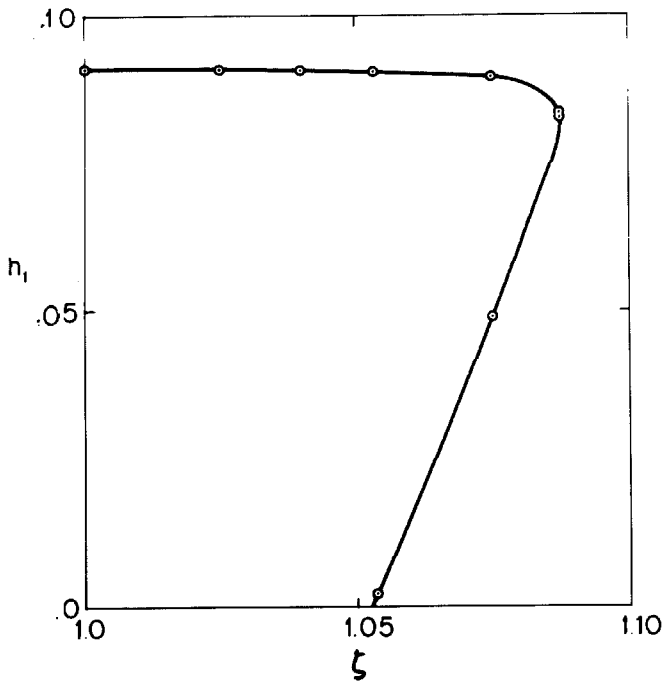

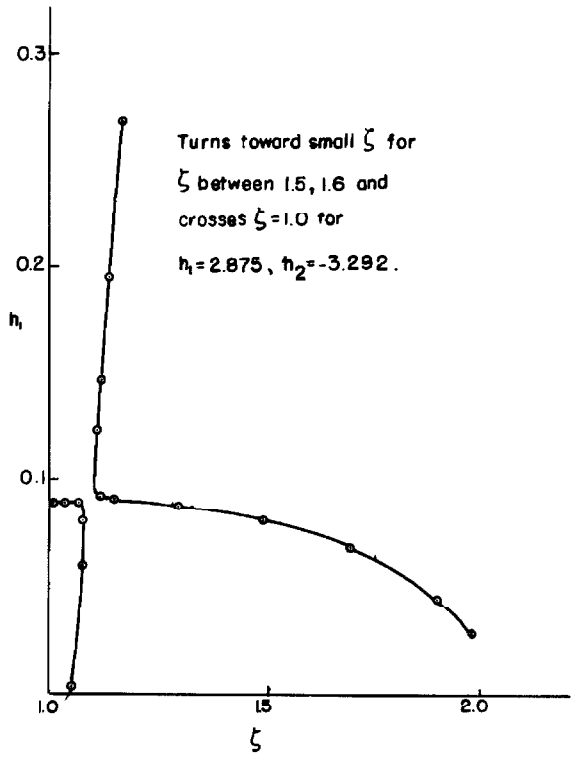

Figure 14. See caption on page 105.

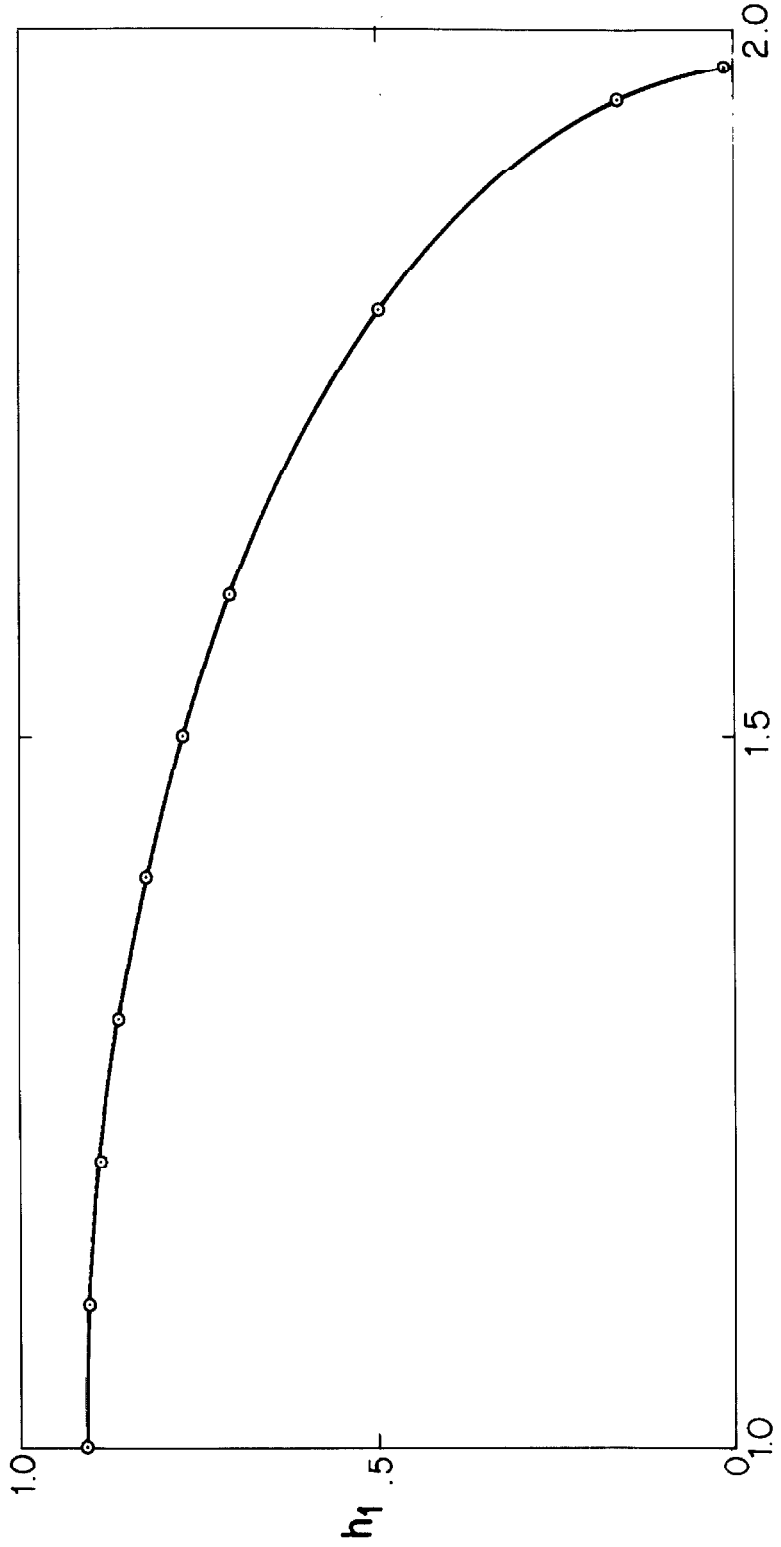

Figure 15. Thickness of the upper layer at the coast as a function of the latitude variable ζ for the case $\theta = 1.0$, $\delta = 10.0$. ($\gamma = 11.0$.) The velocity at the coast, v_2^o becomes negative at the coast for $\zeta > 1.4$. Therefore the limit $\delta \to \infty$ is not physically reasonable.

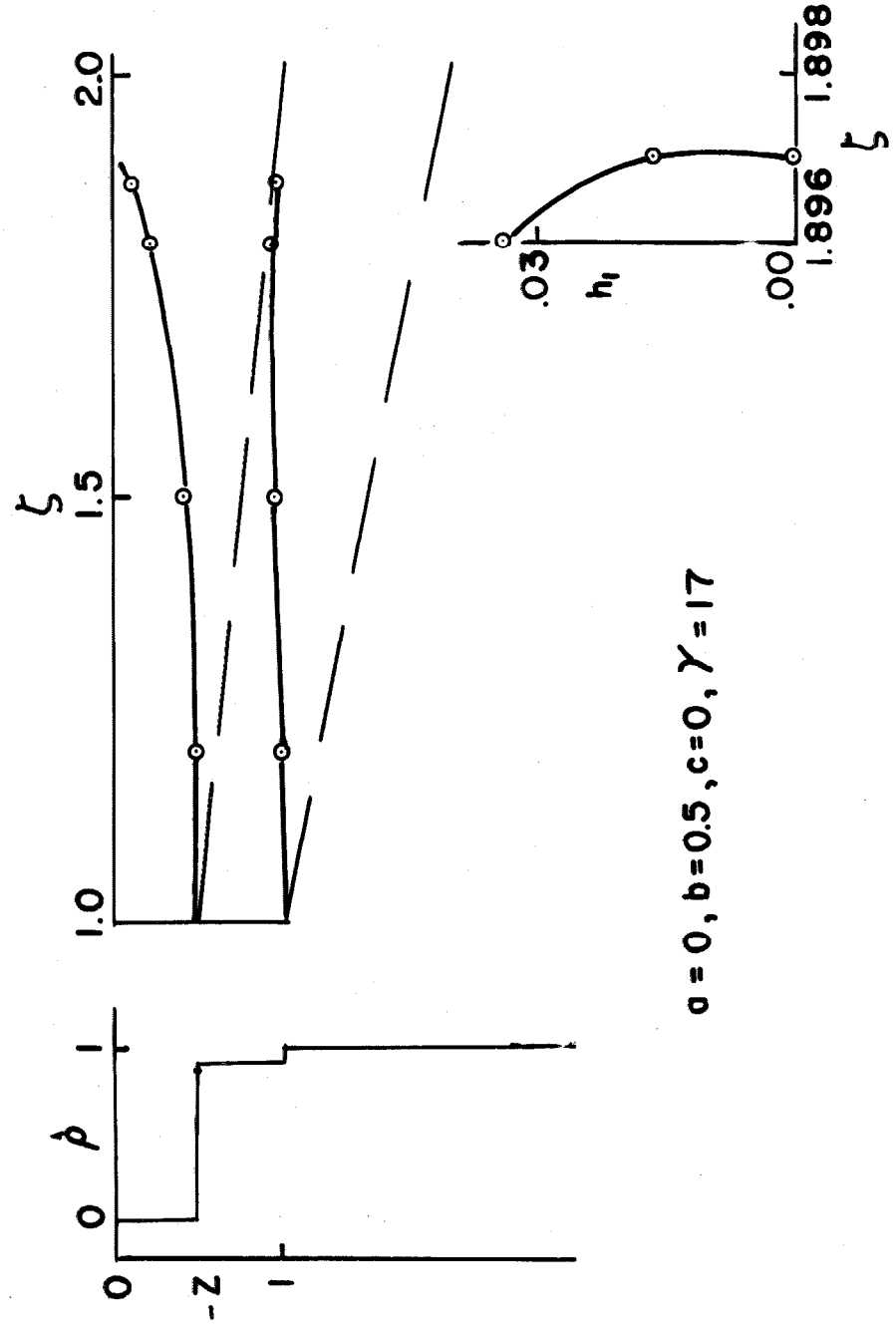

Figure 16. See caption beginning on page 105.

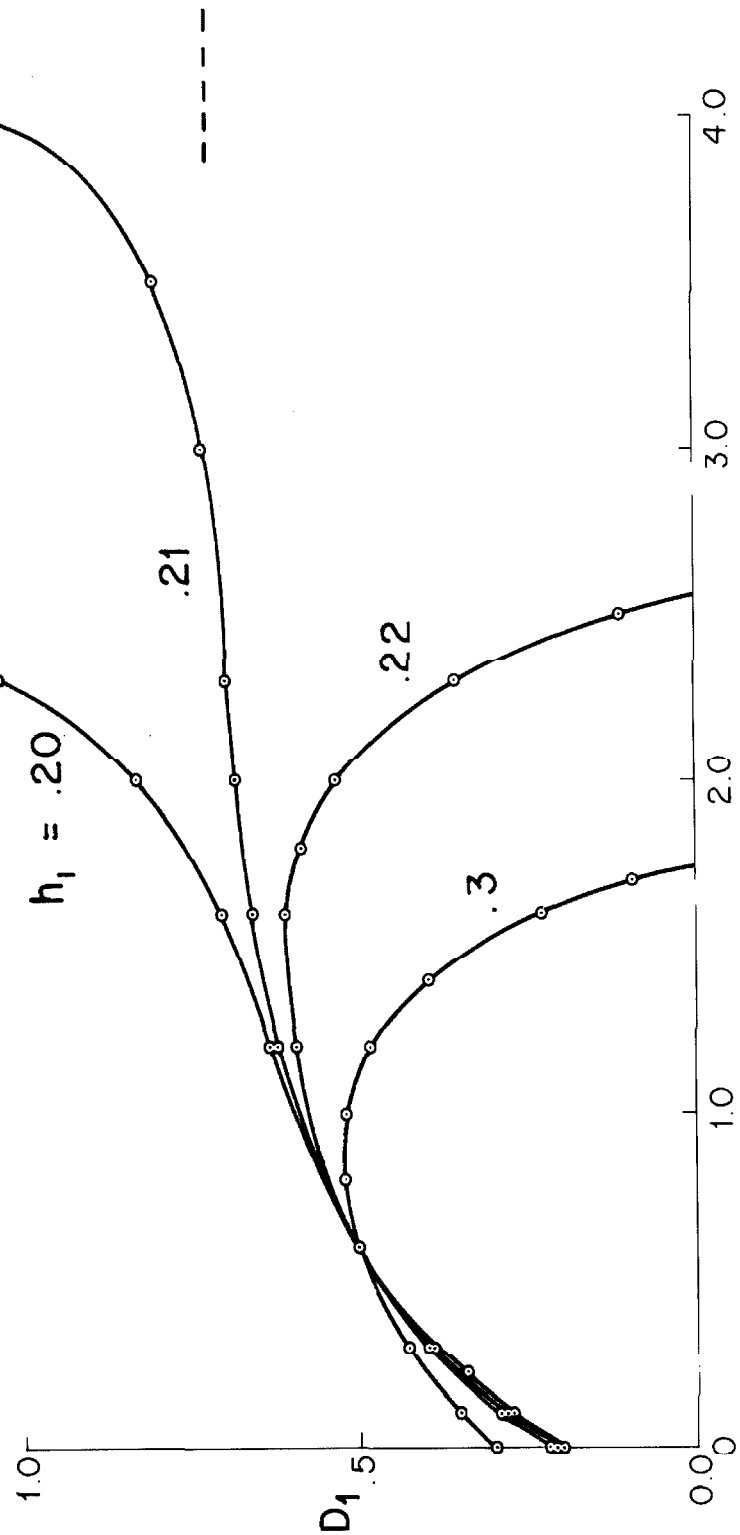

Figure 17. The thickness of the upper layer, h_1, as a function of $\underline{x}$, the east-west coordinate, showing convergence of machine integrations for successive approximations to h_1 for the parameters $a = 0$, $b = 0.5$, $c = 0$, $\gamma = 2.0$, $\zeta = 1.457$. The dashed line shows the correct asymptotic solution.

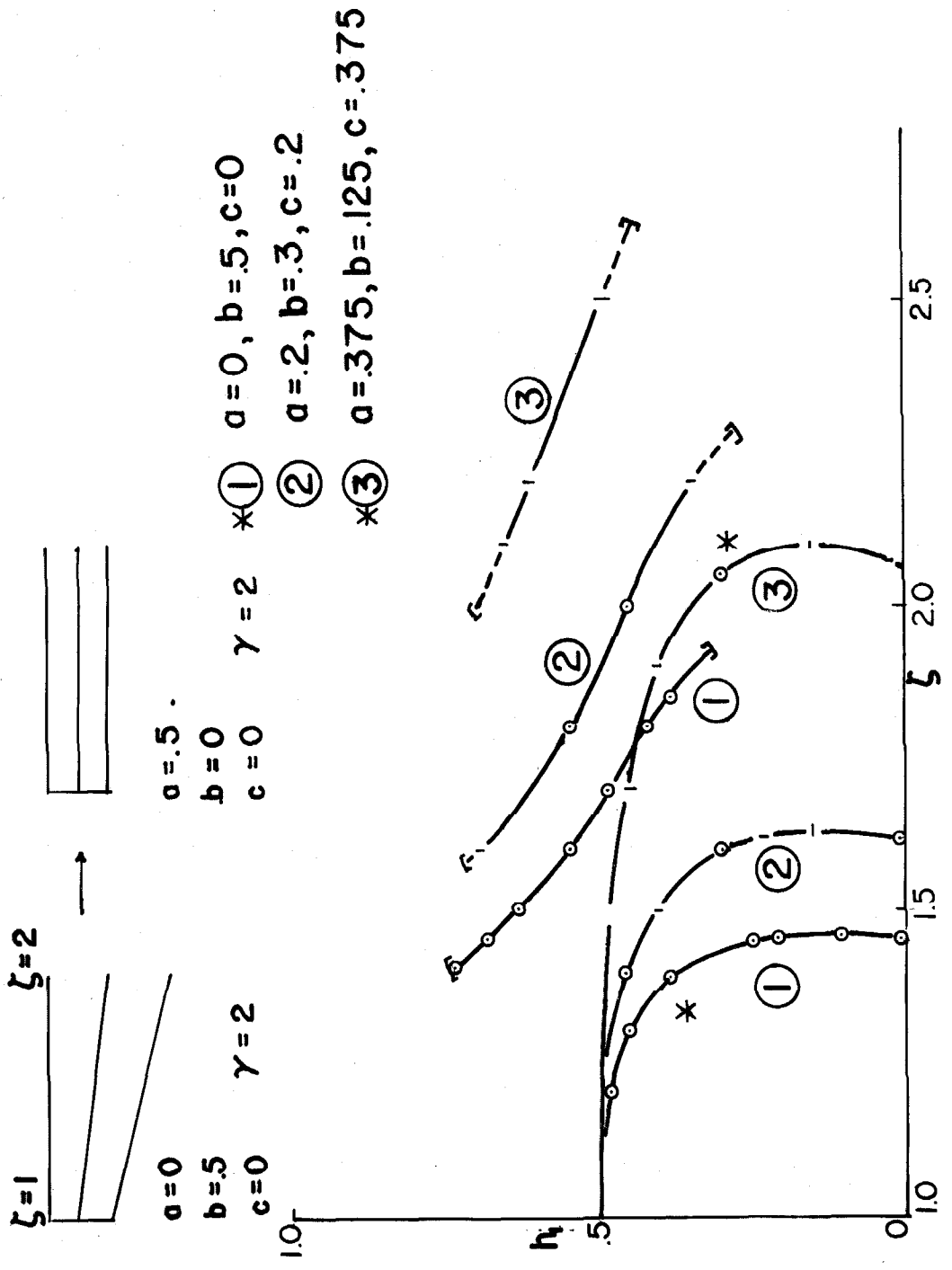

Figure 18. See caption on page 106.

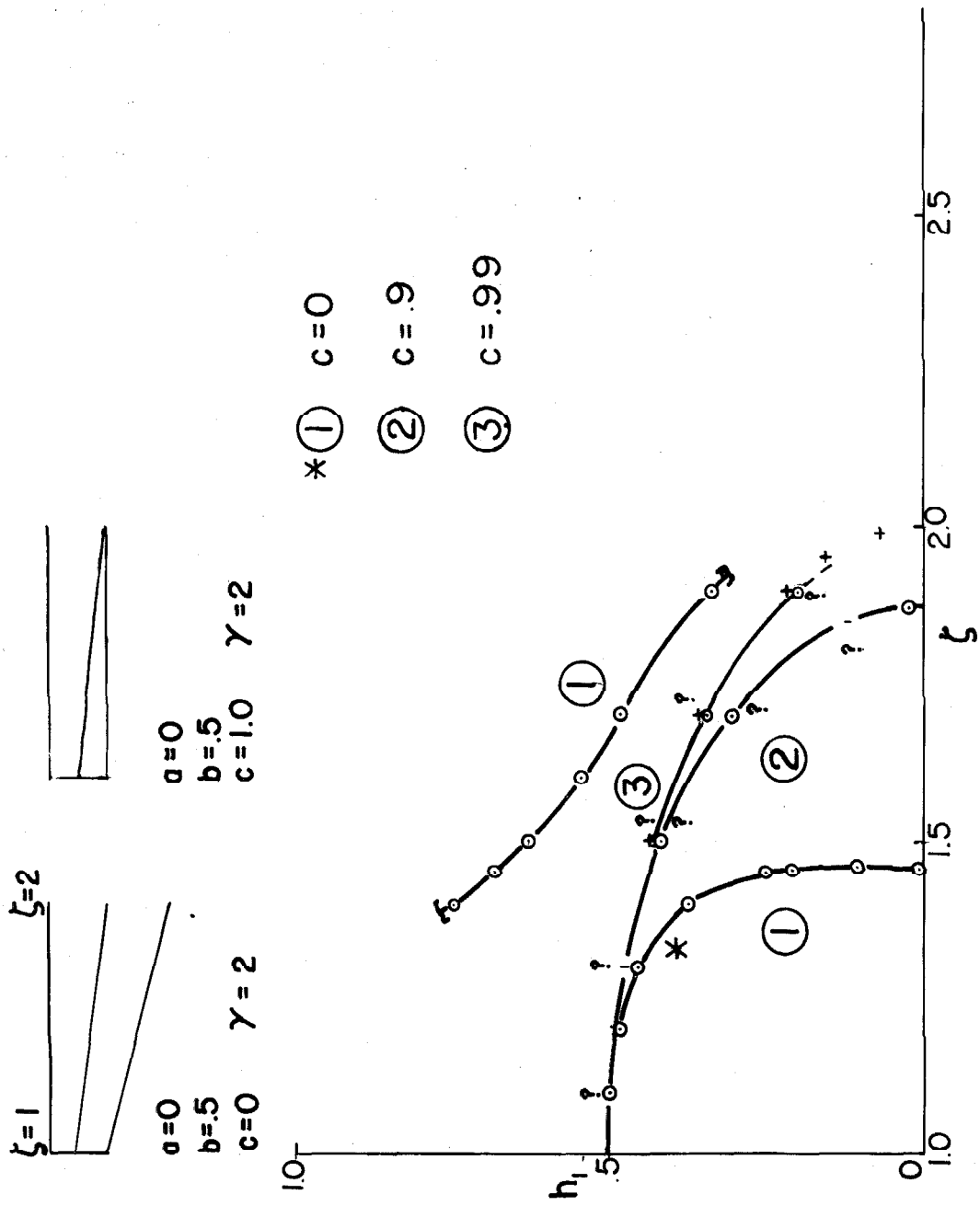

Figure 19. See caption beginning on page 106.

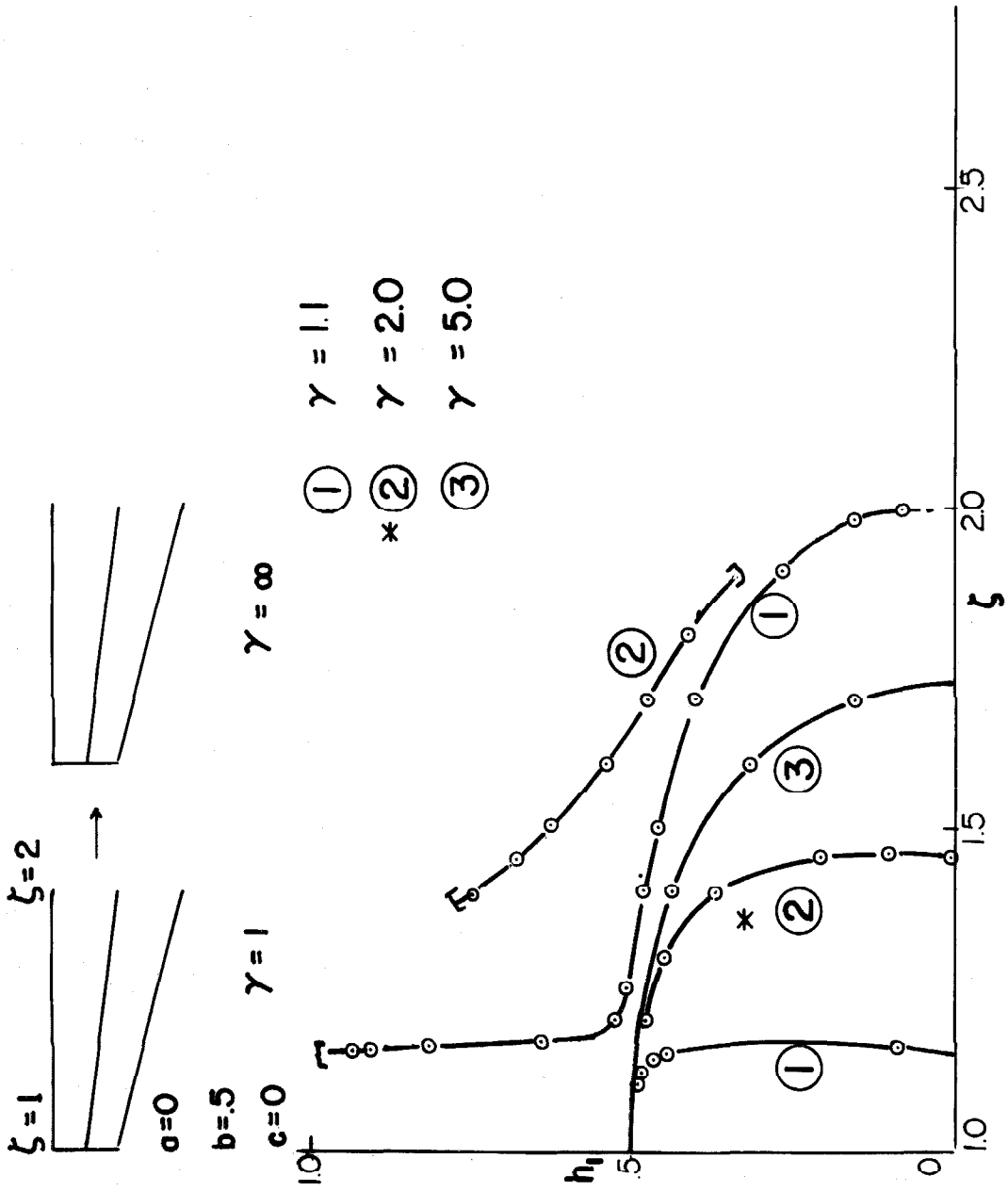

Figure 20. See caption on page 107.

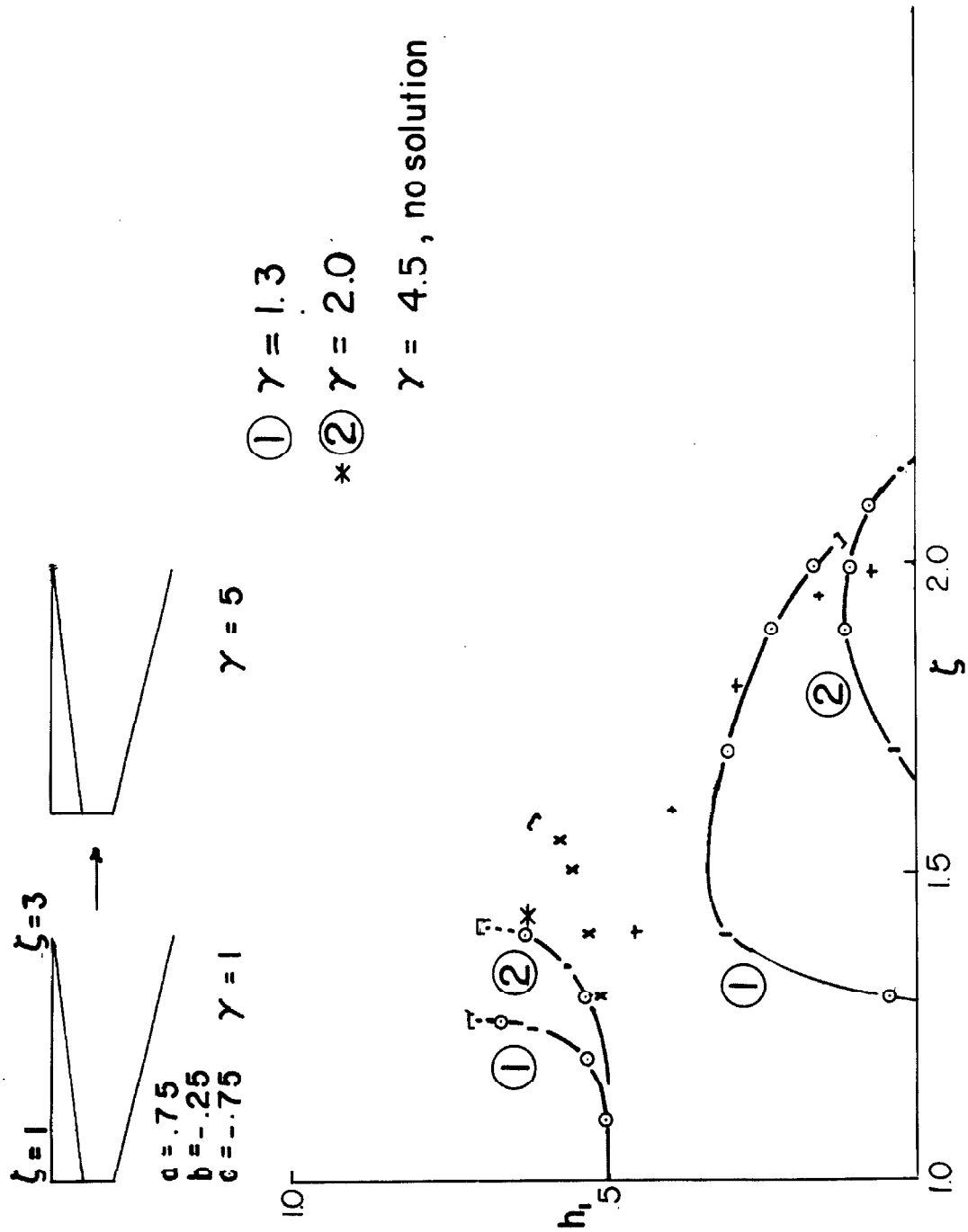

Figure 21. See caption on page 107.

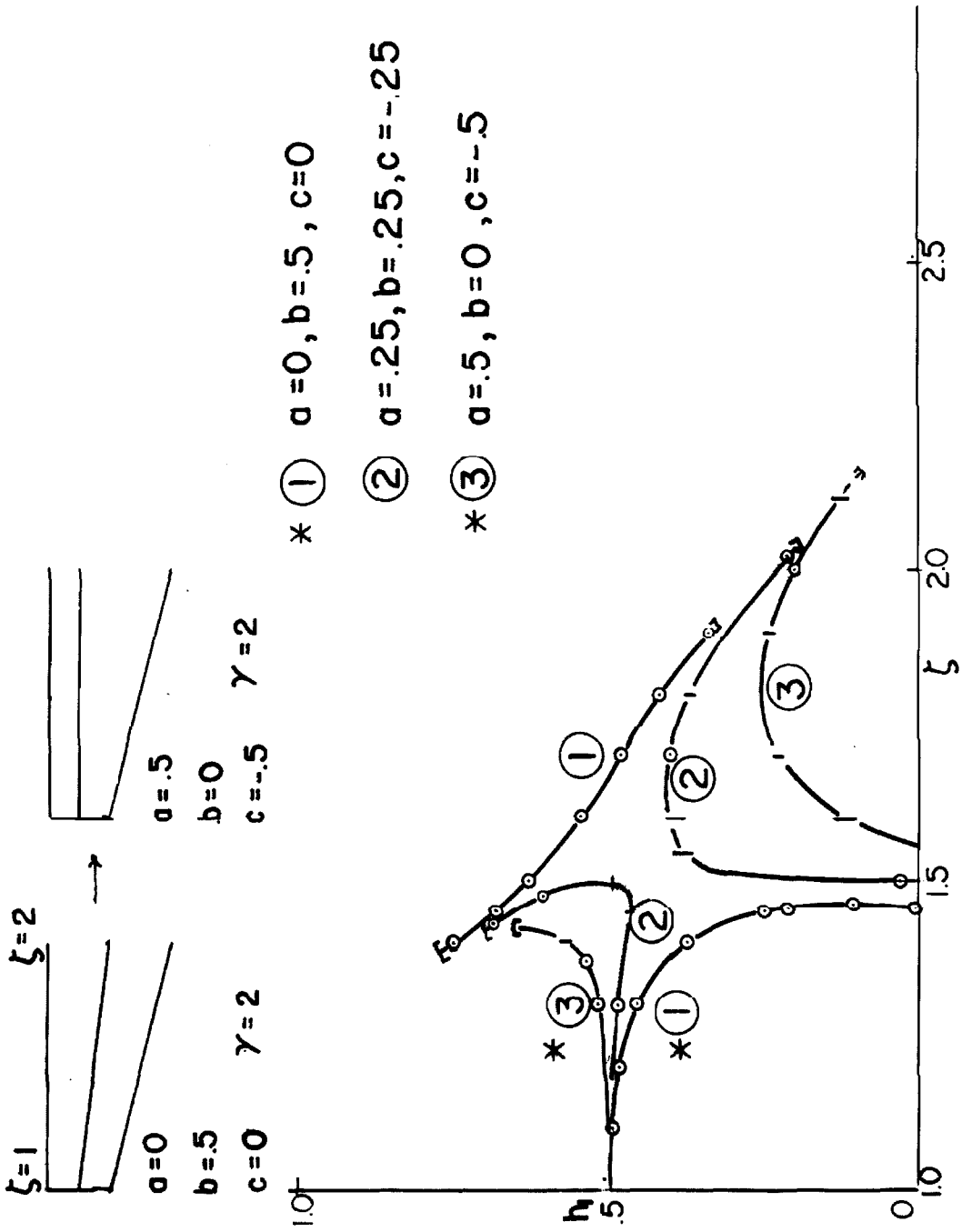

Figure 22. See caption on page 108.

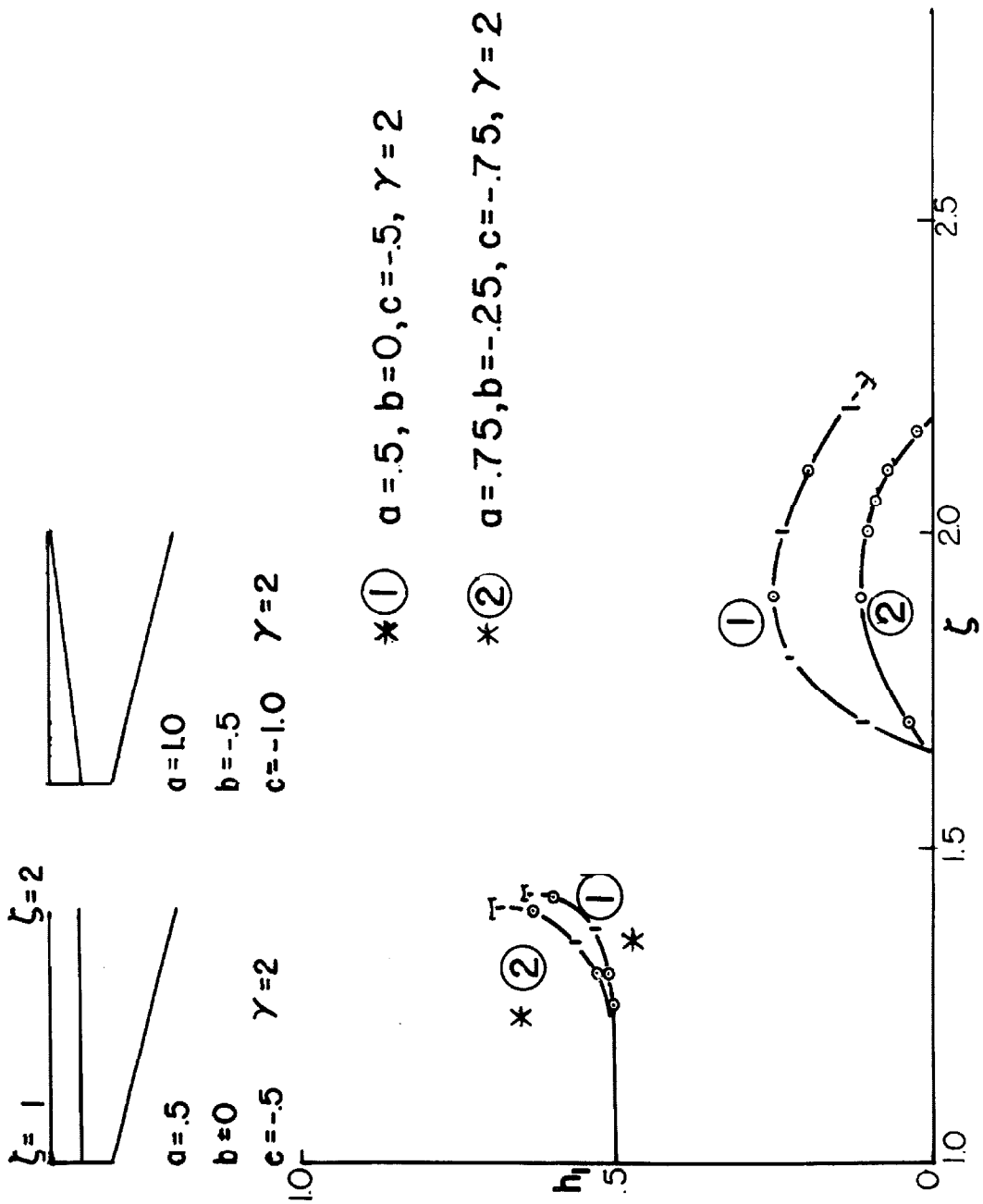

Figure 23. See caption on page 108.

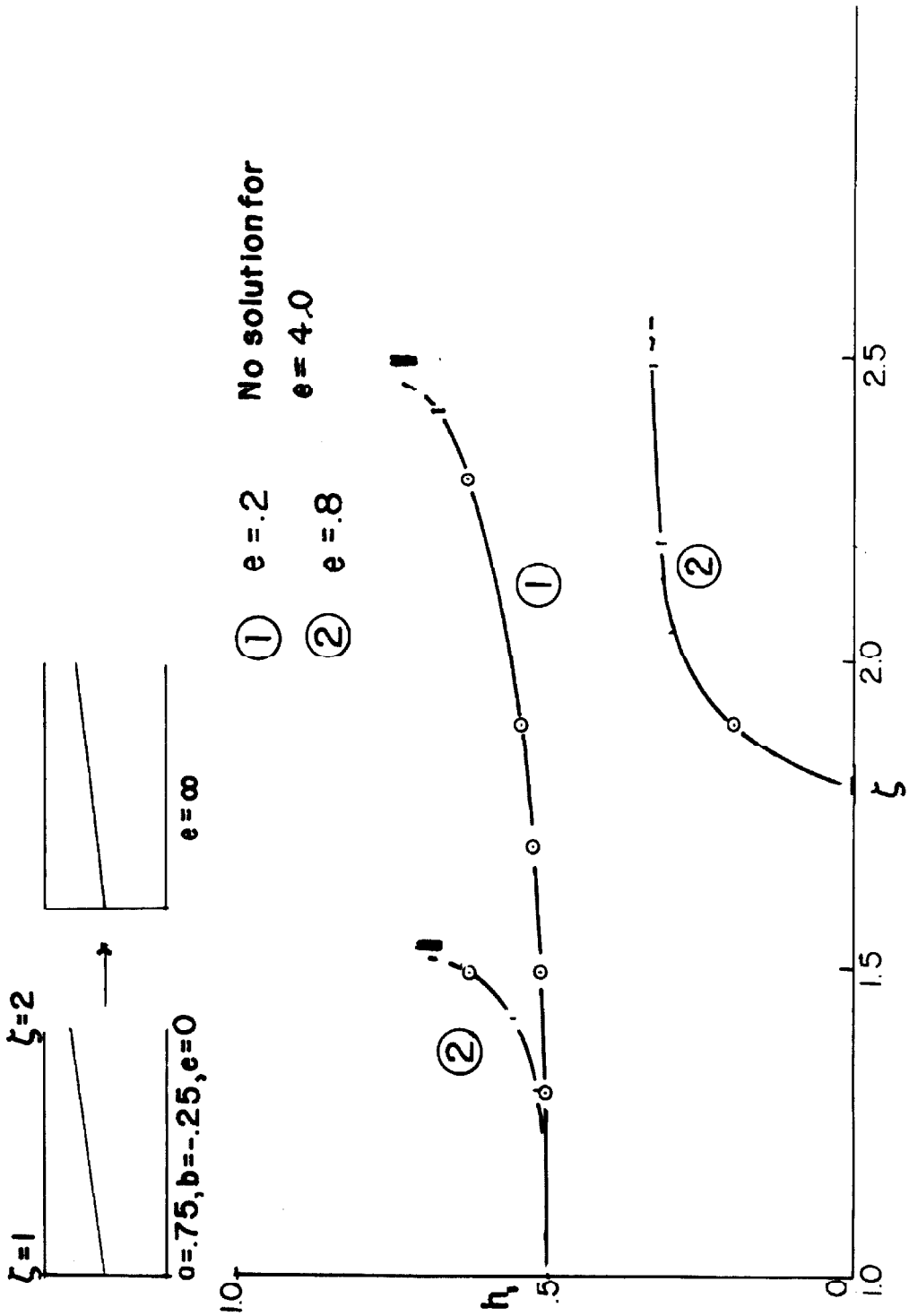

Figure 24. See caption on page 108.

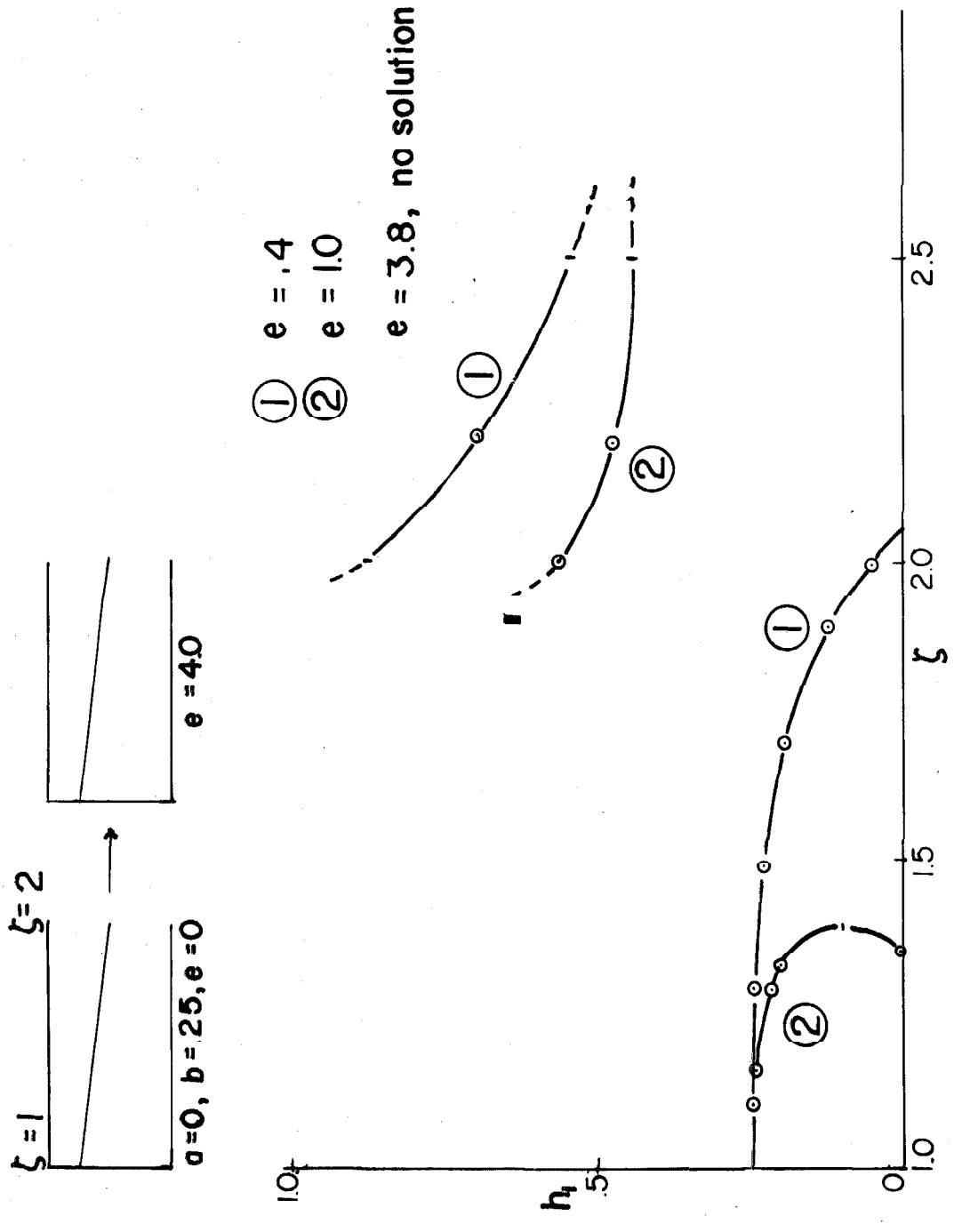

Figure 25. See caption on page 109.

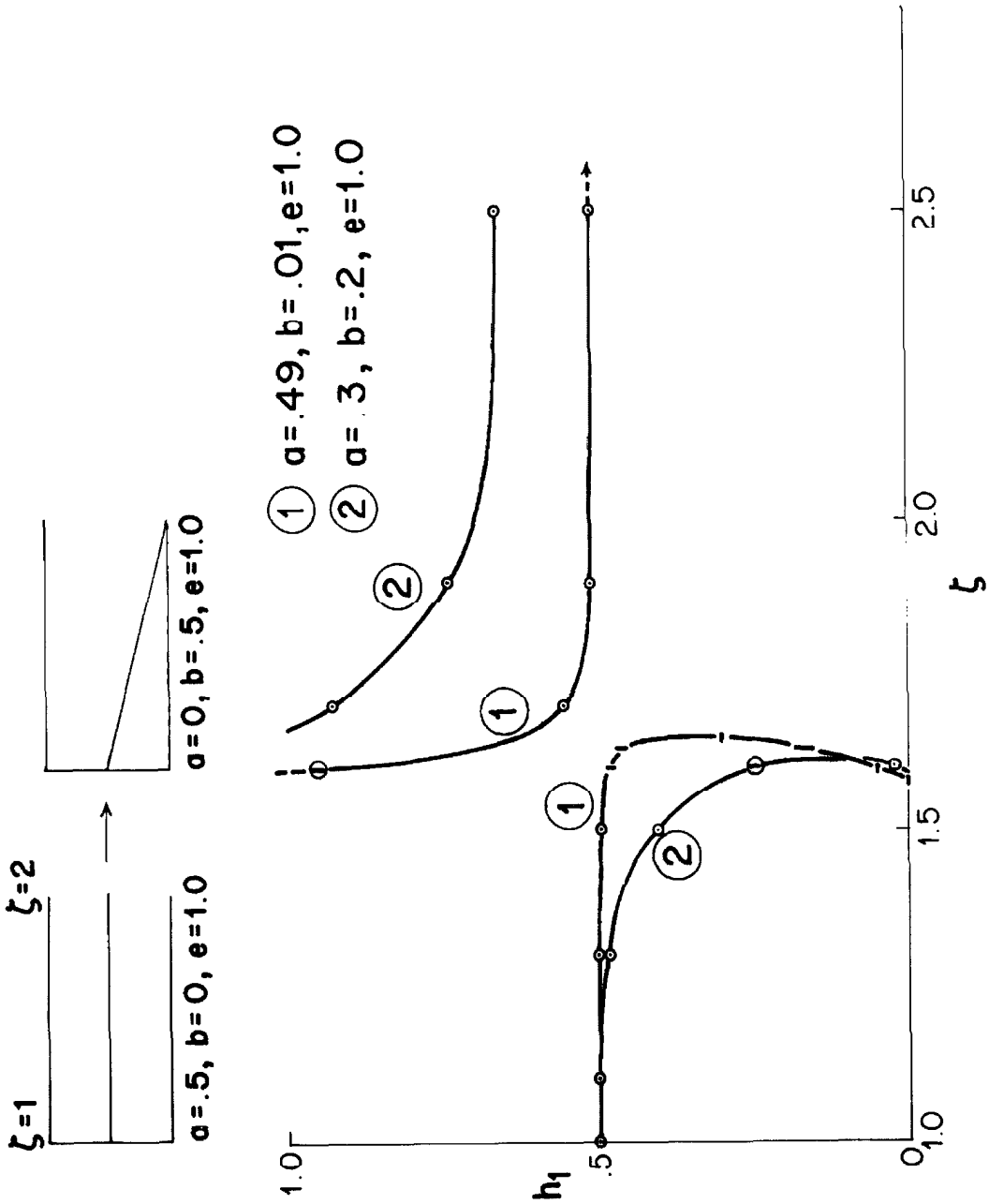

Figure 26. See caption on page 109.

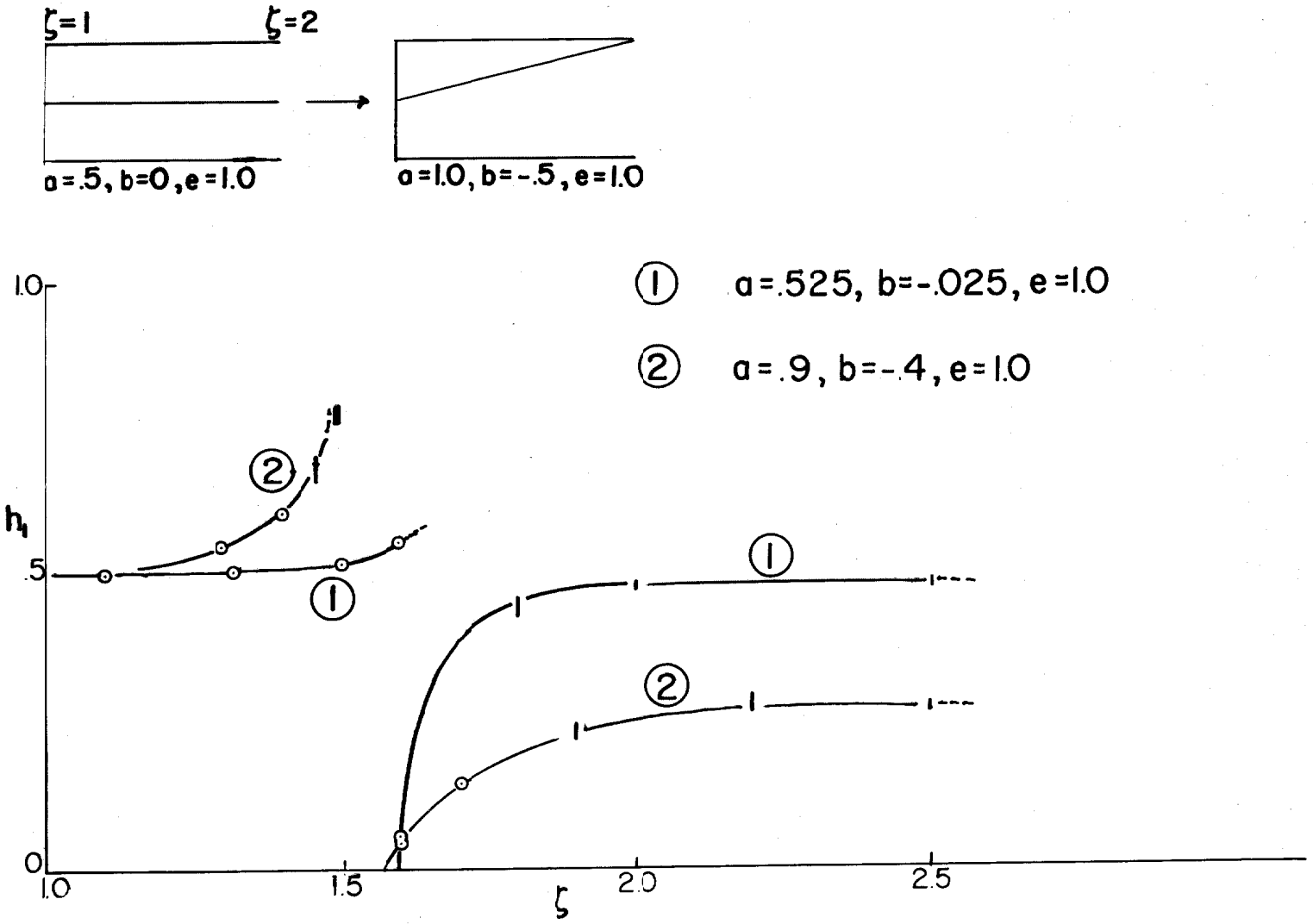

Figure 27. See caption beginning on page 109.

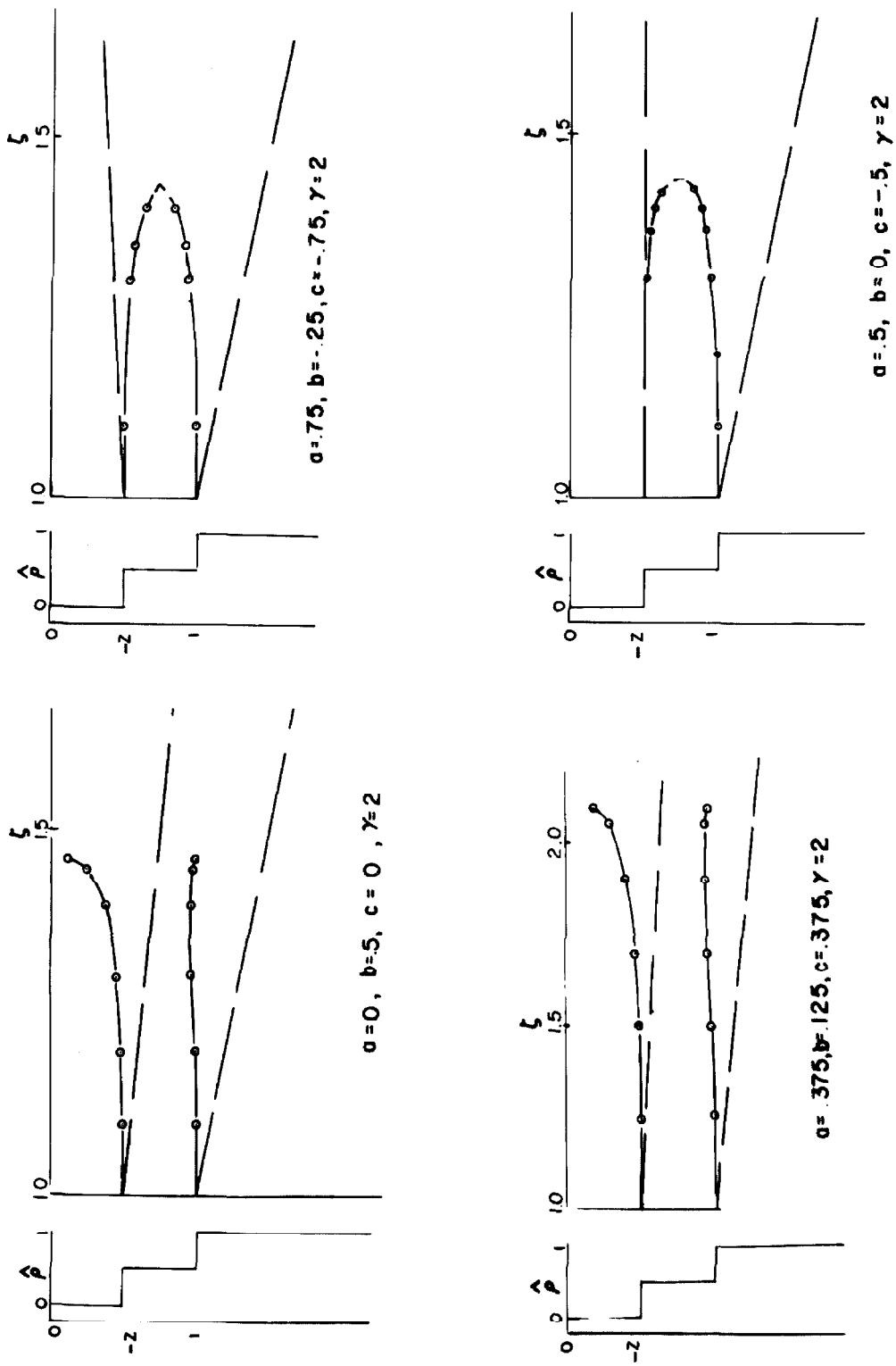

Figure 28. See caption on page 110.

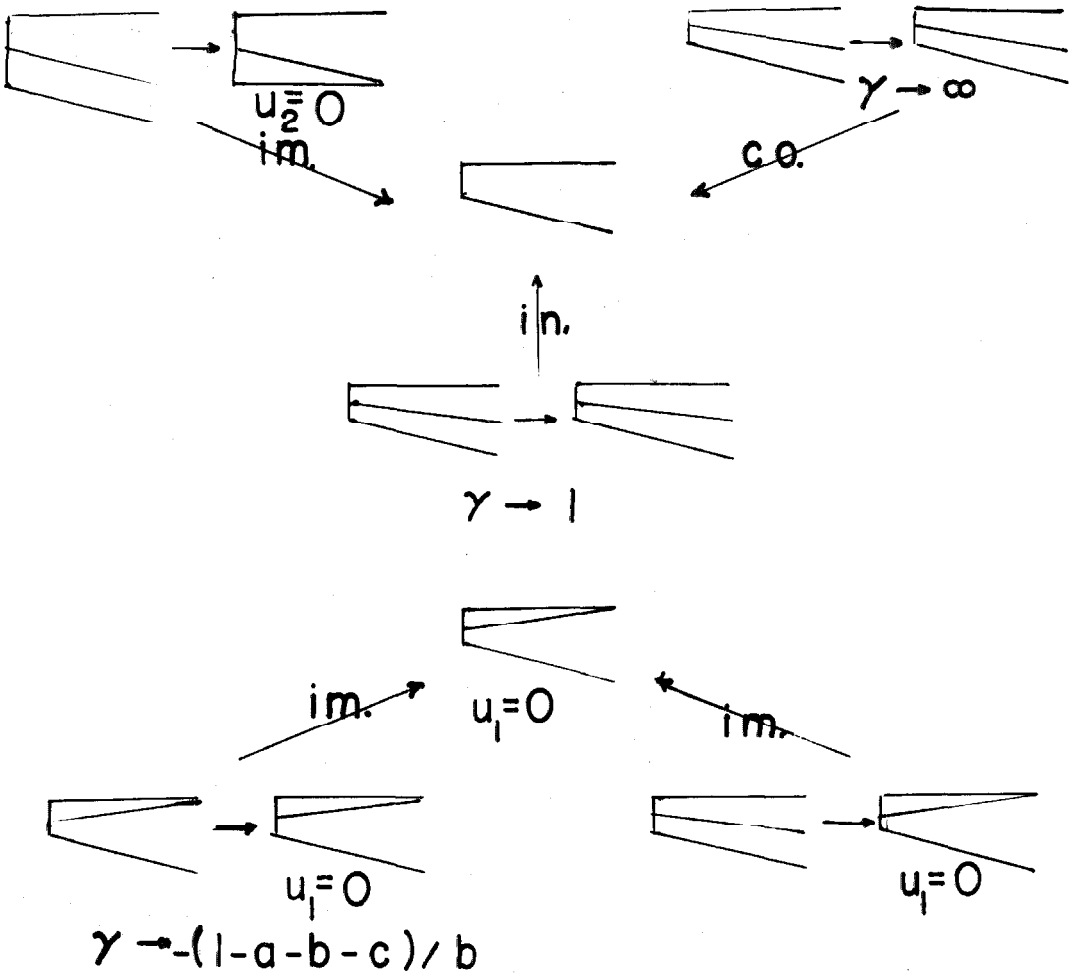

im = impossible, in = incorrect, co = correct

Figure 29. See caption on page 110.

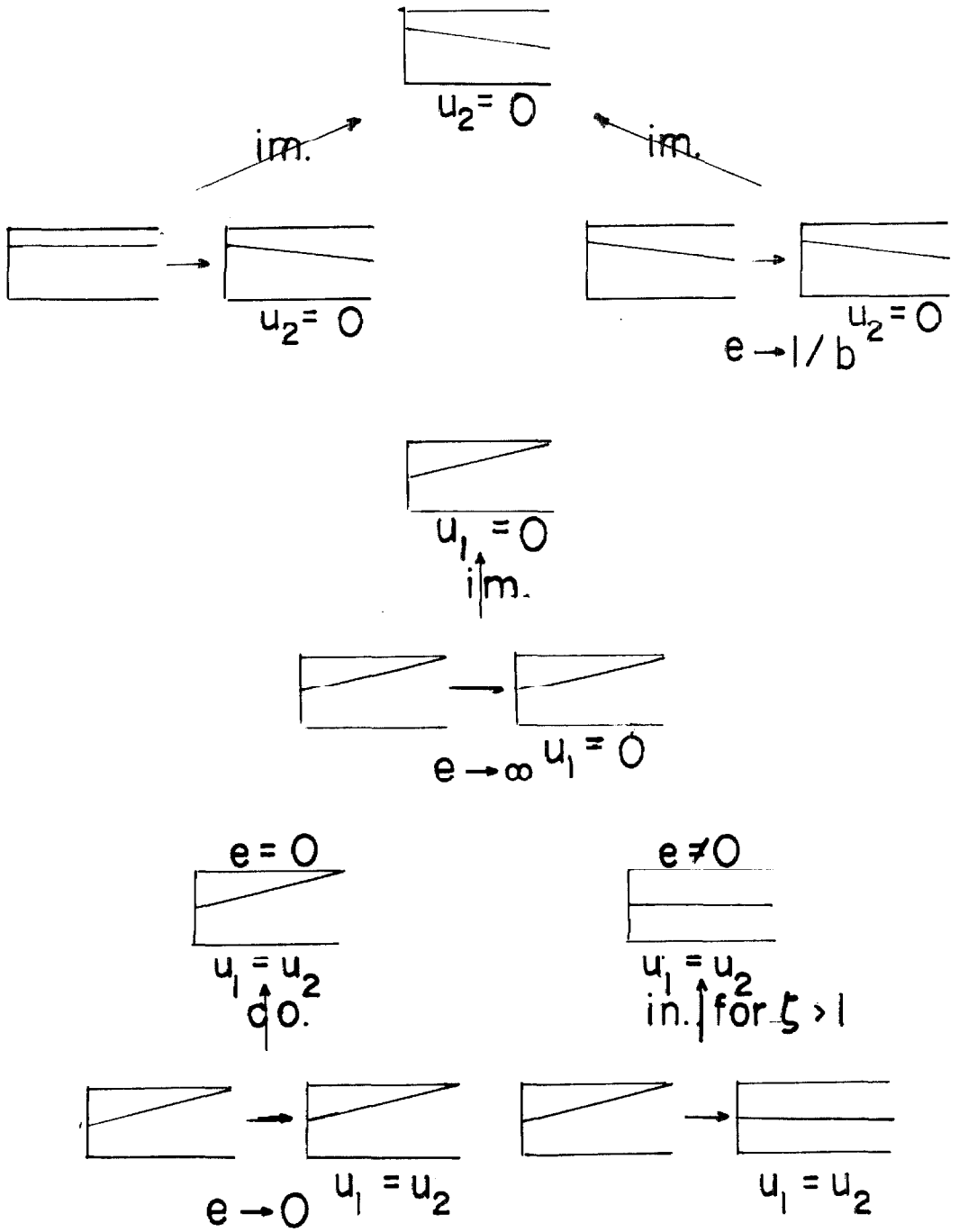

im = impossible, in = incorrect, co = correct

Figure 30. See caption on page 110.

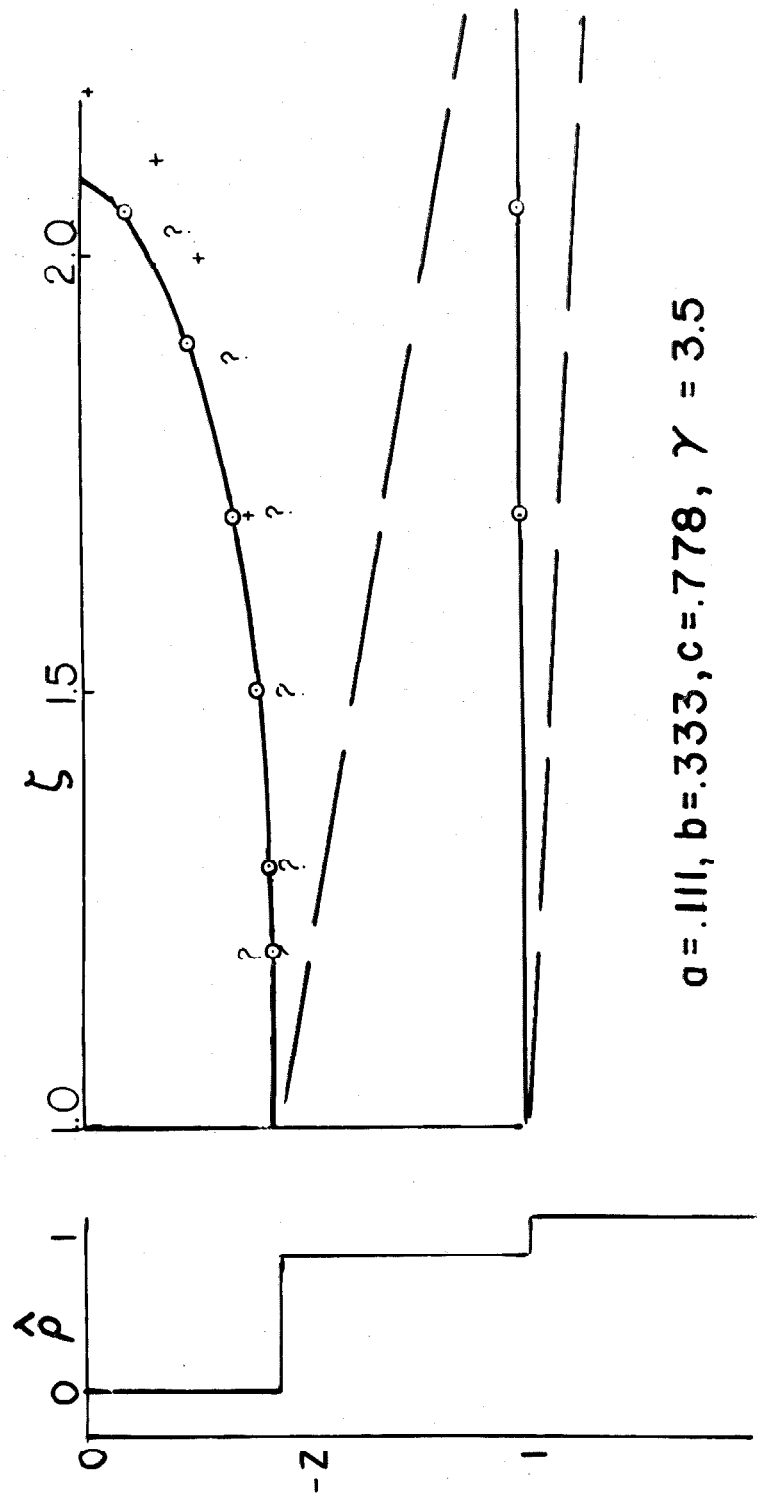

Figure 31. See caption beginning on page 110.

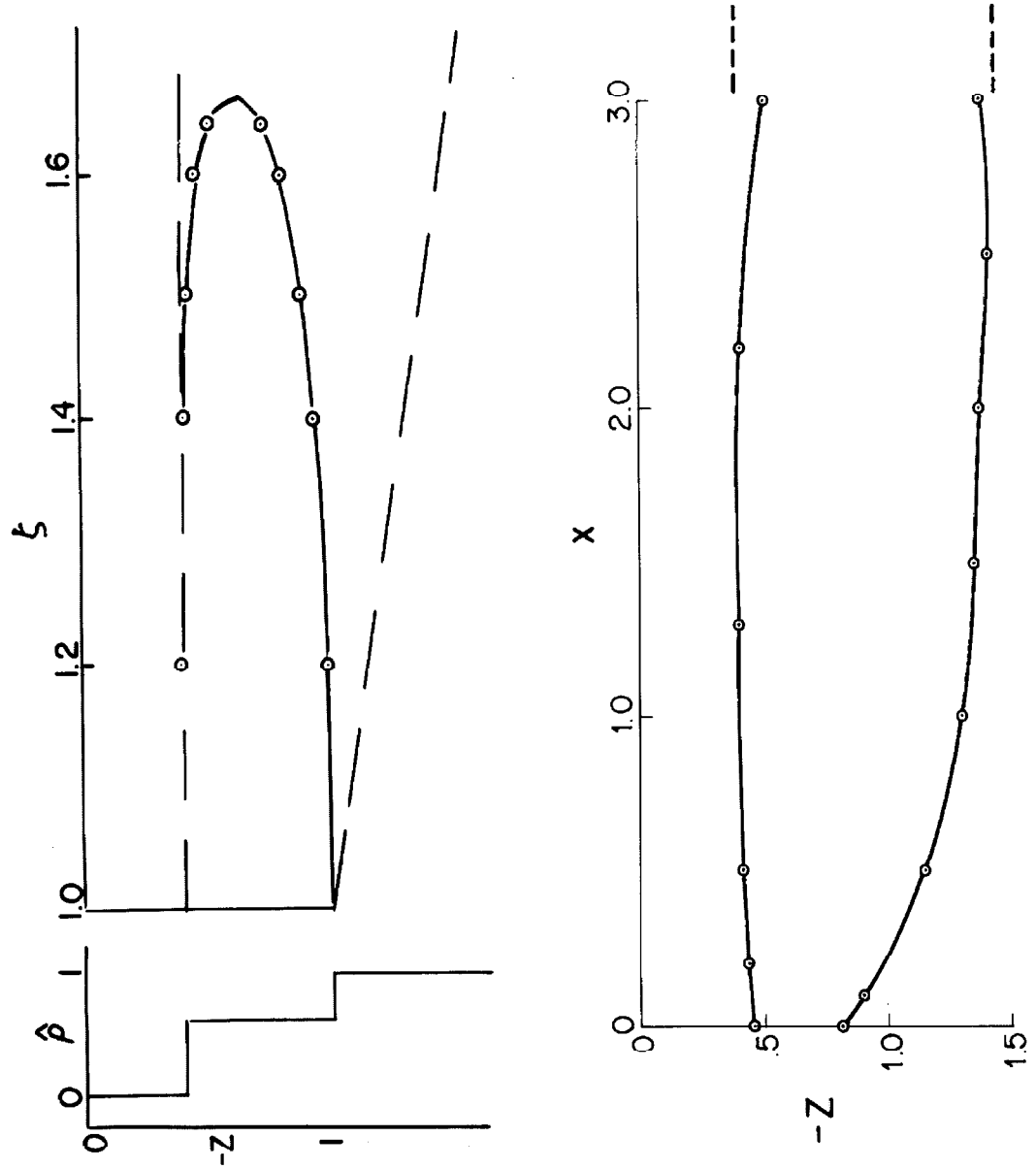

Figure 32. See caption on page 111.

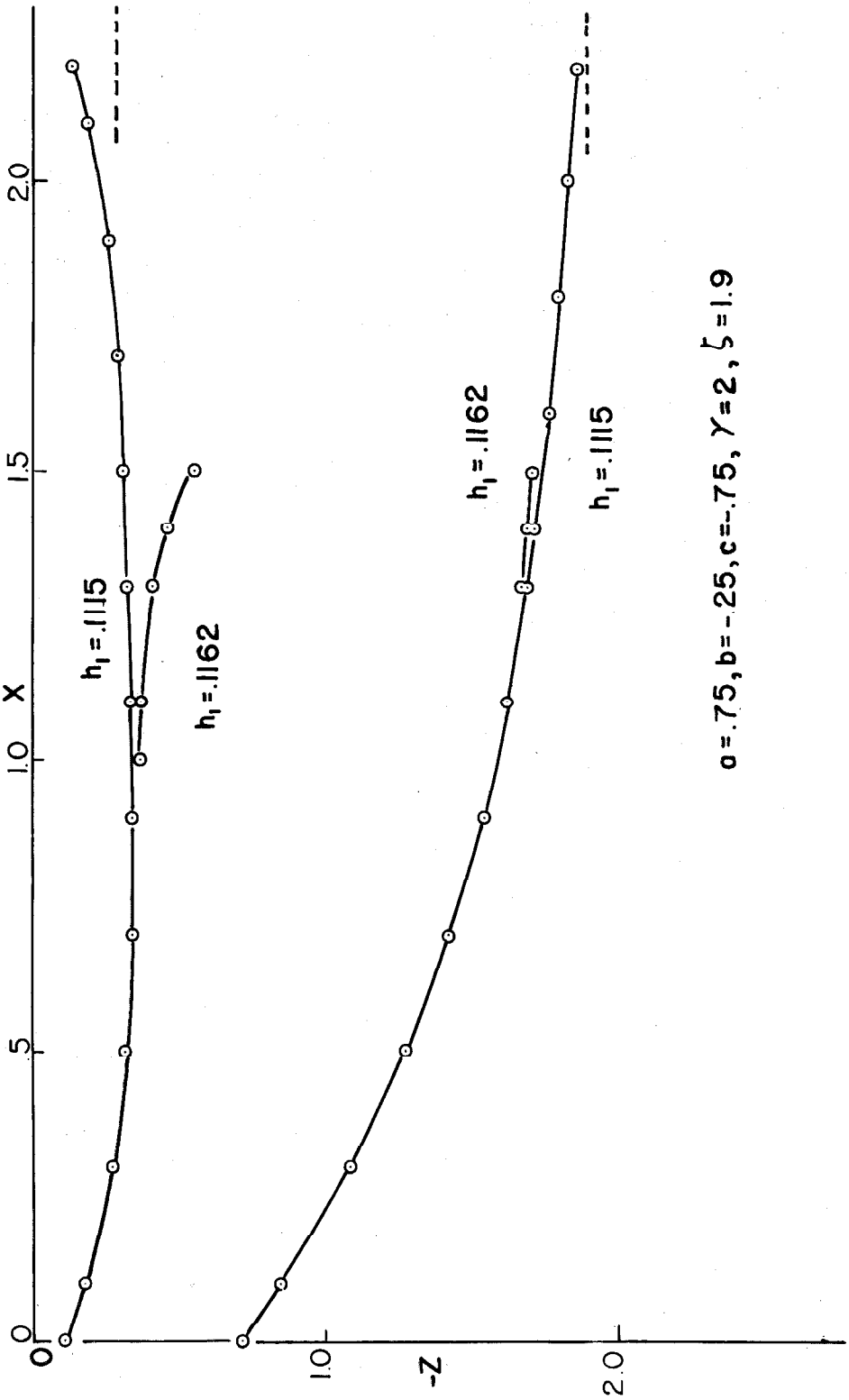

Figure 33. See caption on page 111.

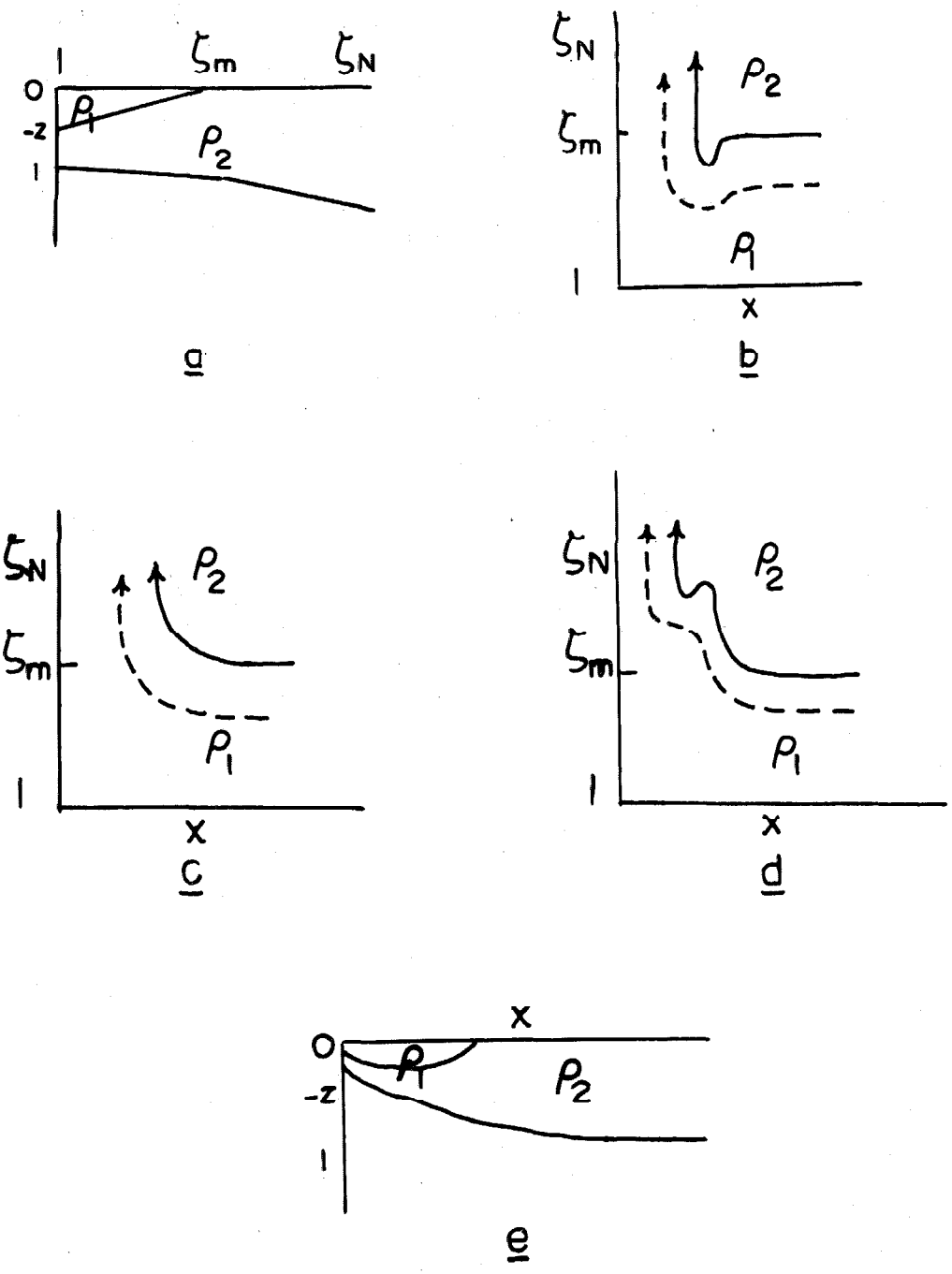

Figure 34. See caption on page 112.

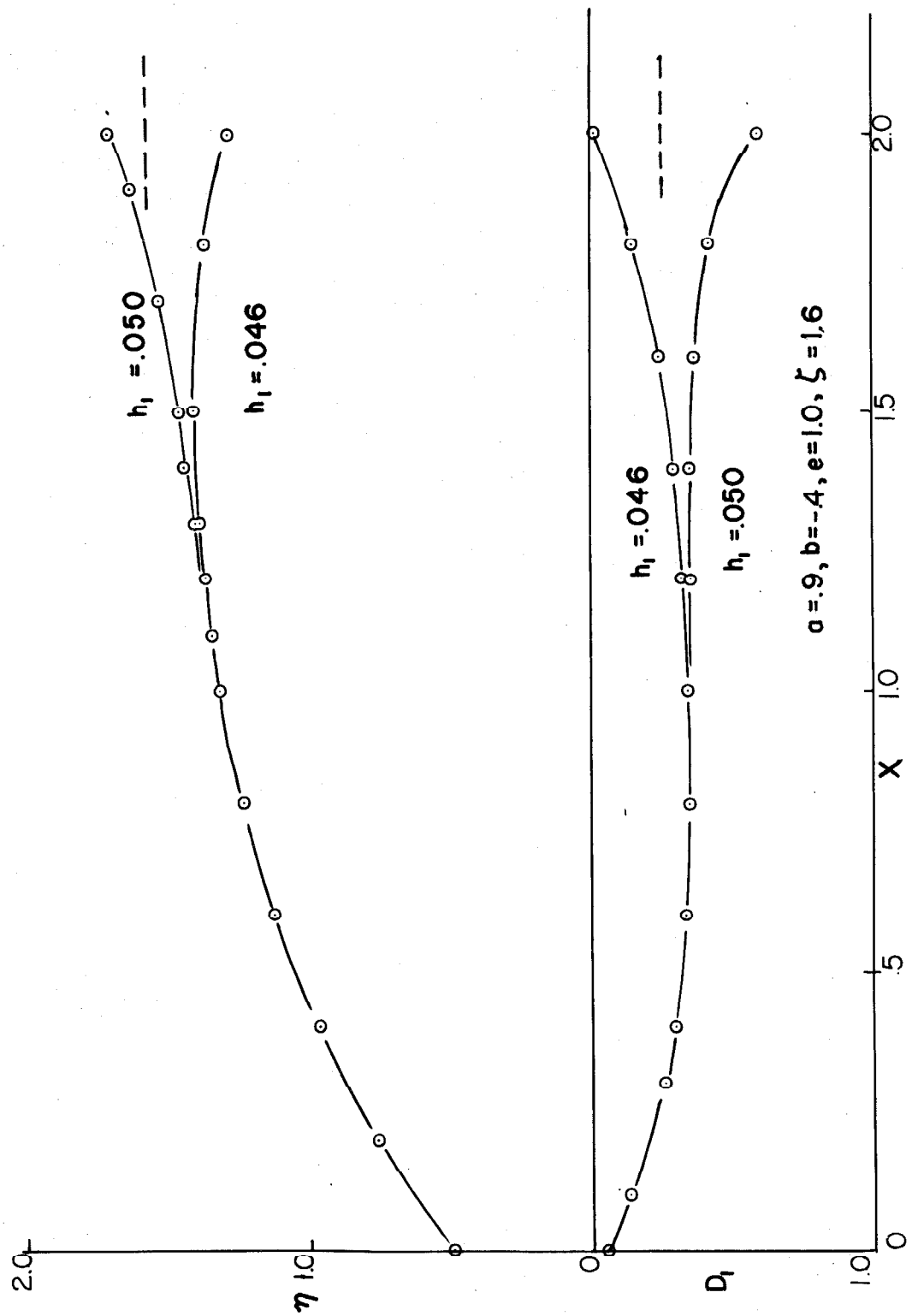

Figure 35. See caption on page 112.

LIST OF SYMBOLS

(a,b,c)	parameters of layer thicknesses
(a_i,b_i)	undetermined coefficients
D_i	layer thicknesses
D_o	constant layer thickness
e	ratio of stratification to free surface effects
F_i	potential vorticity integrals of the motion
f	Coriolis parameter
G_i	Bernoulli integrals of the motion
g	acceleration of gravity
h_i	thickness of layer $\underline{i}$ at the coast
n_i	algebraic combination of the solutions of the characteristic equation for constant potential vorticity
p_i	pressure in layer $\underline{i}$
R	radius of the earth
$\underset{\sim}{V}$	vector velocity
(u,v,w)	horizontal and vertical cartesian velocities
$(\overline{u},\overline{v})$	vertically integrated horizontal velocities
Y_i	dependent variables for numerical integration
(x,y,z)	horizontal and vertical cartesian coordinates
x_t	value of $\underline{x}$ where the upper layer thickness vanishes
α_i	roots of the characteristic equation for constant potential vorticity
β	meridional gradient of the Coriolis parameter
γ	parameter describing stratification

δ ratio of layer thickness in the interior for constant potential vorticity

ϵ small non-dimensional number, the ratio of horizontal scales

ζ a north-south transformed coordinate, the non-dimensional Coriolis parameter

η surface elevation

θ latitude, or ratio of density gradients of the upper to the lower layer in constant potential vorticity case

θ_o latitude of tengency of the beta-plane

λ characteristic scale of $\underline{x}$

ν viscosity of sea water

ρ_i density of layer $\underline{i}$

σ $1000(\rho-1)$

τ shearing stress across a horizontal surface

ψ stream function

Ω earth's angular velocity

REFERENCES

1. Stommel, H. 1958. The Gulf Stream: a physical and dynamical description. University of California Press, Berkeley.

2. Stommel, H. and A. B. Arons. 1960. On the abyssal circulation of the world ocean--I. Stationary planetary flow patterns on a sphere. Deep Sea Res., V 6, pp. 140-154.

3. Stommel, H. and A. B. Arons. 1960. On the abyssal circulation of the world ocean--II. An idealized model of the circulation pattern and amplitude in oceanic basins. Deep Sea Res., V 6, pp. 217-233.

4. Stommel, H., A. B. Arons, and A. J. Faller. 1958. Some examples of stationary flow patterns in bounded basins. Tellus, V 10, pp. 179-187.

5. Robinson, A. R. and H. Stommel. 1959. The oceanic thermocline and the associated thermohaline circulation. Tellus, V 11, pp. 295-308.

6. Stommel, H. and J. Webster. 1962. Some properties of thermocline equations in a subtropical gyre. J. Mar. Res., V 20, pp. 42-56.

7. Robinson, A. R. and P. Welander. 1963. Thermal circulation on a rotating sphere with application to the oceanic thermocline. J. Mar. Res., V 21, pp. 25-38.

8. Blandford, R. Notes on the thermocline. In preparation.

9. Swallow, J. C. and B. V. Hamon. 1960. Some measurements of deep currents in the eastern North Atlantic. Deep Sea Res., V 3, pp. 93-104.

10. Fuglister, F. C. 1960. Atlantic Ocean Atlas. Woods Hole Oceanographic Institution, Woods Hole, Massachusetts.

11. Worthington, L. V. 1954. Three detailed cross-sections of the Gulf Stream. Tellus, V 6, pp. 116-123.

12. Warren, B. 1963. Topographic influences on the path of the Gulf Stream. Tellus, V 15, pp. 167-183.

13. Carrier, G. F. and A. R. Robinson. 1962. On the theory of the wind-driven ocean circulation. J. Fl. Mech., V 12, 1, pp. 49-80.

14. Bryan, K. 1963. A numerical investigation of a nonlinear model of a wind-driven ocean. J. Am. Sci., V 10, 6, pp. 594-606.

15. Sverdrup, H. U. 1947. Wind-driven currents in a baroclinic ocean; with application to the equatorial currents of the eastern Pacific. Proc. Nat. Acad. Sci. Wash., V 33, pp. 318-326.

16. Stommel, H. 1948. The westward intensification of wind-driven ocean currents. Trans. Amer. Geophys. Union, V 29, pp. 202-206.

17. Munk, W. H. 1950. On the wind-driven ocean circulation. J. Meteor., V 7, pp. 79-93.

18. Stommel, H. 1955. Lateral eddy viscosity in the Gulf Stream system. Deep Sea Res., V 3, pp. 88-90.

19. Munk, W. J., G. W. Groves, and G. F. Carrier. 1950. Note on the dynamics of the Gulf Stream. J. Mar. Res., V 9, pp. 218-238.

20. Munk, W. J., and G. F. Carrier. 1950. The wind-driven circulation in ocean basins of various shapes. Tellus, V 2, pp. 158-167.

21. Morgan, G. W. 1956. On the wind-driven ocean circulation. Tellus, V 8, pp. 301-320.

22. Charney, J. G. 1955. The Gulf Stream as an inertial boundary layer. Proc. Nat. Acad. Sci. Wash., V 41, pp. 731-740.

23. Stoker, J. J. 1957. Water Waves; the mathematical theory with applications. Interscience Publishers, New York.

24. Rossby, C. G. 1939. Relation between variations in the intensity of the zonal circulation of the atmosphere and the displacements of the semi-permanent centers of action. J. Mar. Res., V 2, pp. 38-55.

25. Fofonoff, N. P. The Sea, M. N. Hill, editor. 1963. V 1, pp. 323-380, Interscience, New York.

26. Todd, J. 1962. Survey of Numerical Analysis. McGraw-Hill, New York.

27. Ippen, A. T. and D. R. F. Harleman. 1952. Steady state characteristics of sub-surface flows. Natl. Bur. Standards (U.S.), Circ. 521, pp. 79-93.

28. Long, R. R. 1953. Some aspects of the flow of stratified fluids III. Continuous density gradients. Tellus, V 7, pp. 341-357.

29. Yih, C. S. and C. R. Guha. 1955. Hydraulic jumps in a fluid system of two layers. Tellus, V 7, pp. 358-366.

30. Stern, M. E. 1961. The stability of thermoclinic jets. Tellus, V 4, pp. 503-508.

31. Greenspan, H. P. 1962. A criterion for the existence of inertial boundary layers in oceanic circulation. Proc. Natl. Acad. Sci. U.S., V 48, pp. 2034-2039.

32. Starr, V. P. 1945. A quasi-Lagrangian system of hydrodynamical equations. J. Meteor., V 2, pp. 227-237.

33. Ertel, H. 1942. Meteorological Zeitung. V 59, p. 277.

34. Jacobs, S. 1963. Low Rossby number flow over bottom topography. Harvard University doctoral thesis.